universität wien

MASTERARBEIT / MASTER‘S THESIS

Titel der Masterarbeit / Title of the Master’s thesis

“*A phytochemical study on Palicourea glomerulata to reproduce previous findings of quinoline alkaloids*”

verfasst von / submitted by

Alexander Karbalaei Bagher, BSc

angestrebter akademischer Grad / in partial fulfilment of the requirements for the degree of

Master of Science (MSc)

Wien, 2022 / Vienna 2022

Studienkennzahl lt. Studienblatt / degree programme code as it appears on the student record sheet:	A 066 862
Studienrichtung lt. Studienblatt / degree programme as it appears on the student record sheet:	Chemie
Betreut von / Supervisor:	Univ.-Prof. Dipl.-Chem. Dr. Lothar Brecker, Privatdoz.

Statuary declaration

I hereby declare that the thesis submitted is my own unaided work, that I have not used other than the sources indicated, and that all direct and indirect sources are acknowledged as references.

This printed thesis is identical with the electronic version submitted.

Place, Date

Signature

Acknowledgement

First, I want to thank my supervisor Univ.-Prof. Dipl.-Chem. Dr. Lothar Brecker, Privatdoz. for offering me to work on this exciting topic, even though organising laboratory work was especially difficult, due to the global pandemic and social distancing. I am very grateful for his help and advice with any problems that came up during structure elucidation. Overall, it was a pleasant and memorable experience to work in his group.

Next, I want to thank my laboratory supervisor Mag. Dr. Johann Schinnerl for helping me with the isolation processes and the biological and chemical assays that have been conducted during my thesis. I also want to thank him for giving me insight into the large and fascinating topic of specialised plant metabolites and their importance for plant life. Additionally, I want to thank my colleagues at the Department of Botany and Biodiversity Research Vienna for providing me the plant material.

I also want to thank my colleagues in my working group at Organic Chemistry Department for their help and advice. It is unfortunate, that due to the pandemic, social activities were not possible. I want to especially thank Florian Traxler, BSc. MSc. for helping me with the CD, IR and polarimetric measurements and Merve Bodur for her help with the biological and chemical assays.

Additionally, I want to thank the NMR Center and the Mass Spectrometry Center of the University of Vienna, Währinger Strasse 38, A-1090 Vienna, Austria for measuring all my samples.

Lastly, I want to thank my family for financially supporting and encouraging me. I also want to thank my girlfriend and my friends for helping me throughout this time with emotional support and distraction when I needed it.

Abstract

Phytochemical investigation on the leaf extract of *Palicourea glomerulata* resulted in the isolation of five compounds, four known and one novel compound. Their structure was elucidated using ^{1}H, ^{13}C (DEPTq), COSY, TOCSY, NOESY, HSQC, HMBC and ROESY experiments and ESI-MS measurements. The novel compound is structurally related to cyclotryptamines and alstrostines, which are monoterpene indole alkaloids that are not derived from strictosidine. The already known four compounds include 6,8-di-*C*-β-D-glucopyranosylnaringenin, 6'-*O*-β-D-apiofuranosyl-sweroside, glomerulatine A and 1-(6-amino-6-deoxy-α-D-glucosyl)-2,3-dipalmitylglycerol. Interestingly, *C*-glycosylflavonoids and 6-aminosugarsglycerolipids are scarcely found in nature. Both compound classes have been studied intensively due to their bioactivities. However, their occurrence in this species was not yet mentioned. Furthermore, because of the large structural diversity of the substances, the NMR spectra of each compound brought their own unique challenges. Therefore, different approaches were needed for the structure elucidation of these respective compounds. Additionally, chemical and biological assays were conducted with the leaf, stem bark and root extracts using the antioxidant activity assay, the non-choice feeding experiment and the leaf disc choice test. However, apart from radical scavenging activity, no effects were observed. Overall, this thesis emphasises on the vast variety of specialised plant metabolites and that modern isolation techniques can help to find novel structures in already studied species. This work contributed to the further understanding of the chemical profile of *Palicourea glomerulata*.

Zusammenfassung

Die phytochemische Untersuchung von dem Blattextrakt von *Palicourea glomerulata* resultierte in der Isolation von insgesamt fünf Verbindungen, wovon vier bereits bekannt sind und eine neu ist. Die Strukturen wurden mittels ^{1}H, ^{13}C (DEPTq), COSY, TOCSY, NOESY, HSQC, HMBC und ROESY NMR Experimenten und ESI-MS Messungen aufgeklärt. Die neue Verbindung ist strukturell mit der Klasse der Cyclotryptamine und Alstrostine verwandt. Alstrostine gehören zu den Monoterpen-Indolalkaloiden, die nicht Strictosidin als Vorstufe haben. Die bereits bekannten Verbindungen sind 6,8-Di-*C*-β-D-glucopyranosylnaringenin, 6'-*O*-β-D-Apiofuranosyl-sweroside, Glomerulatin A und 1-(6-Amino-6-deoxy-α-D-glucosyl)-2,3-dipalmitylglycerol. Interessanterweise kommen *C*-Glycosylflavonoide und 6-Aminozuckerglycerolipide sehr selten in der Natur vor. Dennoch wurden beide Strukturklassen aufgrund ihrer Bioaktivität intensiv untersucht. Nichtdestotrotz ist ihr Vorkommen in dieser Spezies noch nicht beschrieben. Darüber hinaus brachten die NMR Spektren zu jeder Verbindung aufgrund der großen strukturellen Vielfalt der Substanzen einzigartige Herausforderungen mit sich. Deswegen waren bei der Strukturaufklärung der jeweiligen Verbindungen unterschiedliche Herangehensweisen notwendig. Zusätzlich wurden chemische und biologische Assays mit Blatt-, Stammrinden- und Wurzelextrakten durchgeführt. Dazu zählten der Antioxidans Test, der Non-choice-feeding Test und der Leaf disc choice Test. Jedoch wurden neben der Radikalfängerwirkung keine weiteren Effekte gemessen. Zusammengefasst zeigt diese Arbeit, dass Pflanzen eine große Vielfalt an spezialisierten Pflanzenmetaboliten synthetisieren können und dass moderne Isolationstechniken dabei helfen können neue Strukturen in bereits untersuchten Spezies zu finden. Zudem trägt sie zum weiteren Verständnis zum chemischen Profil von *Palicourea glomerulata* bei.

Table of content

1. Introduction

In human history, plants have been known for their biological activity for many thousands of years [1]. As a multidisciplinary field, phytochemical research aims to describe natural compounds, understand their biosynthetic pathway, their biological activity, and their mechanisms of action. Furthermore, the profile of specialized metabolites distribution can be used as chemotaxonomic markers and bring additional information for the taxonomic classification [2]. Plants rely on specialized metabolites, because beside mechanical defenses, chemicals are their only way of protection against herbivores and pathogens. These chemical defenses are mostly derived from the secondary metabolism, also called specialized metabolism, and include, amongst other, alkaloids, flavonoids, and terpenes [3].

As one of the largest in the Magnoliopsida class, the Rubiaceae includes approximately 637 genera and more than 13 600 species. It is divided into the three subfamilies: Rubioideae, Cinchonoideae and Ixoroideae. Research shows, that of these three subfamilies, Rubioideae, the most ancient one, possesses the highest chemical diversity. Regarding the chemical profile, the Rubiaceae family are shown to possess a large diversity of secondary metabolites such as iridoids, anthraquinones, terpenoids, flavonoids, and indole alkaloids, as the main constituents [2].

1.1. *Palicourea glomerulata*

Palicourea glomerulata (Donn.Sm.) Borhidi, also known as *Psychotria glomerulata* (Donn.Sm.) Steyerm. and *Cephaelis glomerulata* Donn.Sm., belongs to the family of Rubiaceae and the subfamily of Rubioideae. This species is native in the Neotropical realm, mainly Central America and northern South America, where it amongst other plants is used in the traditional medicine [4]. Many species of Rubiaceae are used for traditional medical purposes around the world, as they are an abundant source of biologically active compounds [5]. Other members of the Rubiaceae family that are known for their economic importance include *Cinchona*, which are rich in quinine used to treat malaria and *Coffea arabica*, the source of coffee [6].

In the past decade, molecular phylogenetic analysis as well as phytochemical, ethnobotanical, pharmacological and chemotaxonomic studies have resulted in the

classification of the speciose *Psychotria* alliance, which consists of the two sister tribes Palicoureeae and Psychotrieae. These two sister tribes include about 24 % of Rubiaceae as a whole [5,7,8]. Besides differences in their habitat [8], phytochemical studies show differences in the chemical profile of Palicoureeae and Psychotrieae [5].

1.2. Specialized metabolites (=secondary metabolites)

The following paragraph is dedicated to the different classes of secondary metabolites, that have been isolated and described in this thesis. As many members of the Rubiaceae family have been phytochemically investigated over the past decades, research on *Palicourea glomerulata* describes the finding of three quinoline alkaloids (Figure 1) via acid-base extraction [9]. Acid-base extraction prioritizes the isolation of alkaloids [10]. As of now, no other substance classes have been mentioned to be isolated from *Palicourea glomerulata*.

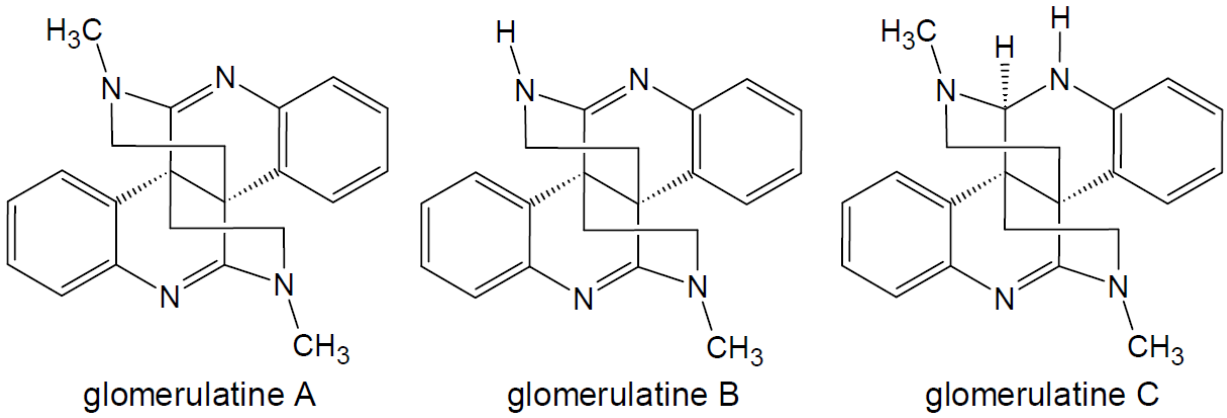

Figure 1. Structures of glomerulatine A, B and C [9].

1.2.1. *C*-Glycosylflavanonoids

Flavonoids are the largest group of plant phenolics [11], and play different roles in the ecology of plants. Because of their attractive colors, they can act a visual signal for pollinating insects. They can even act as protection against herbivores due to their astringency. Additionally, flavonoids can scavenge radical oxygen species (ROS) and absorb UV light to prevent the formation of UV induced radicals [12].

Flavonoids are known for their biological activity and benefits to human health for a long time. The flavonoid intake in human diet can range from 50 to 800 mg/day and can help in the prevention of cancer, diabetes, and cardio vascular diseases [11,12]. The pharmacokinetics of these substances are dependent on the type of glycosylation and the

number of sugar moieties. Flavonoid *C*-monoglycosides are often deglycosylated and degraded in the intestine by the colon bacteria, whereas flavonoid *C*-multiglycosides can reach the blood stream unchained [11]. Additionally, flavonoid *C*-glycosides in general show many benefits *in vitro*, in the case of antioxidant potential even exceeding the effects of their *O*-glycoside and aglycone counterpart [11].

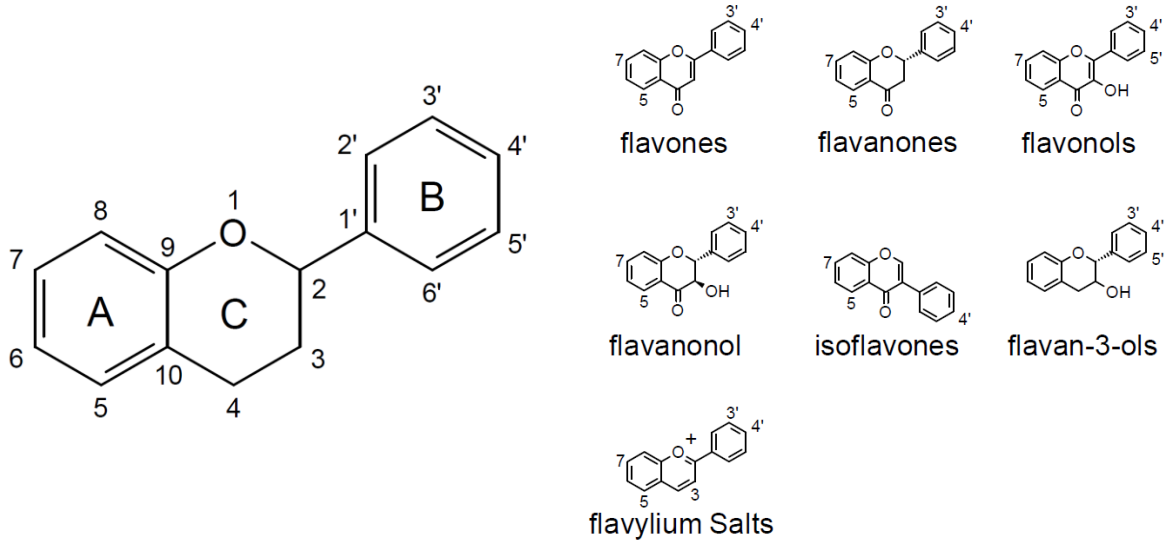

Figure 2. Basic flavan structure (left) and different classes of flavonoids (right). Biosynthetic substituents, mainly hydroxyl groups, can occur on the positions shown [12].

The basic flavonoid structure, the flavan nucleus, consists of 15 carbons arranged in three rings (C_6-C_3-C_6) (Figure 2). The two aromatic rings are labelled A and B, and the third ring is labelled C. Depending on the oxidized state and pattern of substitution of the C ring, flavonoids can be assigned into different classes. These classes include flavones, flavan-3-ols, flavanones, flavylium salts (anthocyanidins), flavonols, flavanonols and isoflavones (Figure 2) [12]. Flavonoids are formed by a sequential condensation of three malonyl coenzyme A with *p*-coumaroyl coenzyme A which is catalyzed by type III polyketide synthase (PKS) (Figure 3). The *p*-coumaroyl coenzyme A is derived from either L-tyrosine or L-phenylalanine, via the phenylpropanoid pathway [13,14]. Then naringenin chalcone is formed by Claisen type condensation of the C6 and C1 and chalcone synthase (CHS) [14]. Chalcone isomerase (CHI) catalyzes the intramolecular cyclization to form the tricyclic naringenin flavonoid [15].

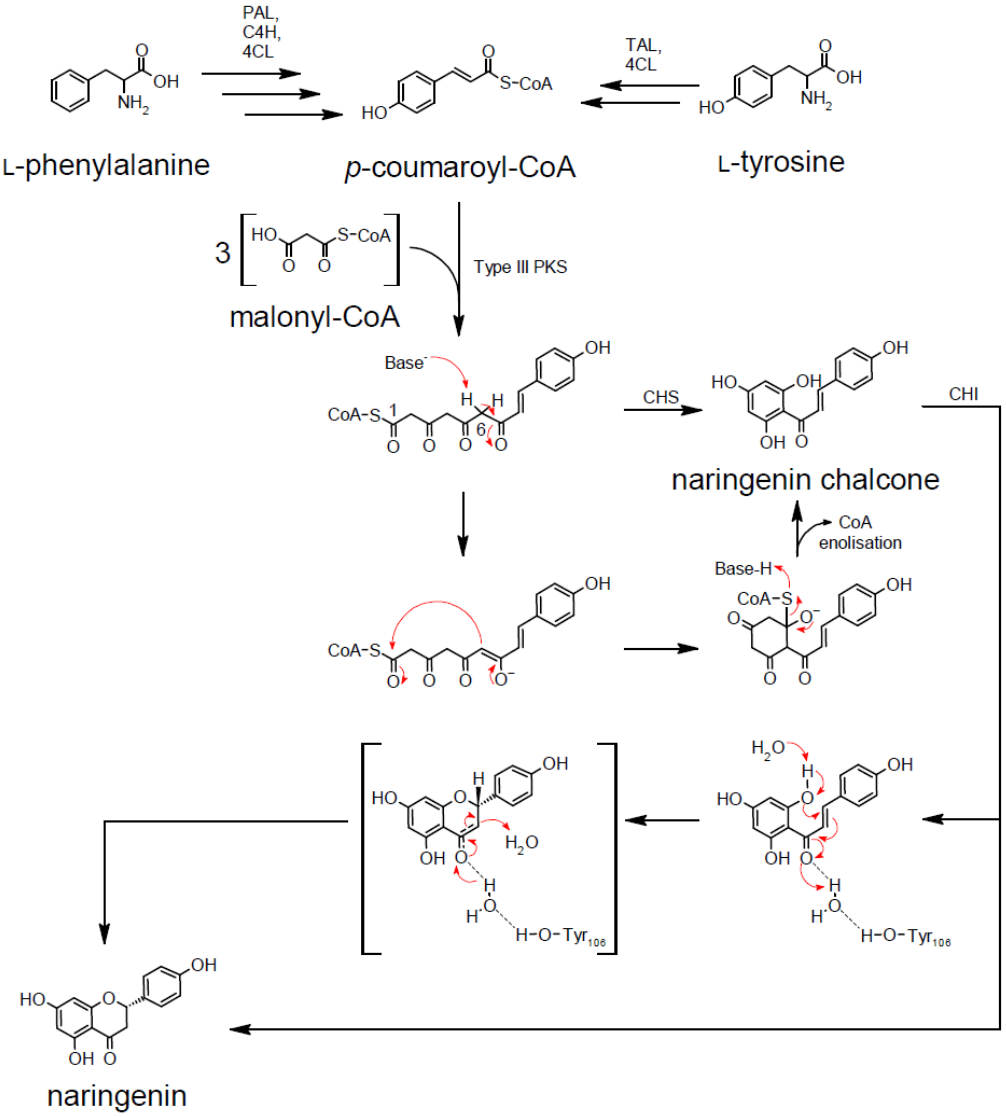

Figure 3. The naringenin pathway. coenzyme A (CoA), L-phenylalanine ammonia-lyase (PAL), L-tyrosine ammonia-lyase (TAL), cinnamate 4-hydroxylase (C4H), 4-hydroxycinnamate:CoA ligase (4CL), Type III polyketide synthase (PKS), chalcone synthase (CHS), chalcone isomerase (CHI) [13–15].

The major modification of flavonoids is glycosylation. It is a way to influence the stability, natural product transport, cellular compartmentalization and autotoxicity. Where contrary to *O*- and *N*-glycosylation, *C*-glycosylation is rather rare [16]. Unlike *O*-glycosidic bonds, *C*-glycosidic bonds are resistant to acid hydrolysis and glycosidase cleavage [17]. Although, *C*-glycosylated natural products have been known for many decades, their biosynthesis and biological roles are still not fully understood [16]. Some studies regarding the biosynthetic pathway of *C*-glycosides used ^{14}C-labelled flavanone and flavone aglycones. Results showed that the flavanone aglycons were converted into flavone *O*-

glycosides and *C*-glycosides simultaneously, while the flavone aglycones were only *O*-glycosylated. Therefore, the *O*-glycosylation step occurs at the terminal step after the flavone aglycone is generated, while *C*-glycosylation occurs before the flavone skeleton formation [13].

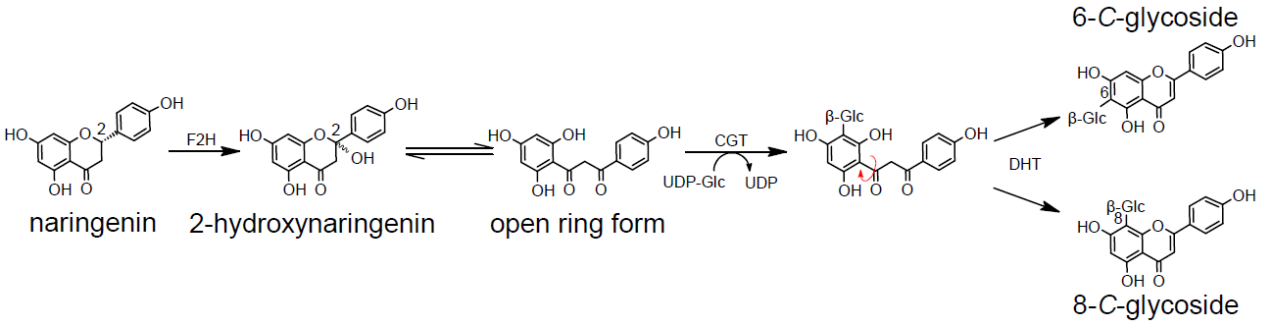

Figure 4. *C*-glycosylation pathway of naringenin. uridine diphosphate (UDP), flavanone 2-hydroxylase (F2H), *C*-glycosyltransferase (CGT), dehydratase (DHT) [13,18].

For the formation of *C*-glycosides, flavonoids are first hydroxylated on the C2 by flavanone 2-hydroxylases (F2H), a cytochrome P450 monooxygenase (Figure 4) [18]. The 2-hydroxyflavone is in equilibrium its open-ring form, which subsequently can be *C*-glycosylated. The *C*-glycosylation is catalyzed by the *C*-glycosyltransferase (CGT) enzyme and uridine diphosphate glucose (UDP-glucose) as donor [17]. There are multiple ways the *C*-glycosylation can occur as shown in Figure 5. However, every glycosylation results in the formation of a β-glycosidic bond from a α-glycosidic donor unto a carbon atom within an aromatic ring, that is at an *ortho* or *para* position relative to a heteroatom-bearing carbon. Overall, the reaction mechanism includes the deprotonation of the heteroatom, a nucleophilic attack on the anomeric carbon, and, unlike in *O*-glycosylation, a subsequent tautomerization to restore the aromaticity [16].

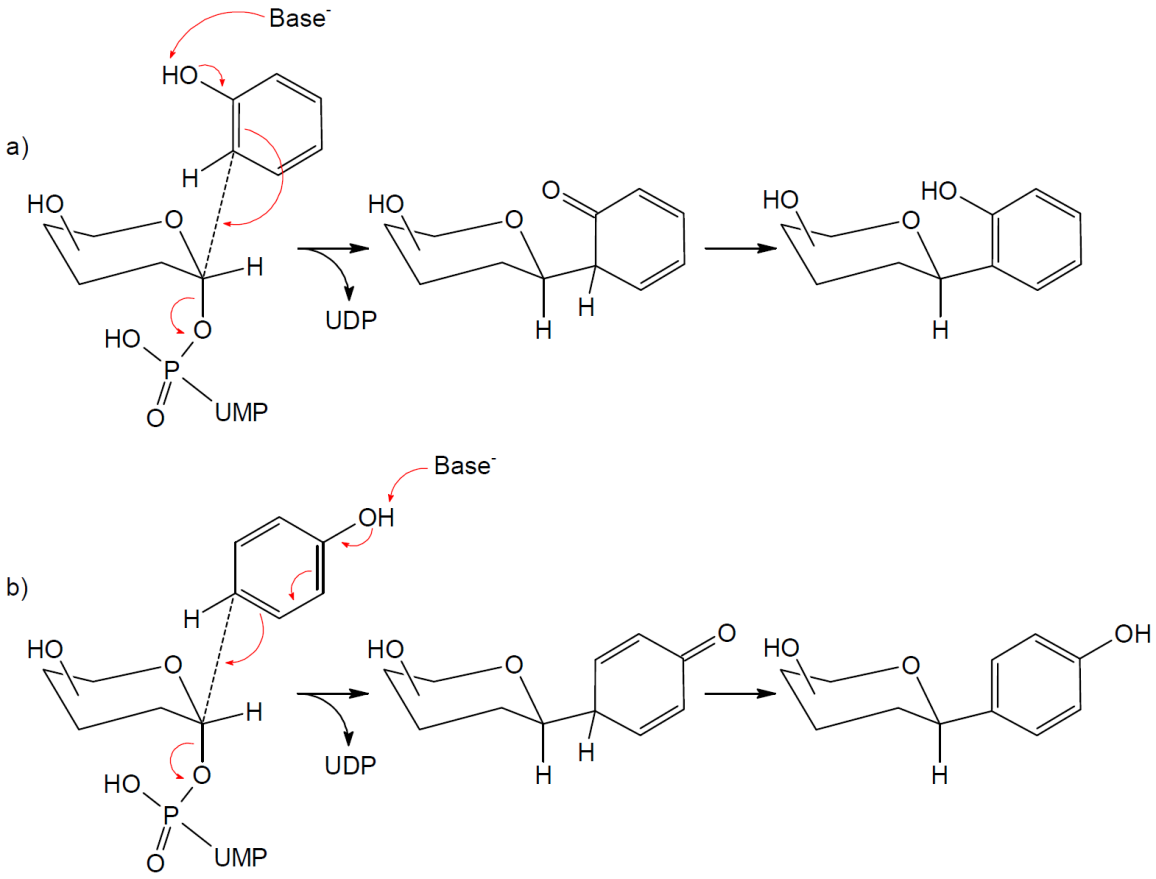

Figure 5. Possible mechanisms of the enzymatically catalysed *C*-glycosylation of flavonoids. The main steps involve deprotonation of a heteroatom that is either in a) *ortho* or b) *para* position, a nucleophilic attack on the anomeric carbon, and a subsequent tautomerisation [16].

1.2.2. Seco-iridoid monoterpenoids

The name iridoid is derived from *Iridomyrmex*, a genus of ants, from which iridomyrmecin, iridolactone, and iridodial were isolated [19]. Mostly present as glycosides, these compounds are almost exclusively of plant origin [19,20]. As chemical protection against herbivores and pathogens, iridoid glycosides generally have a bitter taste and show anti-feedant and growth inhibitory activity against insects [21]. Because iridoids are present in many medicinal plants, their bioactivity was intensively studies. They show a wide range of bioactivity. Some of their bioactive properties are cardiovascular, antitumor, and anti-inflammatory [22].

The iridoid base structure consists of a cyclopentane [c] pyran monoterpenoid containing nine to ten carbon atoms. Cleavage of the cyclopentane ring results in the formation of seco-iridoids (Figure 6). The parent compound of the seco-iridoids is secologanin, which is derived from loganin. Also known as the ultimate nitrogen-free precursor of alkaloids, secologanin is the most important key compound for alkaloid biosynthesis, which is not derived from an amino acid. Over a thousand alkaloids and other natural products are derived from secologanin [20]. The discovery of genes and enzymes involved in the secologanin pathway was of highest interest in the past decades. Some alkaloids that derive from secologanin have pharmacological importance, such as camptothecin, which is used to treat cancer [23]. Researchers were able to characterize every step of the seco-iridoid pathway (Figure 7) of *Catharanthus roseus* (L.) G.Don and reconstitute the entire pathway in the host *Nicotiana benthamiana* Domin, by heterologous gene expression [23].

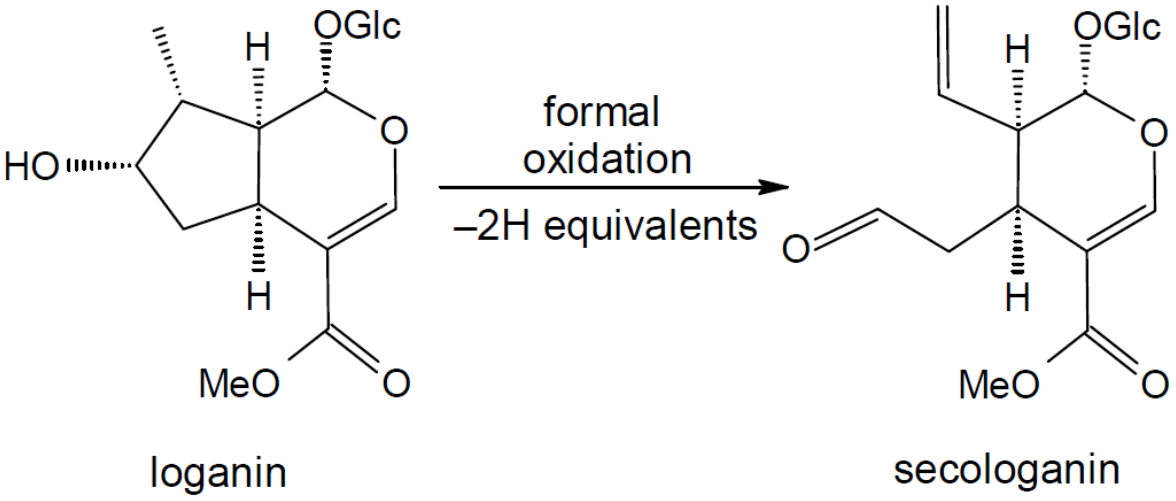

Figure 6. Structures of loganin and secologanin. Cleavage of the cyclopentane ring of loganin via formal oxidation results in the formation of secologanin [20].

The precursor of secologanin, loganin is derived from the monoterpenoid geranyl diphosphate. It was believed that the geranyl diphosphate of the secologanin pathway exclusively stemmed from mevalonate [20,24]. Research has shown that the major precursor is 1-deoxy-D-xylulose-5-phosphate [25,26]. Both ways result in the formation of isopentenyl diphosphate (IPP). The isomerization of IPP to dimethylallyl diphosphate (DMAPP) is catalyzed by IPP isomerase (IDI) [26]. Geranyl diphosphate synthase (GPPS) catalyzes the condensation of IPP and DMAPP to geranyl diphosphate [27]. After geraniol

is formed via geraniol synthase (GES), it is subsequently oxidized to the dialdehyde 8-oxogeranial [23]. Iridoid synthase (IS) catalyzes the reductive cyclization. Two possible mechanisms for this step are proposed. The first describes an inverse electron demand oxo-Diels-Alder reaction (Figure 7 a) and the second an intramolecular Michael addition (Figure 7 b) [28]. Both result in the two substances *cis-trans*-nepetalactol, and the open ring form *cis-trans*-iridodial, that are in equilibrium [28]. After oxidation of the methyl group, *O*-glycosylation, hydroxylation of the cyclopentane ring, and esterification, loganin is formed [23]. The cleavage of the cyclopentane ring is catalyzed by secologanin synthase (SLS), a cytochrome P450 monooxygenase [29].

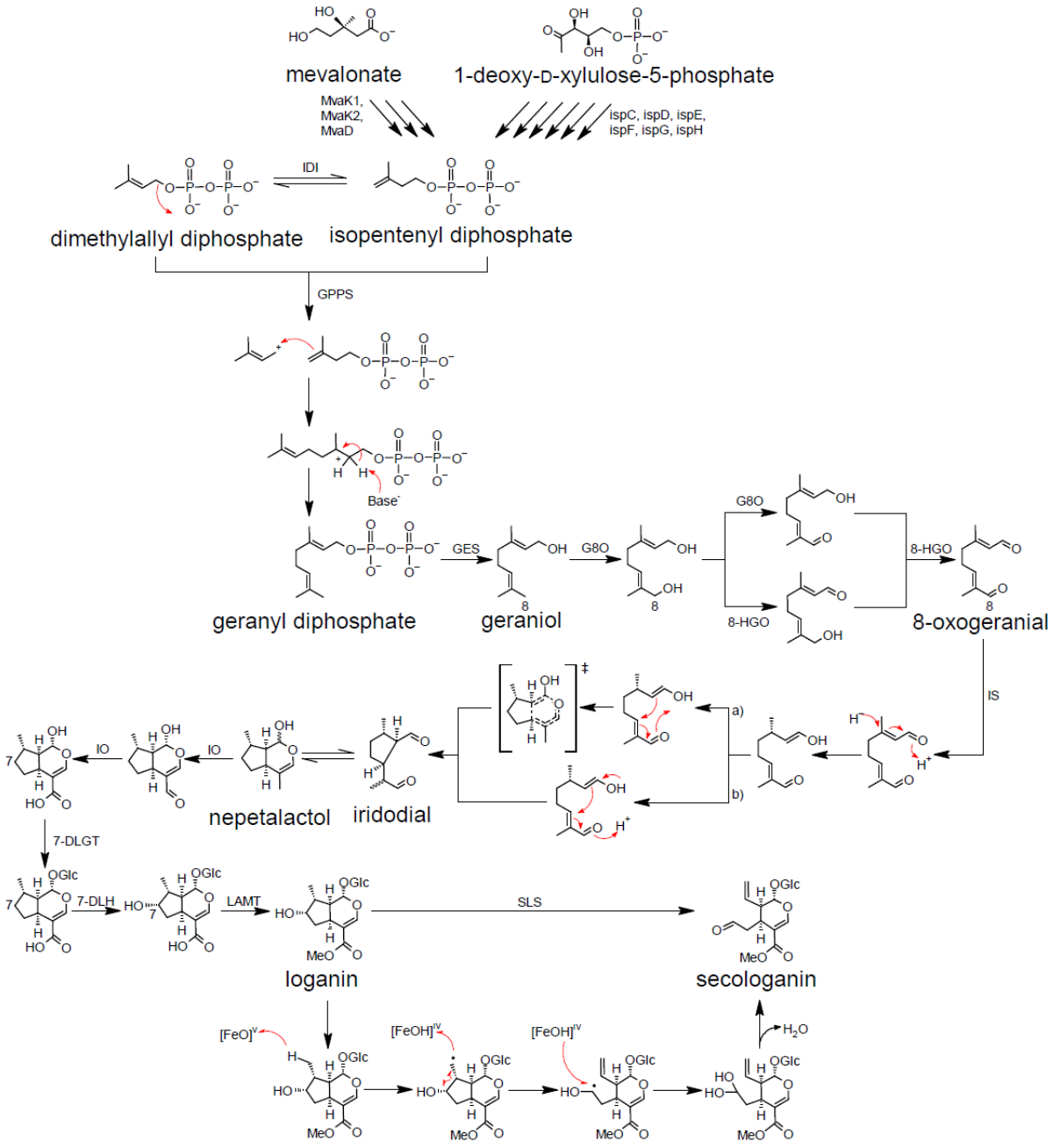

Figure 7. The secologanin pathway. mevalonate kinase (MvaK1), phosphomevalonate kinase (MvaK2), mevalonate diphosphate decarboxylase (MvaD), 2C-methyl-D-erythritol 4-phosphate synthase (ispC), 4-diphosphocytidyl 2C-methyl-D-erythritol synthase (ispD), 4-diphosphocytidyl 2C-methyl-D-erythritol kinase (ispE), 2C-methyl-D-erythritol 2,4-cyclodiphosphate synthase (ispF), 1-hydroxy-2-methyl-2-(*E*)-butenyl 4-diphosphate synthase (ispG), 1-hydroxy-2-methyl-2-(*E*)-butenyl 4-diphosphate reductase (ispH), IPP isomerase (IDI), geranyl diphosphate synthase (GPPS), geraniol synthase (GES), geraniol 8-oxidase (G8O), 8-hydroxygeraniol oxidoreductase (8-HGO), iridoid synthase (IS), iridoid oxidase (IO), 7-deoxyloganetic acid glucosyl transferase (7-DLGT), 7-deoxyloganic acid hydroxylase (7-DLH), loganic acid *O*-methyltransferase (LAMT), secologanin synthase (SLS) [23–29].

1.2.3. Tryptamine-derived alkaloids

The quinoline alkaloids isolated from *Palicourea glomerulata* [9] and monoterpene indole alkaloids (MIA) belong to the class of tryptophan-derived alkaloids. Monoterpene indole alkaloids i.e., tryptamine-derived alkaloids are among the largest subclasses of alkaloids [30]. Furthermore, they are the main chemical marker for Rubiaceae [2]. All of the terpene indole alkaloids derive from the previously mentioned secologanin and tryptamine [31]. The key compound of MIAs, strictosidine, is formed by the condensation tryptamine and secologanin via Pictet-Spengler reaction (Figure 8). This reaction is catalyzed by the "Pictet-Spenglerase" strictosidine synthase (STR). Studies on *Rauvolfia serpentina* (L.) Benth. ex KurzIt show that STR is enantioselective and results in 3-α-(*S*)-stricosidine [32]. Under acidic conditions, a Schiff-base is formed between the aldehyde secologanin and the amine compound. After electrophilic substitution at the C2 position, deprotonation results in the formation of an six membered ring [32].

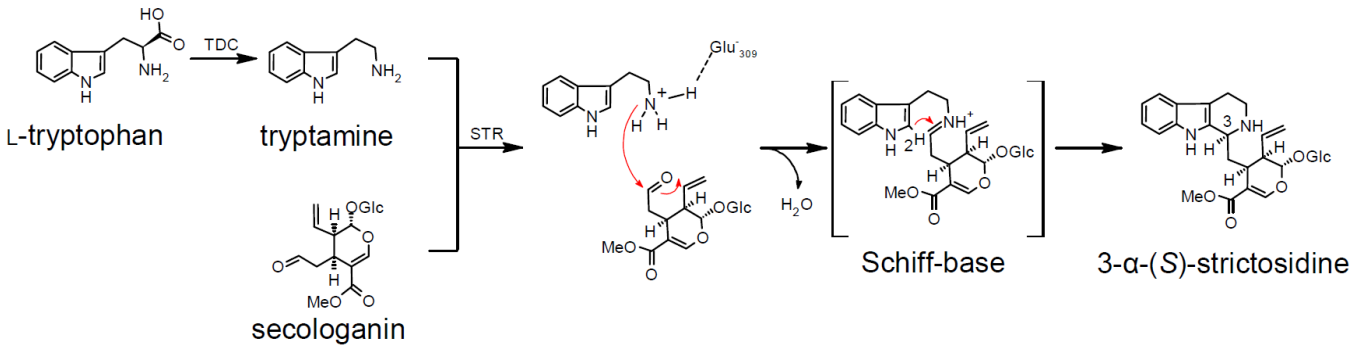

Figure 8. The strictosidine pathway. tryptophan decarboxylase (TDC), strictosidine synthase (STR) [23,32].

Strictosidine is a precursor to many MIAs, some of them include the antimalarial agent quinine [6,23], or camptothecin, which is used to treat cancer (Figure 9 a). Other "Pictet-Spenglerases" such as deacetylipecoside synthase (DIS) and deacetylisoipecoside synthase (DIIS) catalyze the reaction of dopamine with secologanin to form dopamine-iridoids (Figure 9 b) [32]. The analysis on the accumulation of alkaloids type dopamine-iridoid and alkaloids type tryptamine-iridoid contributed to the taxonomic rearrangement of some species of *Psychotria* and *Palicourea* [5].

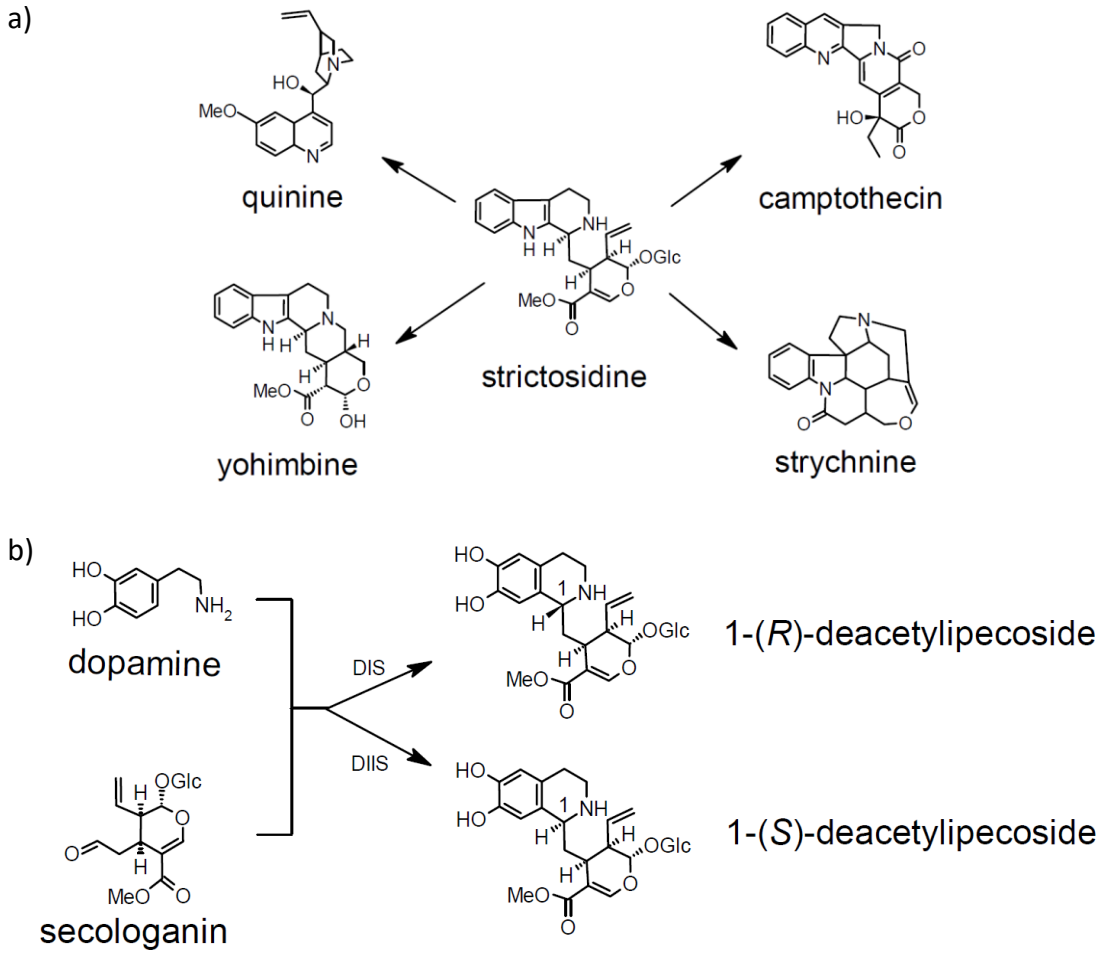

Figure 9. a) Examples of strictosidine as a key compound in the biosynthesis of MIAs. b) Other examples of Pictet-Spenglerases. deacetylipecoside synthase (DIS), deacetylisoiceposide synthase (DIIS) [32].

Even though strictosidine is known as the universal MIA precursor [23], and sometimes even described to be the common biosynthetic precursor of all MIAs [32], isolated compounds from *Palicourea luxurians* (Rusby) Borhidi suggest different reaction mechanisms between tryptamine and secologanin leading to MIAs that do not derive from strictosidine (Figure 10) [30]. Pathway a) describes two possible ways resulting in the MIA

javaniside, and pathway b) describes the formation of alstrostine A and isoalstrostine A. In a_1) the iminium ion is formed like in the Pictet-Spengler reaction, but unlike before resulting in a cyclopentane ring, by deprotonation of the indole nitrogen. Subsequent oxidation results in an amide group. In a_2) the indole moiety is first oxidized to an amide, and subsequently cyclized. After lactam ring formation javaniside is formed. In the pathway b) tryptamine is cyclized by oxidation, forming an intermediate with two secondary amine functions. After the formation of the enamine with two secologanin moieties, protonation can occur in two different ways. Both, b_1) and b_2) result in the formation of a six membered ring. After deprotonation alstrostine A and isoalstrostine A are formed [30].

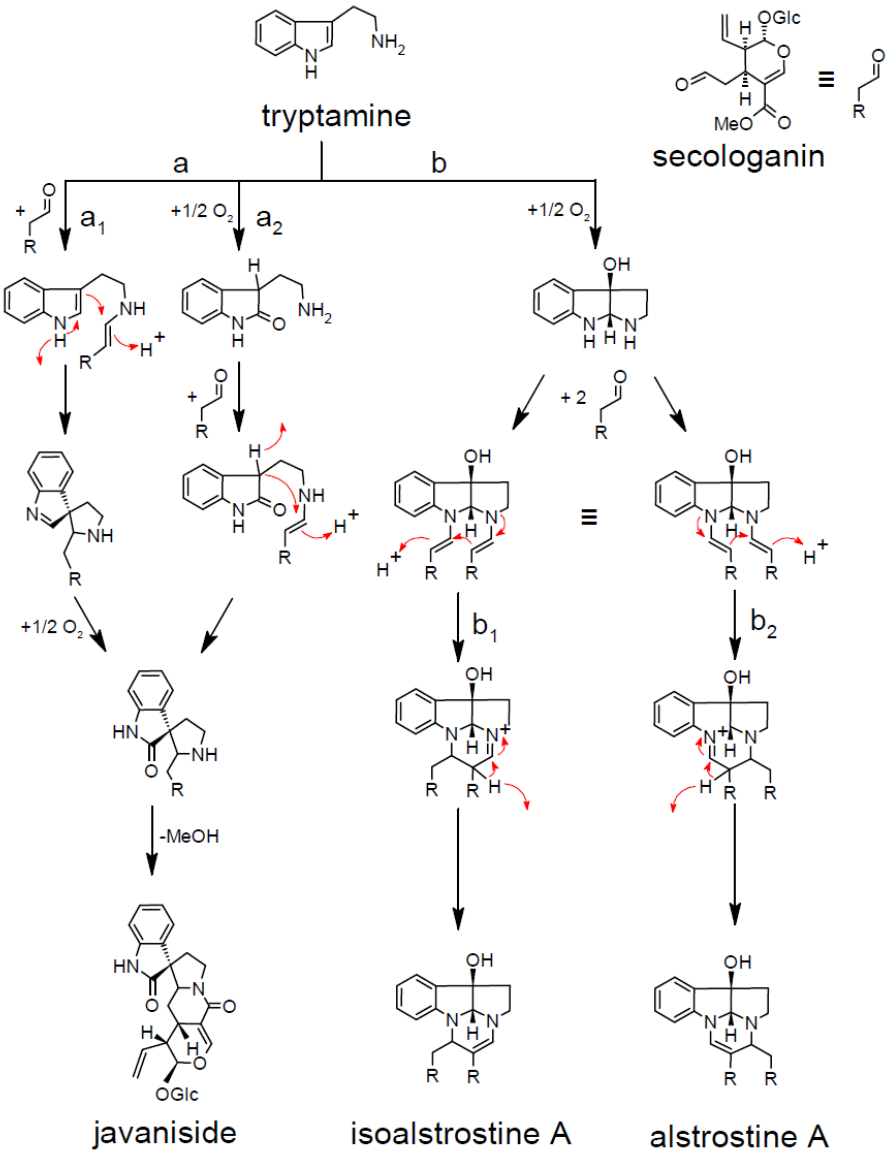

Figure 10. Possible pathways resulting in the formation of javaniside, alstrostine A and isoalstrostine A. Three MIAs that are possibly not derived from strictosidine [30].

Additional indole alkaloids include cyclotryptamines such as the tryptamine dimers glumerulatine A, B and C, and tryptamine multimers (Figure 11 a). The core structure of cyclotryptamines is the cyclic pyrrolidine [2,3-*b*]indoline (Figure 11 b). The biosynthetic pathway (Figure 11 c) of the tryptamine dimer 3a,3a'-bispyrrolidine [2,3-*b*]indoline starts with the one-electron-oxidation of tryptamine. Then, deprotonation results in the formation of two different radicals. The dimerization occurs either on position C3a or C7 resulting in the typical link pattern of cyclotryptamines [33].

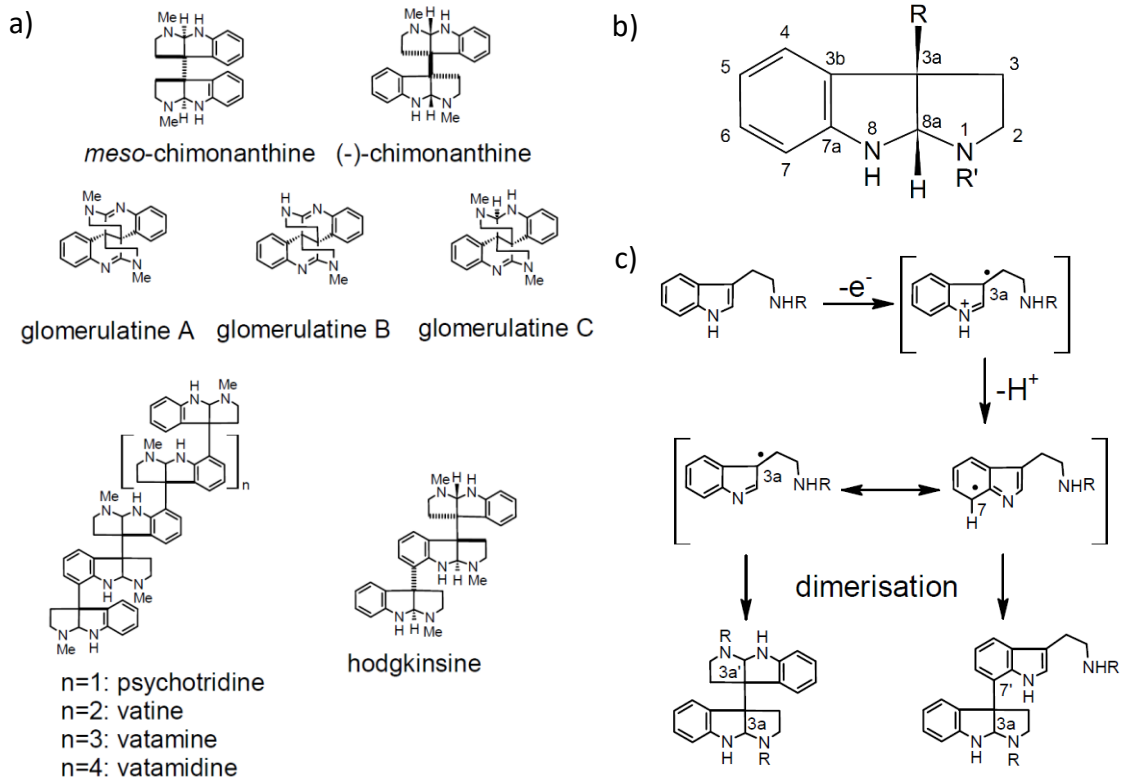

Figure 11. a) Examples of cyclotryptamine dimers and oligomers. b) The basic structure of cyclotryptamines. c) Biosynthetic pathway of 3a,3a'-bispyrrolidine [2,3-b]indoline [9,33].

After cleavage of the two pyrrolidine rings, the tetraaminoaldehyde can react with four different amino functions to form five different isomers (Figure 12 a). The tryptamine moieties are colored differently to visualize the different linking combinations. The isomerization of (–)-chimonanthine to (+)-calycanthine has been observed under acidic conditions (Figure 12 b) [33,34]. Calycanthine is the thermodynamically most stable isomer, and contains 6 six-membered rings [33,34]. Because of the spontaneous conversion of chimonanthine to calycanthine, it has been questioned whether the isomeric form,

calycanthine, is a real natural occurring compound or an artefact of acid-base extraction [33,35].

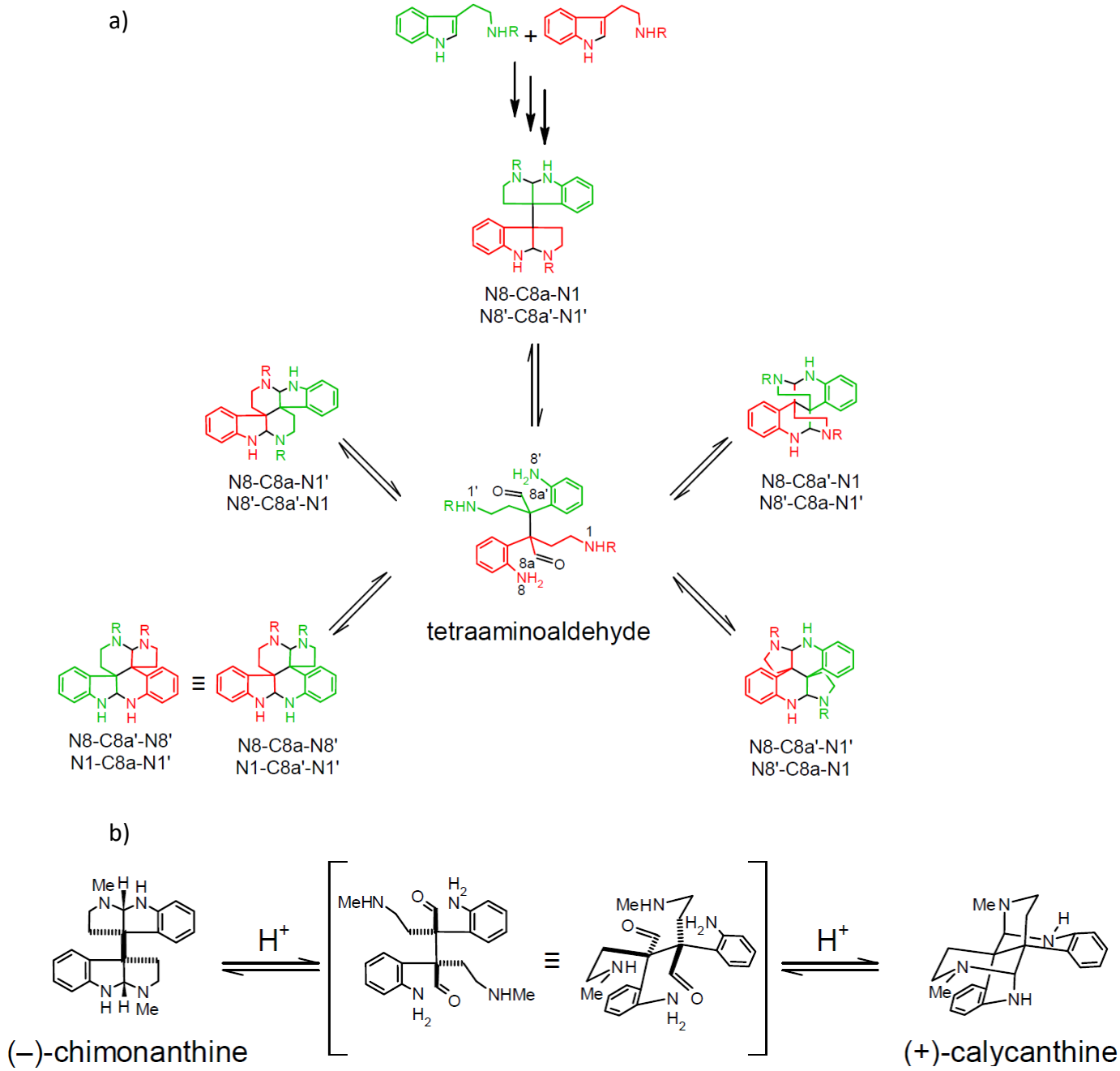

Figure 12. a) The formation of five different isomers via dehydration of tetraaminoaldehyde. b) The spontaneous formation of (–)-chimonanthine to (+)-calycanthine under acidic conditions [33].

1.2.4. 6-Amino-6-deoxy-glycoglycerolipids

Additional compounds isolated from *P. glomerulata* were identified to be glycoglycerolipids. The general structure of these compounds consists of a carbohydrate that is either alpha or beta connected to the *sn*-3 position of a glycerol, which is diacylated

on the other two hydroxyl groups. The fatty acids can differ in their chain length and degree of unsaturation [36]. These compounds are widespread in nature, where they can be found in the thylakoid membranes of chloroplasts and cyanobacteria [36]. Even though glycoglycerolipids and their 2-deoxy-2-amino (or 2-acetamido) sugar containing counterparts are commonly found in algae, the 6-deoxy-amino glycosides are extremely rare. This is a very small class of compounds with hardly any mentions in literature [37]. A few examples of 6-deoxy-amino glycoglycerolipids and their origins are shown in Figure 13 [37–39].

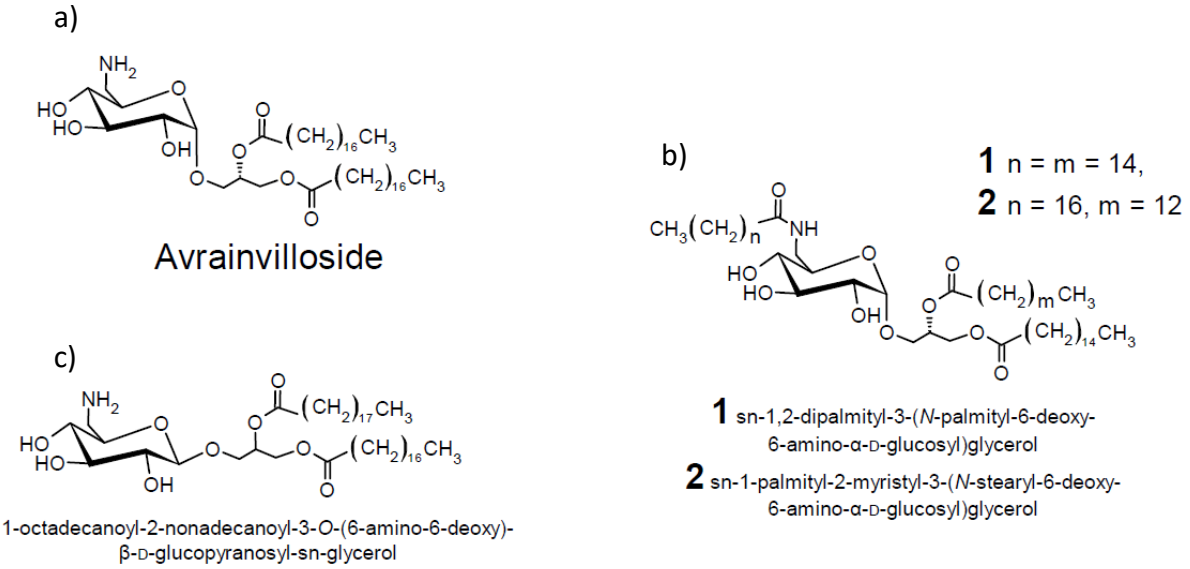

Figure 13. Examples of 6-amino-6-deoxy-glycoglycerolipids found in plants and algae. a) Compound isolated from *Avrainvillea nigricans* (Andersen et Taglialatela-Scafati, 2005). b) Compound isolated from an unidentified alga (Zhou et al., 2005). c) Compound isolated from *Livistona chinensis* (Jacq.) R.Br. ex Mart. (Zeng et al., 2012) [37–39].

Interestingly, 6-amino-6-deoxy-glycoglycerolipids show anti-bacterial, anti-tumor, anti-stress, free-radical scavenging, and human Myt1 kinase inhibiting activities [36]. Myt1 kinase is important for the regulation of mitosis, inhibition of this enzyme can kill rapidly proliferating cells, such as tumor cells [38]. The pharmacological activities can vary depending on the fatty acid chains and the group that is attached to the nitrogen [40]. Recent studies on the anti-tumor activity show that, even though 6-amino-6-deoxy-glycoglycerolipids were able to inhibit the activation of Epstein-Barr virus-early antigens (EBV-EA) in Raji cells and tumor promotion in mice, their activity was much less when compared to the 6-*O*-acylated glycoglycerolipids, where the only difference is the replacement of the nitrogen with an oxygen [36].

1.3. Aim of this study

The aims of this present thesis are to further understand and add information to the chemical profile of the plant *Palicourea glomerulata*, as well as to try to recreate the isolation of cyclotryptamines. Furthermore, the findings of this thesis demonstrate the capability of plants to produce a wide range of chemical substances, and the advantages of mild conditions when extracting natural compounds. Although leaf, stem bark and root extracts were prepared, the compounds isolated in this study solely stem from the leaf extract.

The first part of the thesis focused thoroughly on the isolation and structure elucidation of constituents of the leaf extract. The plant material was collected from the neotropic region, Costa Rica. The main working steps included the methanolic extraction of the plant material, the separation of the components in the crude extract via liquid-liquid extraction, the chromatographic separation of the solvent extracts via size exclusion chromatography (SEC), preparative thin layer chromatography (prep. TLC), normal phase (NP), and reverse phase (RP) column chromatography (CC). Additionally, TLC and high performance liquid chromatography (HPLC) measurements were performed, to evaluate the separation results, using staining agents and a UV-Vis detector. On isolates with sufficient purity, one-dimensional and two-dimensional Nuclear Magnetic Resonance (NMR) experiments, and Mass Spectrometry (MS) measurements were performed. To further describe the physical properties of the isolated compounds, infrared (IR) spectroscopic, polarimetric and photometric measurements were performed. The second step of the thesis was dedicated to biological and chemical assays using the crude leaf, stem bark and root extracts. The biological tests were performed on the herbivore generalist *Spodoptera littoralis* Boisduval. (Noctuidae) and included the non-choice feeding experiment and the leaf disc choice test. The measurement of the antioxidative activity of the extracts was performed using the 2,2-diphenyl-1-picrylhydrazyl (DPPH) method.

The findings in this thesis emphasize on the vast variety of secondary plant metabolites, and that modern extraction methods could yield new results. Additionally, because plant constituents do not occur isolated in nature, antagonistic or synergistic interactions between the substances of this chemical cocktail are of much interest.

2. Materials and methods

Product and manufacturer information for all devices (Table 1), chemicals, column material and eluents (Table 2), websites and software (Table 3) used for this thesis are listed below.

Table 1. Devices.

Product	Manufacturer	
Agilent 1100 HPLC System	Agilent Technologies	USA
BUCHI UV-Vis Detector C-640	BUCHI Corporation	CH
Bruker Avance III 400, 600 and 700 MHz	Bruker	GER
Chemistry vacuum sys. MZ 2C NT +AK+EK	Vacuubrand	GER
Chirascan plus	Applied Photophysics	UK
FT-IR spectrometer ALPHA	Bruker	GER
Huber Minichiller 280 OLÉ	Huber	GER
Infinite M Nano plate reader	Tecan	CH
Perkin Elmer polarimeter 341	Perkin Elmer	USA
Precision balance Entris®	Sartorius	GER
Rotary evaporator	Heidolph Instruments	GER
Specord 205 colorimeter	Analitik jena	GER
TRIVAC Vacuum pump	Leybold	GER
Ultrasonic bath	VWR International	USA

Table 2. Chemicals, column material and eluents.

Product	Manufacturer	
96-well plates	VWR International	USA
Acetone	Sigma-Aldrich	USA
Agar-Agar	Carl Roth	GER
Ammonia solution	Carl Roth	GER
Ammonium acetate, ≥ 97%	Carl Roth	GER
Anisaldehyde	Carl Roth GmbH	GER
L-Ascorbic acid, ≥99 %	Sigma-Aldrich	USA
1-Butanol	Merck	GER

Caffeine	Sigma-Aldrich	USA
Chloramphenicol	Sigma-Aldrich	USA
Chloroform	Merck	GER
Diaion® HP-20	Supelco® Analytical	USA
Diethyl ether	Merck	GER
Dimethyl sulfoxide	Merck	GER
Dragendorff's reagent	Sigma-Aldrich	USA
Ethyl acetate	Merck	GER
n-Heptane	VWR International	USA
Hypersil BDS-C18 column	Agilent	USA
Methanol ≥99.8 % for HPLC	VWR International	USA
Methanol	Merck	GER
CD_3OD	Eurisotop	GER
(–)-Nicotine	Sigma-Aldrich	USA
D-(–)-Salicin	Sigma-Aldrich	USA
Silica gel 60, 0.2–0.5 mm	Carl Roth GmbH	GER
Silica gel 60, 0.04–0.063 mm	Carl Roth GmbH	GER
Silica gel C8-Reversed phase	Sigma-Aldrich	USA
Silica gel under 0.08 mm	Merck	GER
Sephadex® LH-20	Sigma-Aldrich	USA
TLC Plates: Cellulose	VWR International	USA
TLC Plates: Kieselgur	VWR International	USA
TLC Plates: Silica	VWR International	USA
(±)-α-Tocopherol, ≥96 %	Sigma-Aldrich	USA
Water for HPLC	VWR International	USA

Table 3. Websites and software.

Product	Use
Agilent Chemstation	Evaluation of the HPLC chromatograms
ImageJ	Image Analysis
Opus 7.2	IR measurement software
TopSpin 4.0.8	NMR spectrum analysis
https://www.chemcalc.org/mf-finder	MS spectrum interpretation
http://www.ic50.tk	IC_{50} calculation
https://www.nmrdb.org/	NMR spectrum prediction
https://www.reaxys.com	Research of chemical structures

2.1. Plant material

Palicourea glomerulata samples 1481 and 1481-B were collected in the Heredia province in Costa Rica by co-workers of the Department of Botany and Biodiversity Research Vienna. Root, stem bark and leaf material were separated, air-dried under exclusion of light and shredded to small pieces with a mixer.

2.2. Experimental

The isolation of natural components is a multistage process that includes preparation of the plant material, solid-liquid extraction, liquid-liquid extraction, preparative thin layer chromatography (prep. TLC), atmospheric and medium pressure column chromatography (AP/MPLC). Additionally, each isolation step was monitored with TLC and HPLC measurements. The structures of isolated components were elucidated with spectral data obtained from 1D and 2D NMR spectroscopy, as well as ESI-MS spectrometry. Then, IR spectroscopic, polarimetric and photometric measurements were performed for each isolated compound. Lastly, several biological and chemical assays were conducted, which included a non-choice feeding experiment, an antioxidant capacity assay, and a leaf disc choice test.

2.2.1. Extraction

First, the dry weights of the *P. glomerulata* 1481 and 1481-B leaf, stem bark and root samples were determined as shown in the table below (Table 4). Afterwards, each sample was transferred in a glass vessel and covered with redistilled methanol. Then, the vessel was put in an ultrasonic bath at room temperature for a duration of 20 min, for further breaking down of matrix elements and higher extraction yields. Subsequently, the samples were put in a dark closet for 48 h. The samples were treated with redistilled methanol for a total of three times. After each extraction step, the samples were filtered into an Erlenmeyer flask. After the first filtration, 10 mg per mL solutions were prepared for HPLC analysis to assess differences between the samples 1481 and 1481-B. Because of the similarities in the HPLC chromatograms of the extracts of 1481 and 1481-B, the samples were pooled for total extraction yields of 4.1 g, 1.5 g and 1.1 g from leaf, stem bark and root material respectively (Table 4). The solvent was removed in a rotary evaporator set at 40 °C and 200 mbar to prevent destruction of components.

Next, to separate the extracts components due to their polarity, a liquid-liquid extraction was performed. First, by transferring the sample into a round bottom flask and adding 100 mL of pure H_2O and 100 mL solvent. After the sample was completely dissolved, the dispersion was transferred into a separating funnel. After firmly shaking and phase separation, the organic phase was poured into a separate round bottom flask and connected to a rotary evaporator at 40 °C and 200 mbar. Recollected solvent was used for further extraction. The solvents used were *n*-heptane with 3 % ethyl acetate, chloroform, and ethyl acetate. As TLC plates performed on the leaf extract indicated that most of the content of interest was present in the H_2O phase, an additional extraction step with 1-butanol was performed. Each extraction step was repeated two to four times. Then, the samples were connected to a rotary evaporator at 40 °C and 200 mbar. For faster evaporation of water and 1-butanol, a small amount of 1-butanol was added to the water phase and vice versa, as the azeotrope has a lower boiling point. Afterwards, the samples were evacuated for 20 min and their dry weight was determined (Table 5). The *n*-heptane with 3 % ethyl acetate phases had a green colouration, because of the higher chlorophyl content, while the ethyl acetate, 1-butanol and water phases were orange in colour.

HPLC measurements of the crude extract and each solvent extract were performed with the UV detector set to 230 nm. TLC with silica plates performed on the solvent extracts were stained with the Dragendorff's reagent, to give indication of the present of alkaloids. The Dragendorff's staining agent shows orange coloration when reacting with alkaloids, which was the compound class of primary interest. The running solvents used were $CHCl_3$:MeOH ratio 90:10 and 80:20, and EtOAc:*n*-heptane ratio 60:40. Most of the alkaloid content was present in the polar phases, EtOAc, 1-butanol and H_2O.

Table 4. *P. glomerulata*: material weight.

Palicourea glomerulata dry weight [g]				
Sample	1481	1481-B	Total	Extract
Leaf	63.7	22.8	**86.5**	**4.1**
Stem bark	26.5	23.2	**49.7**	**1.5**
Root	20.5	1.9	**22.4**	**1.1**

Table 5. *P. glomerulata*: solvent extract weight.

Solvent extracts dry weight [g]					
Sample	*n*-Hep +3 % EtOAc	$CHCl_3$	EtOAc	1-ButOH	H_2O
Leaf (4.1 g)	0.3	0.4	0.2	2.3	0.5
Stem bark (1.5 g)	0.4	<0.1	<0.1	-	0.9

2.2.2. Chromatographic separation

Multiple different separation methods were combined to separate the components of interest from the complex plant matrices. The methods of choice include atmospheric pressure column chromatography (APCC), medium pressure chromatography (MPLC) and preparative thin layer chromatography (PTLC). The APCC and MPLC allowed for coupling with an UV-detector, where the UV-absorbance of the components of interest can be monitored.

Overall, column chromatography allows for easy tweaking of separation conditions, by using different stationary phases, eluents, and a gradient of multiple eluents. Depending on the stationary phase, the components can be separated by either their polarity or their hydrodynamic radius, which is dependent of the molecular size. For the separation due to polarity, the polarities of the stationary and mobile phase need to be opposed. In normal phase chromatography the stationary phase consists of a polar material such as Silica gel, whereas in reverse phase chromatography, usually an alkyl chain is attached to the silicon to make it non-polar. Size-exclusion chromatography (SEC), on the other hand, separates components by their hydrodynamic radius. This can be achieved by materials such as Sephadex LH-20, a beaded, cross-linked hydroxypropylated dextran [41]. The travel distance in highly porous materials differs depending on the molecular mass. Larger molecules do not fit through smaller passages of the Sephadex LH-20, and therefore have a shorter retention time.

In addition to the same advantages of a regular APCC, the MPLC allows for the separation of much larger sample sizes. The sample is injected into a circular system, where it runs through the same column once each cycle. This way the size of the column is artificially lengthened, depending on how long the system runs and therefore achieve better separation results. A pump is constantly applying pressure at 2–5 bar. After 2–3 h the cycle is stopped, and the sample is led towards an outlet where the UV-absorbance of the sample is measured before collecting.

Occasionally, when APCC and MPLC did not suffice, prep. TLC was performed as a final purification step for small amounts of extract. For this, the sample is applied on a SiO_2 coated glass plate, which allowed for removing bands by scratching off the SiO_2 from the glass. Afterwards, the SiO_2 crumbs are covered in MeOH and put in an ultrasound bath for 10–15 s, to resolve the adsorbate. Then, the colloidal dispersion is vacuum filtered using a ceramic frit G5.

For a better overview of each separation step, Figure 14 shows the isolation scheme and Table 6 lists the separation conditions and eluent usage. The name of each performed column consists of a letter, S for sephadex LH20, K for kieselgel (engl. silica gel) or M for MPLC and a number for ordering.

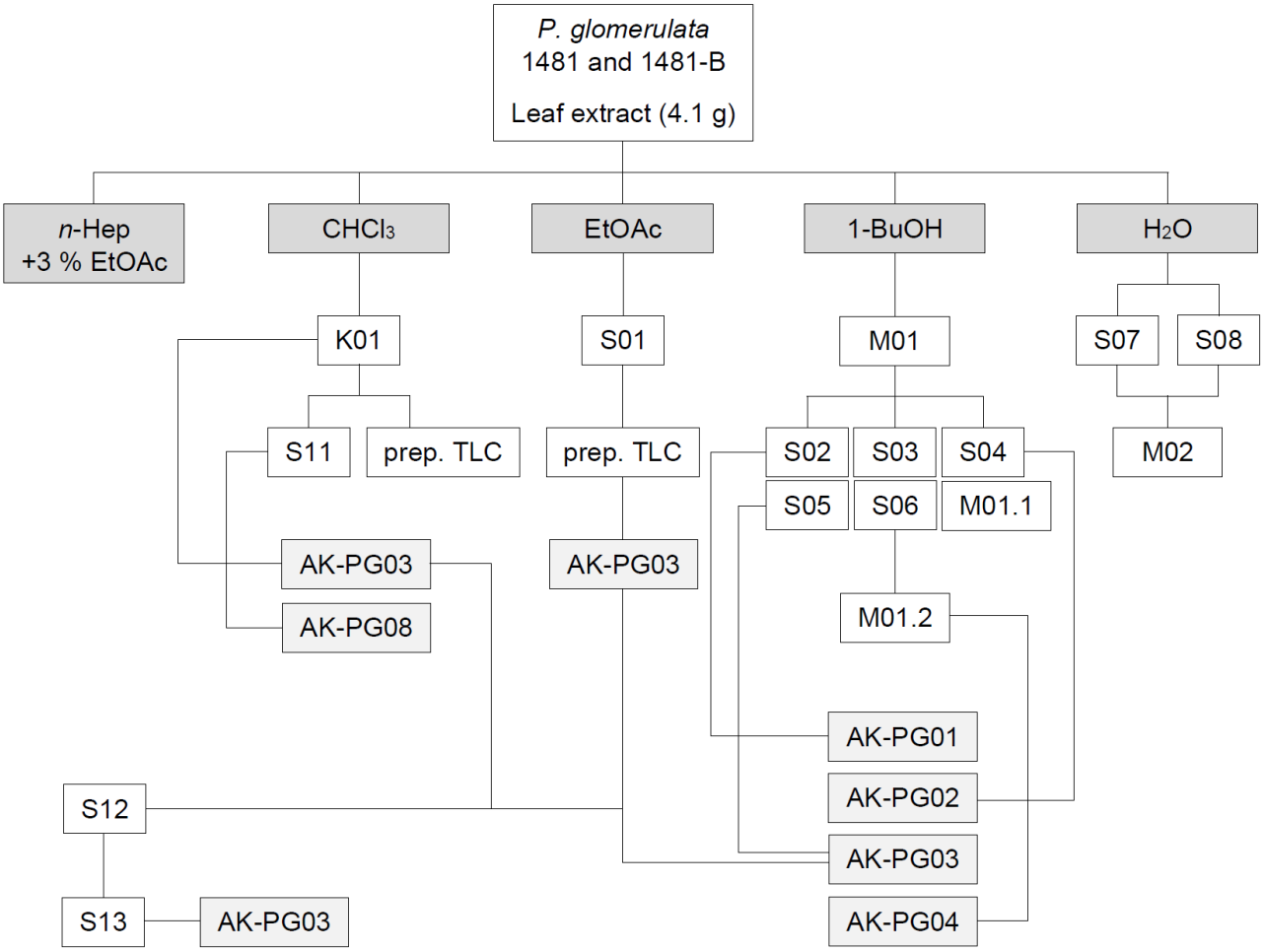

Figure 14. Isolation scheme of the *P. glomerulata* leaf extract. Not all separation attempts led to an isolation of a compound with sufficient purity. Additionally, separation attempts of the aquatic phase resulted in fractions that appeared pure in the HPLC and MS measurements. However, the yield was not measurable on the precision balance. As after the separation of the carbohydrate residues, not much substance was left in the aquatic phase. The materials and solvent amounts used for each separation step are shown in Table 6.

Table 6. List of material and solvent usage for chromatography separation.

Column	Solvent used (estimated consumption [mL])	Column	Solvent used (estimated consumption [mL])
S01	pure MeOH (N/A)	S07	pure MeOH (190)
S02	pure MeOH (N/A)	S08	pure MeOH (150)
S03	pure MeOH (N/A)	S11	pure MeOH (112)
S04	pure MeOH (115)	S12	pure MeOH (125)
S05	pure MeOH (265)	S13	pure MeOH (181)
S06	pure MeOH (375)		

Column	Solvent gradient used (estimated consumption [mL])			
M01	redist. MeOH (1334):$CHCl_3$ (2316):			
(Silica gel under 0.08 mm)	V [mL]	Gradient	V [mL]	Gradient
	200	0:100	160	50:50
	1200	10:90	140	60:40
	400	20:80	450	80:20
	400	30:70	350	100:0
	350	40:60		
M01.1	pure MeOH (880):pure H_2O (720):			
(Diaion® HP-20)	V [mL]	Gradient	V [mL]	Gradient
	300	5:95	100	60:40
	100	20:80	100	70:30
	100	25:75	100	80:20
	100	30:70	100	90:10
	100	40:60	400	100:0
	100	50:50		
M01.2	pure MeOH (435):pure H_2O (365):			
(RP-8)	V [mL]	Gradient	V [mL]	Gradient
	100	5:95	50	60:40
	100	10:90	50	70:30
	50	20:80	50	80:20
	50	30:70	50	90:10
	50	40:60	200	100:0
	50	50:50		

M02	pure MeOH (290):pure H_2O (1110):			
(RP-18)	V [mL]	Gradient	V [mL]	Gradient
	500	2:98	100	50:50
	400	5:95	100	70:30
	100	15:85	100	100:0
	100	25:75		
K01	*n*-heptane(460):EtOAc(690):MeOH(250):			
(Silica gel 60, 0.04-0.063 mm)	V [mL]	Gradient	V [mL]	Gradient
	100	95:5:0	100	0:100:0
	100	85:15:0	100	0:90:10
	100	75:25:0	100	0:80:20
	100	70:30:0	100	0:70:30
	100	60:40:0	100	0:60:40
	100	50:50:0	100	0:50:50
	100	25:75:0	100	0:0:100

2.2.3. Biological and chemical assays

In addition to the isolation and structure elucidation, multiple biological and chemical assays have been performed to assess possible effects of the plant constituents of *P. glomerulata* on the antioxidative activity, on growth of neonatal herbivores and on the gustatory system. The methods used are as followed: The antioxidant capacity assay, the non-choice feeding experiment and the leaf disc choice test. The substances were tested against *Spodoptera littoralis*, a polyphagous species which is frequently used in toxicity tests as a model organism [42].

2.2.3.1. Antioxidant activity assay

The radical scavenging activity of root, stem bark and leaf extract of *P. glomerulata* was measured. In addition, the known antioxidants L-ascorbic acid and α-tocopherol were used as controls. To photometrically measure the antioxidant activity, the DPPH method was used [43]. The DPPH solution was prepared by solving 4 mg of DPPH in 50 mL of MeOH.

First, multiple concentration ranges were evaluated until the inflection point of the measured sigmoid dose-effect curve was in the middle of the concentration range. Then, the EC50 was evaluated using the http://www.ic50.tk website. The concentration ranges were 0.25 mg/mL–0.12 µg/mL for L-ascorbic acid, 0.5 mg/mL–0.24 µg/mL for α-tocopherol, 8.35 mg/mL–8.15 µg/mL for the root extract, 10.05 mg/mL–9.81 µg/mL for the stem bark extract and 3.1 mg/mL–1.51 µg/mL for the leaf extract. Each concentration was measured as a triplicate. The samples were prepared by adding 50 mL MeOH in the columns 2–11 and adding 100 µL of the sample solutions in the first column. Then, 50 µL of from the first column were transferred to column two for a 1:1 dilution. This step was repeated until the last column, where the remaining 50 µL were discarded. The samples were measured at 517 nm (DPPH radical absorbance peak) and 700 nm as a reference before the addition of DPPH (blank) and after an incubation period of 30 min in the dark. Each well contained 50 µL of the DPPH solution. The differences of these two measurements were used for calculating the EC50 values.

2.2.3.2. Non-choice feeding experiment

The non-choice feeding experiment was performed to evaluate whether extracts of *P. glomerulata* inhibit growth of the herbivore generalist *S. littoralis*. The extracts were tested against neonatal larvae of *S. littoralis*. Unspiked samples were used as negative control and samples containing (–)-nicotine served as positive control. The food powder consisted of 150 g white beans, 3 g nipagin, 30 g yeast, 3 g ascorbic acid and 460 mL of tap water. There was a total of 40 samples: 7 negative controls (NC), 6 positive controls and 9 per tested extract. Concentrations were tested as triplicates and the concentrations used were 500 and 1500 ppm (–)-nicotine for the positive control and 500, 1000 and 2000 ppm for each extract solutions. The preparation of the food pellets is described as followed. First, 184 mg of the food powder was weighed per sample. Then, specific volumes of (–)-nicotine and plant extract were added, covered with 2-3 mL of acetone/water and left over the night for the solvent to evaporate. Afterwards, 363 µL of aqueous solution containing 3 % v/v vitamin solution and 0.05 % m/v chloramphenicol was added to each sample. Next, agar-agar solution was prepared by solving 1.1 g of agar-agar in 30 mL of H_2O at 50 °C. Lastly, 0.6 g of this solution was added to each sample while gently stirring. After the food pellet cooled down, it could be placed in a petri dish. Then, ten neonatal larvae were added

to each Petri dish. The samples were incubated at 26 °C and 90 %humidity over a period of 4 d.

2.2.3.3. Leaf disc choice test

The leaf disc choice test was performed to evaluate gustatory effects of *P. glomerulata* extracts on *S. littoralis*. Caffeine and D-(–)-salicin were used as controls, as these substances are known to taste bitter to the test subject [44]. Each sample contained one 10-day-old larvae, which was given a choice of two to three leaf discs to eat. Leaf discs had a diameter of 13 mm and have been treated with either 10 µL solvent (H_2O:acetone 80:20), 10 µL of 10 mg/mL plant extract, 10 µL of 10 mg/mL caffeine or 10 µL of 10 mg/mL D-(–)-salicin. Leaf discs stem from the outer part of the leaves of commercially available salad (*Lactuca sativa* L.). Leaf discs treated with different testing solutions have been tested against each other. Each combination was done in triplicates. First, root, stem bark and leaf extract have been tested against the solvent. Next petri dishes contained all the extracts and the solvent. Lastly, each extract was tested against each positive control. Then, the *S. littoralis* was gently added to the Petri dish and covered. The test was stopped after an exposition period of 105 min. If there were dishes, where no leaf has shown bite marks, the test was not stopped until the other day. The eaten area has been evaluated with ImageJ software.

2.2.4. Measurements

2.2.4.1. High performance liquid chromatography

HPLC measurements are very useful for the isolation of natural components, as it is very sensitive and can measure a large number of samples automatically. Chromatograms give information of the variety of components in the sample, their polarity, and their purity. Additionally, when the HPLC conditions are identical, chromatograms of different measurements can be compared. This is especially useful, when evaluating the chromatography separation of an extract, by comparing its HPLC chromatogram to those of each fraction. Depending on the amount, the samples were diluted and measured in either HPLC vials or 96-well plates, where they were covered with 10 µL of dimethyl sulfoxide (DMSO).

As for the measurement conditions, the stationary phase was a Hypersil BDS-C18 (250 x 4.6 mm, 5 µm particle size) column and as the eluent a gradient of 20 % to 100 % MeOH in 10 mM $NH_4^+CH_3COO^-$ was used. A UV diode array detected the absorbance of

wavelengths at 230 nm and 360 nm as reference. Lastly, the flow rate was set to 1.0 mL/min and the runtime of one measurement was 15–22 min.

2.2.4.2. Nuclear magnetic resonance spectroscopy

NMR spectroscopy is the non-plus-ultra method for elucidating molecular structures in organic chemistry. For this, compounds need to be of high purity and enough amounts. Sample preparation steps included, removing the solvent, evacuating, resolving the sample in 0.7 mL of deuterated methanol (CD_3OD) and transferring the solution into a 5 mm NMR tube. 1D ^{1}H spectroscopy was performed on a 400 MHz device, whereas ^{13}C and 2D measurements were done on 600 or 700 MHz devices. The much faster ^{1}H measurements were used to screen samples whether they were pure enough for further investigations.

To gain most information about the sample, following pulse experiments were needed to be performed: ^{1}H spectroscopy, distortionless enhancement by polarisation transfer including the detection of quarternary nuclei (DEPTq), correlated spectroscopy (COSY), total correlated spectroscopy TOCSY, nuclear Overhauser effect spectroscopy (NOESY), heteronuclear single quantum correlation (HSQC), hetero multiple bond correlation (HMBC) and rotating frame Overhauser enhancement spectroscopy (ROESY). Spectral data was analysed with the TopSpin 4.0.8 Software.

2.2.4.3. Mass spectrometry

Mass spectrometry (MS) and NMR spectroscopy complement each other very well in the information both deliver. As one of the most sensitive measurements in analytical chemistry, MS has found its way into many fields. Therefore, there are many combinations of MS with different kinds of ionisation sources, ion filters and detectors. For this study, as the analytes were natural organic compounds with a medium to large molecular size, the ionisation source needed to be soft. Therefore, the method of choice was electrospray ionisation (ESI). Because of that, the MS spectra have a large peak of the molecule ion and almost no fragments. Sample preparation was performed by the department of mass spectrometry.

2.2.4.4. Infrared spectroscopy

Infrared spectroscopy (IR) measurements were included to receive more data on the physical properties of the isolated compounds, rather than to elucidate their structure.

Measurements were performed on an attenuated total reflection (ATR) Fourier-transformation-IR (FT-IR) device. Sample preparation was trivial as the device allows for direct application by pipetting 1-2 drops on the diamond. After the background has been measured and the solvent evaporated, the measurement could be started. Resolution was set to 4 and samples were measured for a total of 256 times, to obtain a good signal to noise ratio in the fingerprint area. The Opus 7.2 software was used for operating the device.

2.2.4.5. Polarimetry

Polarimetry measurements of isolated compounds were performed by preparing methanolic solution of specific concentrations and transferring them into a cell with a length of 1 dm. Methanol served as blank. Measurements were obtained at room temperature and 589 nm (sodium D-line). Results were calculated using Equation 1.

$$\text{optical rotation } [\alpha]_D^{20} = \frac{\text{measured value} * 100}{\text{cell length [dm]} * \text{concentration } [\frac{\text{g}}{100 \text{ mL}}]}$$

Equation 1. Formula for the calculation of the optical rotation.

2.2.4.6. Photometry

Additionally, the molecular extinction coefficients (ε) have been evaluated for each of the isolated compounds. The wavelengths at which there is a peak in the UV absorbance spectrum has been chosen for the measurement of the ε values. Methanol served as blank. The ε values have been calculated using Lambert Beer's law. Stock solutions of each sample was prepared by removing the solvent and resolving it in 1 mL MeOH. Then concentrations where the extinction of the wavelength of highest absorption was between 3–4 units were evaluated for each sample. Extinction values between 3–4 units mean a transmission of approximately 1 ‰–0.1 ‰ of the initial light intensity.

2.2.4.7. Circular dichroism (CD) spectroscopy

The CD measurement was carried out to gain additional information of the absolute configuration. Methanol served as blank, and the samples were measured in cuvettes with a thickness of 1 cm. A mean spectrum was calculated from five measurements. The detection ranges were 200–400 nm.

3. Results and discussion

3.1. Isolation process

The HPLC chromatograms of the leaf crude extract and the solvent extracts are shown in Figure 15. Only plant constituents that can absorb a wavelength of 230 nm were detected. Hydrophilic substances with smaller retention times appear on the left side of the chromatogram, while lipophilic substances appear on the right side. The most abundant

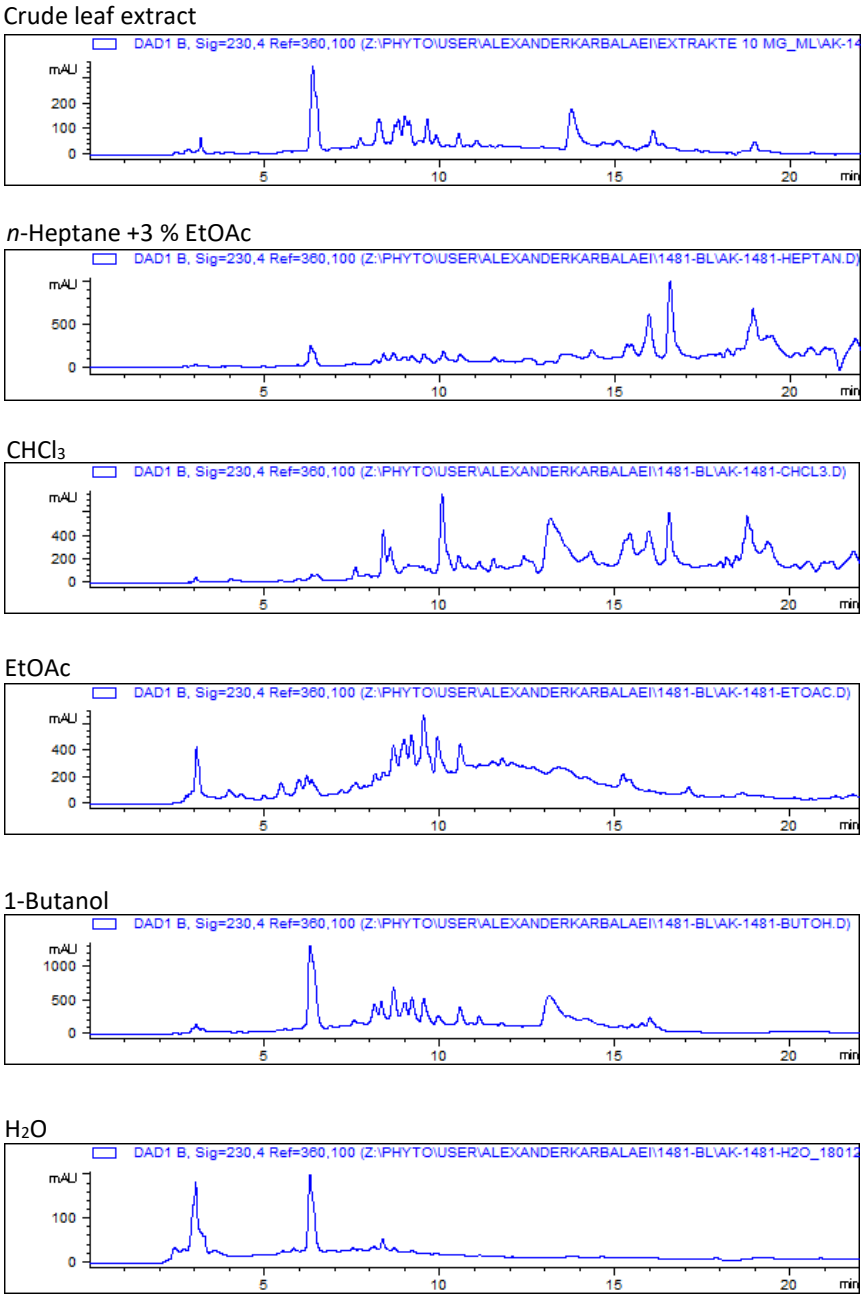

Figure 15. HPLC chromatograms of the crude extract (top) and the solvent extracts ordered in their lipophilicity from top to bottom. UV absorption at 230 nm was detected.

peak of the crude extract with a retention time between 6–7 min, reappears in the 1-butanol and water phases. The majority of the dragendorff-positive compounds are present in the 1-butanol phase (Figure 16). However, the $CHCl_3$ and the EtOAc phases also showed orange spots. Therefore, these three phases were primarily focused for further isolation. Nevertheless, because of the HPLC-chromatogram of the H_2O phase, further chromatographic separation attempts were performed. However, the H_2O phase did not yield significant amounts of substances that were detected in the HPLC, suggesting that most of the hydrophilic content were carbohydrates.

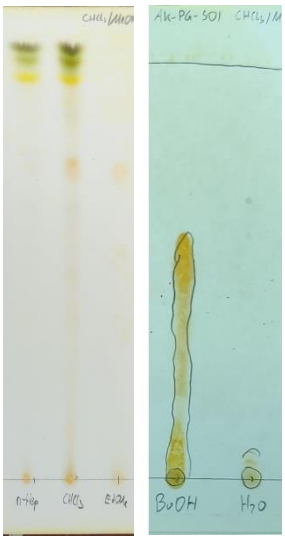

Figure 16. TLC plates of the different solvent phases stained with the Dragendorff's reagent. Eluent used was $CHCL_3$:MeOH 90:10. The solvent phases from left to right include: n-Hep+3 % EtOAc, $CHCl_3$, EtOAc, BuOH and H_2O.

3.1.1. Isolation of AK-PG01

The first isolated substance stems from the 1-butanol phase. With a retention time between 6–7 min (Figure 17), it is one of possibly more constituents contributing to the large peak of the HPLC-chromatogram of the crude, 1-butanol and H_2O extract (Figure 15). A total amount of 2.2 mg was isolated and used for further measurements. AK-PG01 did not show a coloration after applying the Dragendorff's reagent.

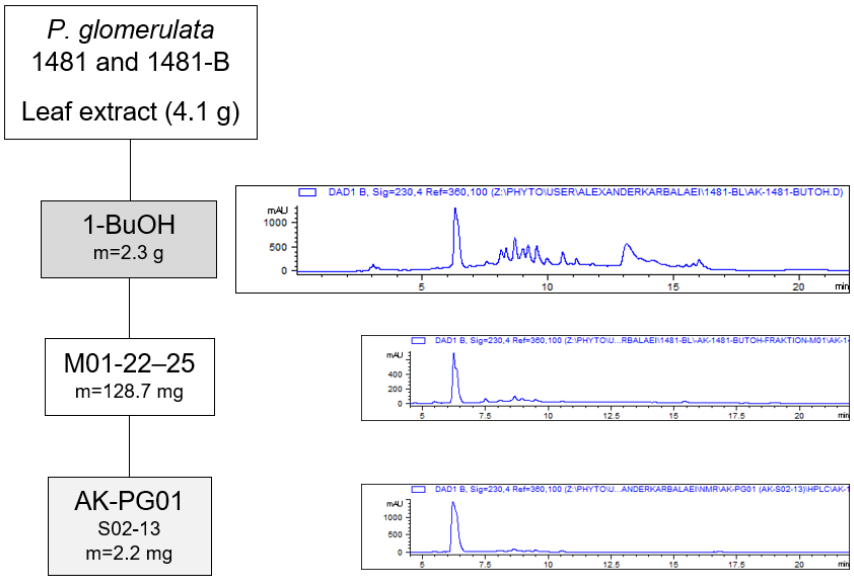

Figure 17. Isolation scheme of AK-PG01. HPLC chromatograms of each fraction as well as the amount is shown. HPLC chromatograms of samples with DMSO as an additive are shown between 4.5 min and 22 min. UV absorption at 230 nm was detected.

3.1.2. Isolation of AK-PG02

AK-PG02 was the second compound isolated from the 1-butanol phase. The isolation scheme with the HPLC chromatograms is shown in Figure 18. A total amount of 2.8 mg was isolated and AK-PG02 did not show a coloration with the Dragendorff's regent.

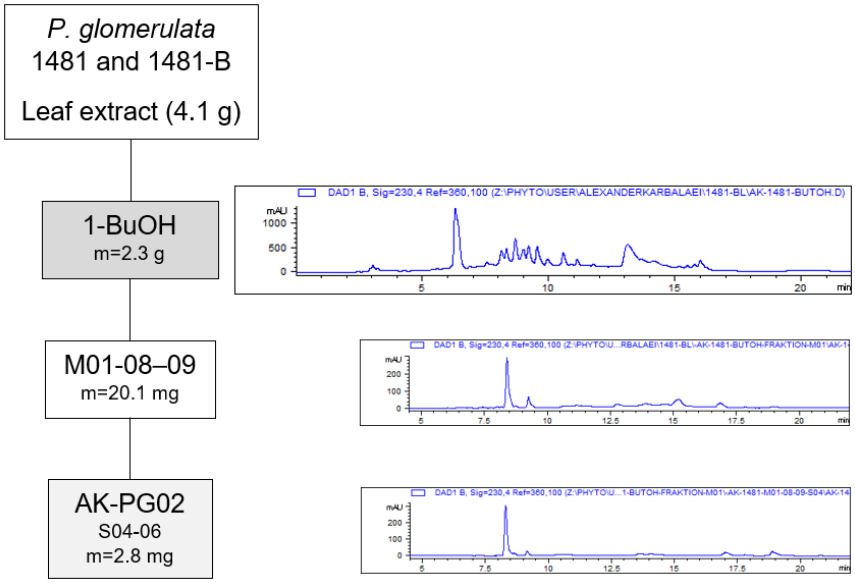

Figure 18. Isolation scheme of AK-PG02. HPLC chromatograms of each fraction as well as the amount is shown. HPLC chromatograms of samples with DMSO as an additive are shown between 4.5 min and 22 min. UV absorption at 230 nm was detected.

3.1.3. Isolation of AK-PG03

The first Dragendorff-positive compound that was isolated was found in the $CHCl_3$, EtOAc and 1-butanol phases. The complete isolation scheme is shown in Figure 19. It was first isolated from the EtOAc phase, where the total yield amounted to 1.5 mg. As structure elucidation indicated, that this compound is structurally related to glomerulatine A, B and C (Figure 1), the isolation of this compound from the other phases was of highest interest. After further purification processes the total yield was 9.1 mg.

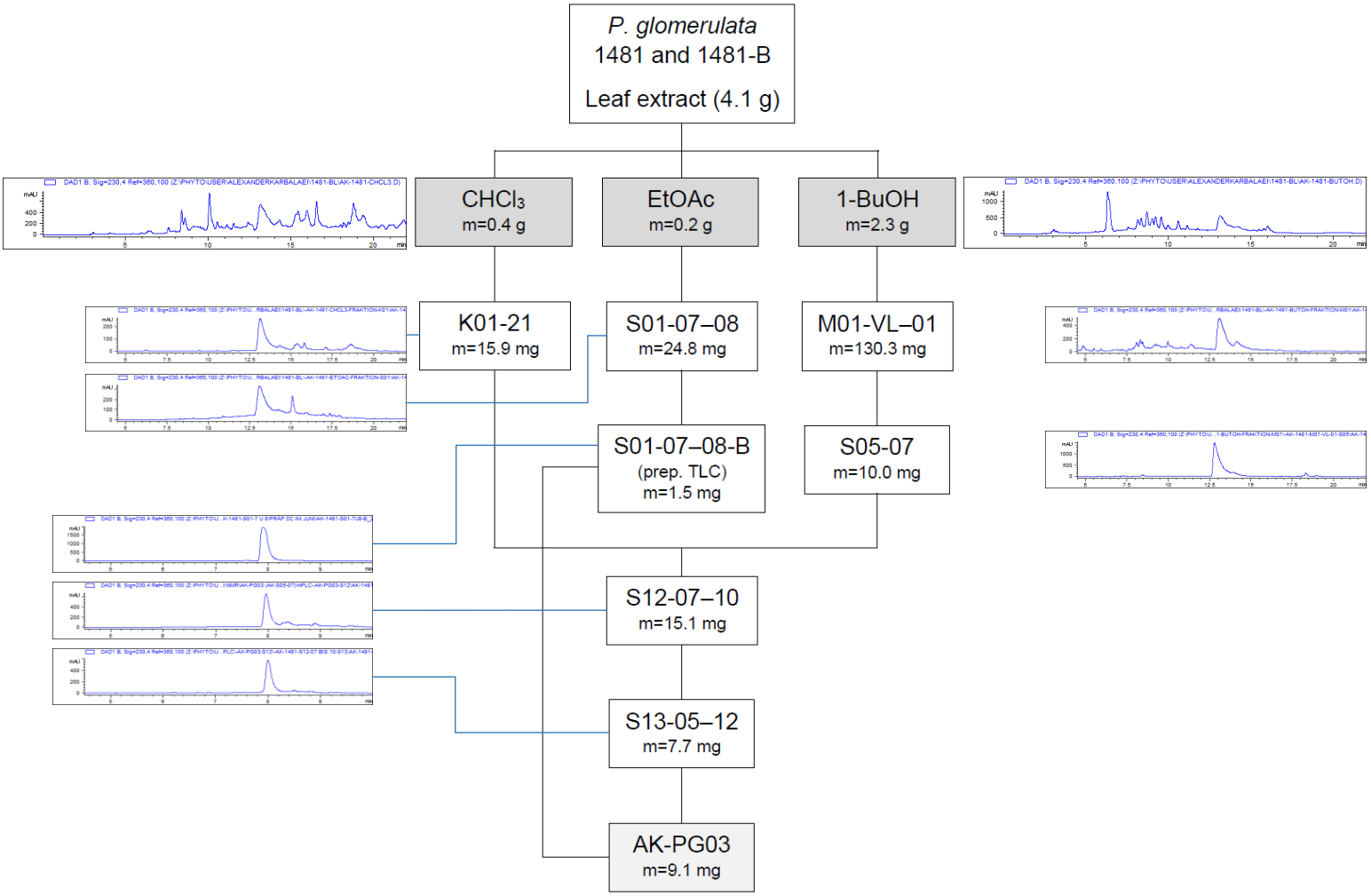

Figure 19. Isolation scheme of AK-PG03. HPLC chromatograms of each fraction as well as the amount is shown. HPLC chromatograms of samples with DMSO as an additive are shown between 4.5 min and 22 min. HPLC measurements of the fractions S01-07–08-B, S12-07–10 and S13-05–12 were performed using a shorter column and different method parameters. Therefore, there is a difference between the retention times. UV absorption at 230 nm was detected.

3.1.4. Isolation of AK-PG04

The fourth isolated compound and the second compound that was Dragendorff-positive also stems from the 1-butanol phase. The isolation scheme and HPLC chromatograms are shown in Figure 20. The double peak of the HPLC-chromatogram did not disappear after further separation attempts, indicating that it might be a mixture of isomers. The total amount isolated was 3.2 mg.

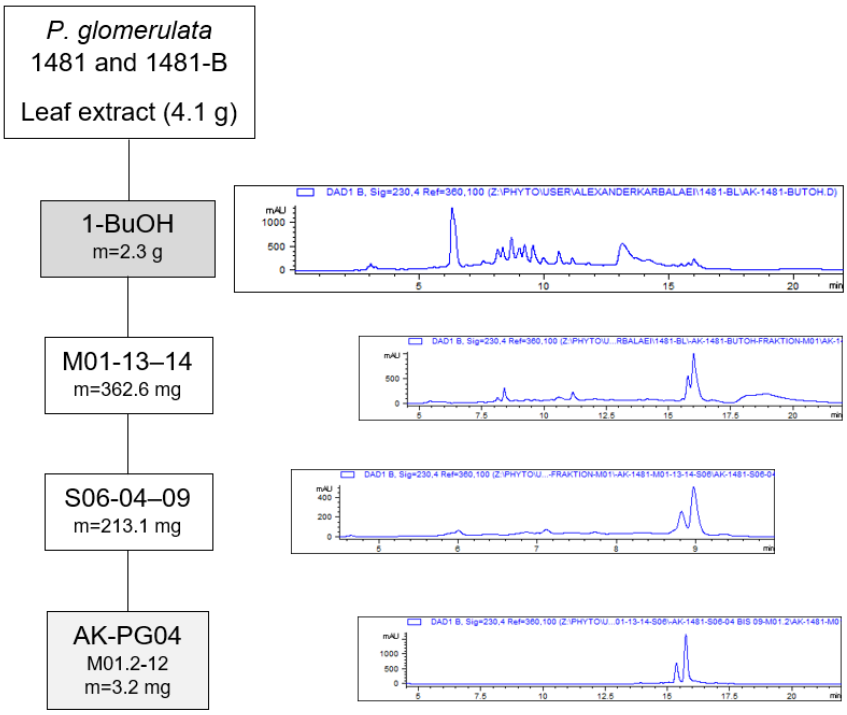

Figure 20. Isolation scheme of AK-PG04. HPLC chromatograms of each fraction as well as the amount is shown. HPLC chromatograms of samples with DMSO as an additive are shown between 4.5 min and 22 min. HPLC measurement of the fraction S06-04–09 was performed using a shorter column and different method parameters. Therefore, there is a difference between the retention times. UV absorption at 230 nm was detected.

3.1.5. Isolation of AK-PG08

The fifth compound was isolated from the $CHCl_3$ phase. Figure 21 shows the isolation scheme and the HPLC chromatograms. This compound was not Dragendorff-positive, and the total yield amounted to 5.9 mg.

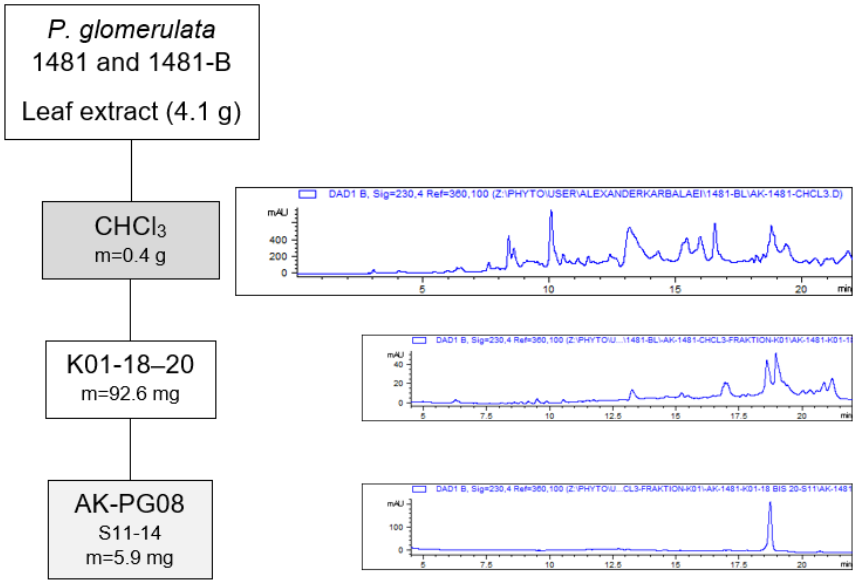

Figure 21. Isolation scheme of AK-PG08. HPLC chromatograms of each fraction as well as the amount is shown. HPLC chromatograms of samples with DMSO as an additive are shown between 4.5 min and 22 min. UV absorption at 230 nm was detected.

3.2. NMR, MS, IR, polarimetric and photometric results

3.2.1. 6,8-Di-*C*-β-D-glucopyranosylnaringenin (AK-PG01)

The NMR results of AK-PG01 are summarized in Table 7. Reference values stem from measurements of synthesized 6,8-di-*C*-β-D-glucopyranosylnaringenin in deuterated pyridine (^{13}C) and deuterated methanol (^{1}H) [45]. The suggested structure with important COSY, NOESY and HMBC couplings is shown in Figure 22. The flavanone basic structure has many prominent peaks. The protons H2' and H3' show ^{1}J and ^{3}J couplings onto the same carbons in the HSQC and HMBC (Figure 23). This observation suggested the presence of a *p*-substituted aromatic B-ring. Initially, the presence of a second aromatic ring was not apparent, due to the lack of signals in the usual aromatic area. However, increment calculation explains aromatic ^{13}C shifts of ~106 and ~165 ppm (Equation 2), as similar values can be obtained by a methyl substituted model molecule (Figure 24) and Table 8 [46]. The carbohydrate moiety most likely has a β-glucose configuration, as MS signals of $[M+Na]^+$ at 619.1634 m/z suggested two missing hexose moieties, the large coupling constant of 9.96 Hz of the anomeric protons imply axial protons on position H1''$^{(\prime)}$ and H2''$^{(\prime)}$ and NOESY crosspeaks of H5''$^{(\prime)}$ with H6''$^{(\prime)}$ and H1''$^{(\prime)}$. Moreover, biosynthetic wise UDP-glucose is the most common sugar donor [16].

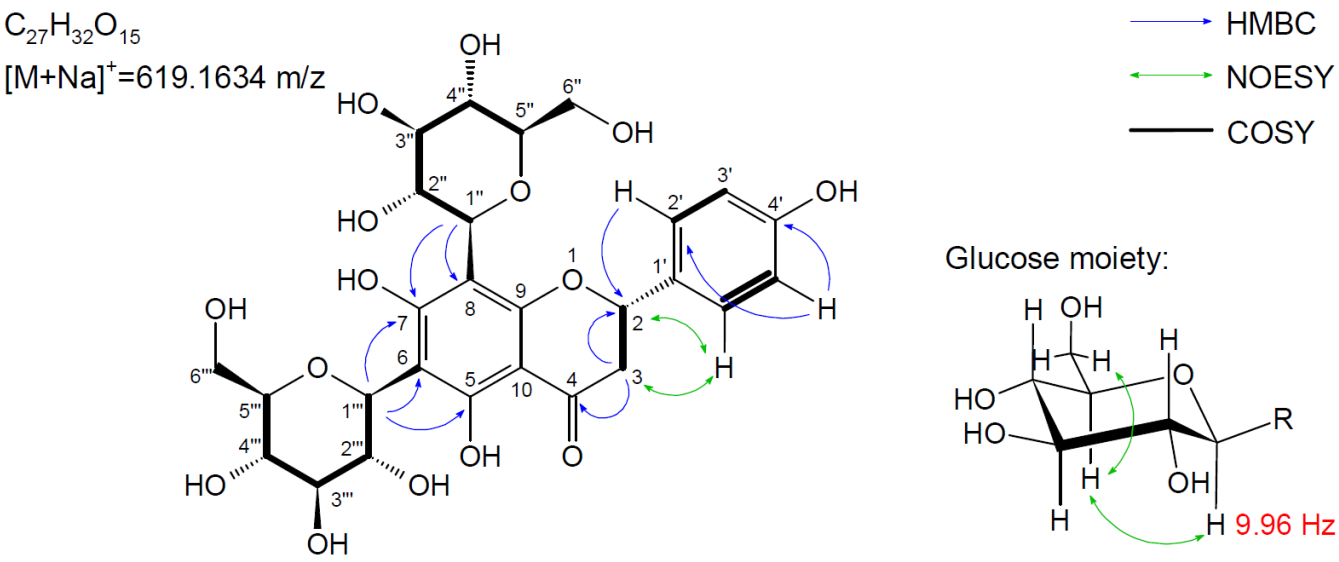

Figure 22. Structure of 6,8-di-*C*-β-D-glucopyranosyl-2(*S*)-naringenin (AK-PG01). HMBC crosspeaks are displayed as blue arrows, NOESY crosspeaks are displayed as green arrows and COSY crosspeaks are displayed as thick bonds. The characteristic large coupling constant of a β-glycosidic anomeric proton is shown in red.

Table 7. NMR shift table of 6,8-di-*C*-β-D-glucopyranosylnaringenin (AK-PG01).

No.	Group	δ ^{13}C	Reference [45] C_5D_5N	δ ^{1}H (multiplicity) s: singlet, d: duplet, t: triplet, m: multiplet, br: broad	Reference [45] CD_3OD	HMBC coupling
Flavanone moiety						
2	CH	80.4	80.1	5.41 (dt)	5.40	H-2’ (7.39, 7.36), H-3 (3.14)
3	CH_2	44.4/43.3	44.1/43.1	3.14/3.08 (br), 2.84/2.77 (dd)	3.11, 2.80	-
4	C_q	198.9/198.8	199.0/198.9	-	-	H-3 (3.14, 2.84/2.77)
5	C_q	~165	163.2	-	-	H-1’’$^{(\prime)}$ (4.88, 4.81)
6	C_q	~106	106.7	-	-	H-1’’$^{(\prime)}$ (4.88, 4.81)
7	C_q	~165	165.5	-	-	H-1’’$^{(\prime)}$ (4.88, 4.81)
8	C_q	~106	105.7	-	-	H-1’’$^{(\prime)}$ (4.88, 4.81)
9	C_q	n.d.	162.7	-	-	-
10	C_q	103.4	103.4/103.3	-	-	-
1’	C_q	131.2/130.8	131.0/130.7	-	-	H-3’ (6.82), H-3 (3.14)
2’	CH	129.2/128.8	129.1/128.8	7.39/7.36 (d)	7.37, 7.34	H-2’ (7.39, 7.36)
3’	CH	116.4	116.4	6.82 (d)	6.84	H-2’ (7.39)
4’	C_q	158.9/159.0	158.7/158.6	-	-	H-2’ (7.39, 7.36), H-3’ (6.82)
Glucose moieties						
1’’$^{(\prime)}$	CH	75.6	79.7	4.88 (4.81$^{(\prime\prime\prime)}$) (d)	4.91-4.82	-
2’’$^{(\prime)}$	CH	72.8	75.4	3.93 (br)	3.97-3.71	H-1’’$^{(\prime)}$ (4.88, 4.81)
3’’$^{(\prime)}$	CH	79.8	80.0	3.50-3.34 (br)	3.53-3.32	H-1’’$^{(\prime)}$ (4.88, 4.81)
4’’$^{(\prime)}$	CH	71.6	73.0/71.3	3.50-3.34 (br)	3.53-3.32	-
5’’$^{(\prime)}$	CH	82.4/82.6	82.8/82.6	3.50-3.34 (br)	3.97-3.71	H-1’’$^{(\prime)}$ (4.88, 4.81)
6’’$^{(\prime)}$	CH_2	62.4	62.2	3.84 (t, br), 3.76 (dd), 3.71 (dd)	3.97-3.71	-

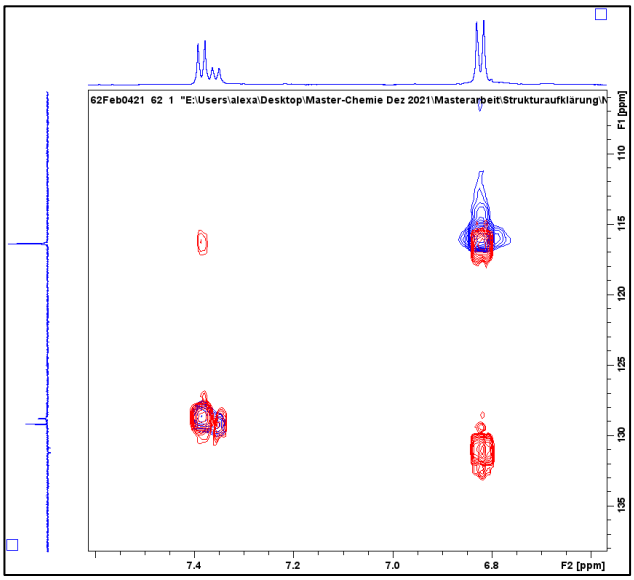

Figure 23. HMBC (red) and HSQC (blue) signals of protons and carbons of the symmetric aromatic B-ring. The overlapping of HMBC and HSQC signals implies ^{1}J and ^{3}J couplings onto the same carbon atom.

$$\delta_C = 128.5 + I_{ipso} + I_{ortho} + I_{meta} + I_{para}$$

Equation 2. Formula for the ^{13}C-shift calculation of substituted benzenes [46].

Table 8. Increment values for substituted benzenes [46].

Substituent	I_{ipso}	I_{ortho}	I_{meta}	I_{para}
–CH_3	9.2	0.7	-0.1	-3.1
–OH	26.9	-12.8	1.4	-7.4
–OCH_3	31.4	-14.4	1.0	-7.7
–CO–CH_3	8.9	0.1	-0.1	4.4

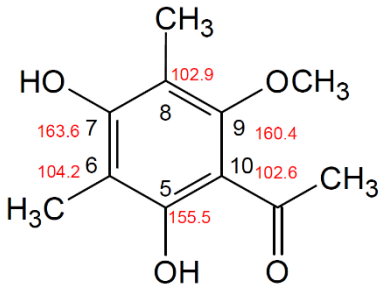

Figure 24. Calculated ^{13}C-shift values of a polysubstituted benzene ring.

Interestingly, some signals in the ^{1}H spectrum as well as in the ^{13}C spectrum appear twice at different intensities. For example, the signals of the carbons C2’ and C3 and the protons H2’ and H3a (Figure 25). This is due to a rotational hindrance of the C8–C1’’-bond that can be caused by an aromatic B-ring on the position C2 or substitution on position C7. However, a 7–OH group would not be large enough to cause this effect [47,48]. Moreover, 6-*C*-glycosyl flavanonoids can show rotamer signals, also depending on the substitution on C7. The separation of these signals is dependent on temperature. As higher temperatures would mean a fast exchange of the two rotamers, the signals would merge [48].

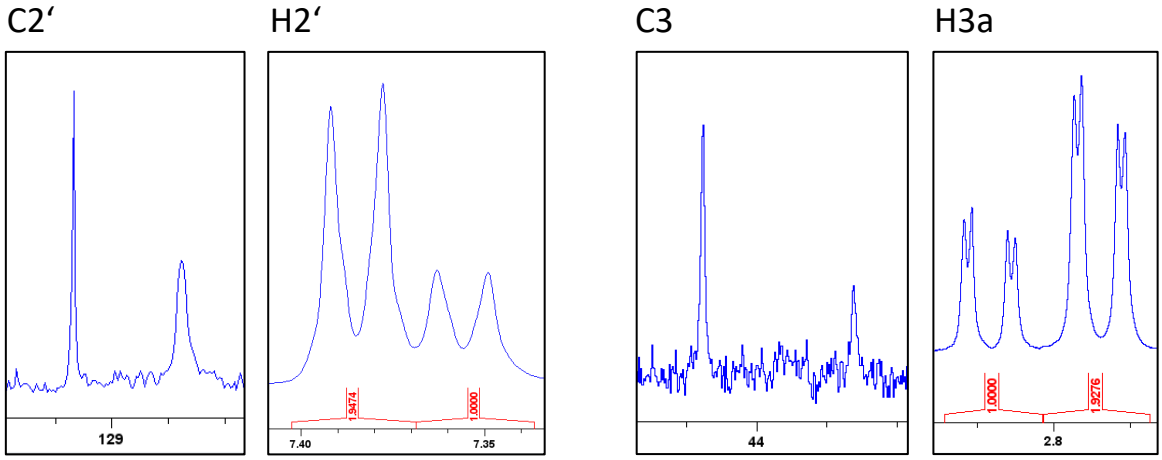

Figure 25. ^{13}C (left) and ^{1}H (right) signals of the positions C2’ (left) and C3 (right). The doubling of the signals is possibly due to rotational isomerism. According to the integrals of the ^{1}H signals the rotamers occur in a ratio of approximately one to two.

Considering the glucose moiety is present in D-configuration, there remains one chiral center, which is on the position C2. These two diastereomers can be distinguished by their ^{1}H shifts of the H3b. As a reference, the acetylated derivate with the *R* configuration on position 2 has a H3b shift of 3.01 ppm and with the *S* configuration a H3b shift of 3.11 ppm. However, ^{1}H signal doubling due to rotamers is not mentioned [45]. H3b shift of AK-PG01 are at 3.14 and 3.08. NOESY signals between the aromatic H2' and the H3b are shown in Figure 26. Considering the doubling of the H2' signal is due to rotamers, there would be a crosspeak between the H2' signals and each H3b signal, if the H3b signal doubling is because of diastereomers. However, the H2' protons of each rotamer only show a crosspeak to one of the two H3b. Therefore, it can be deduced that the doubling of the H3b signal is also the result of the rotation hindrance. The shifts of the H3b protons of 3.14 and 3.08 suggest the *S* configuration on C2.

This absolute configuration is confirmed by the results of the CD-measurements (c= 2.88*10^{-5} mol/L, MeOH) as shown in Figure 27. The CD spectrum of AK-PG01 is more similar to the findings of the *S* configuration, where the CD-values were reported as +5.38° (336 nm), –8.14° (305 nm) and +3.76° (253 nm), whereas the CD-values of the *R* configuration were –3.95° (335 nm), +3.16° (303 nm), +10.95° (257 nm) [49].

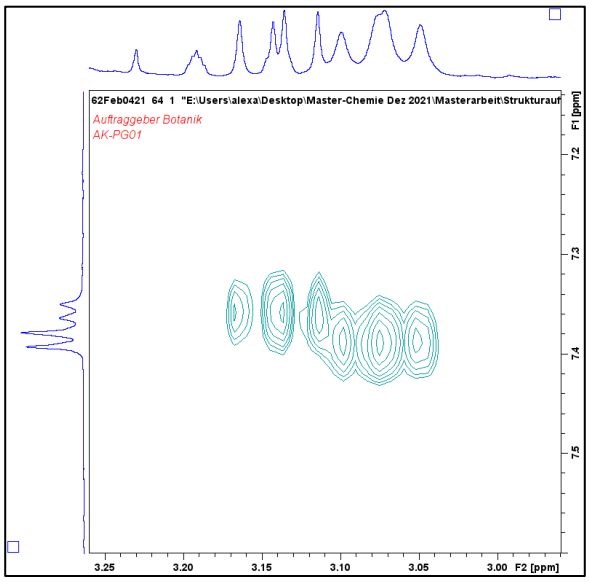

Figure 26. NOESY crosspeaks between the protons at the positions 2' and 3b.

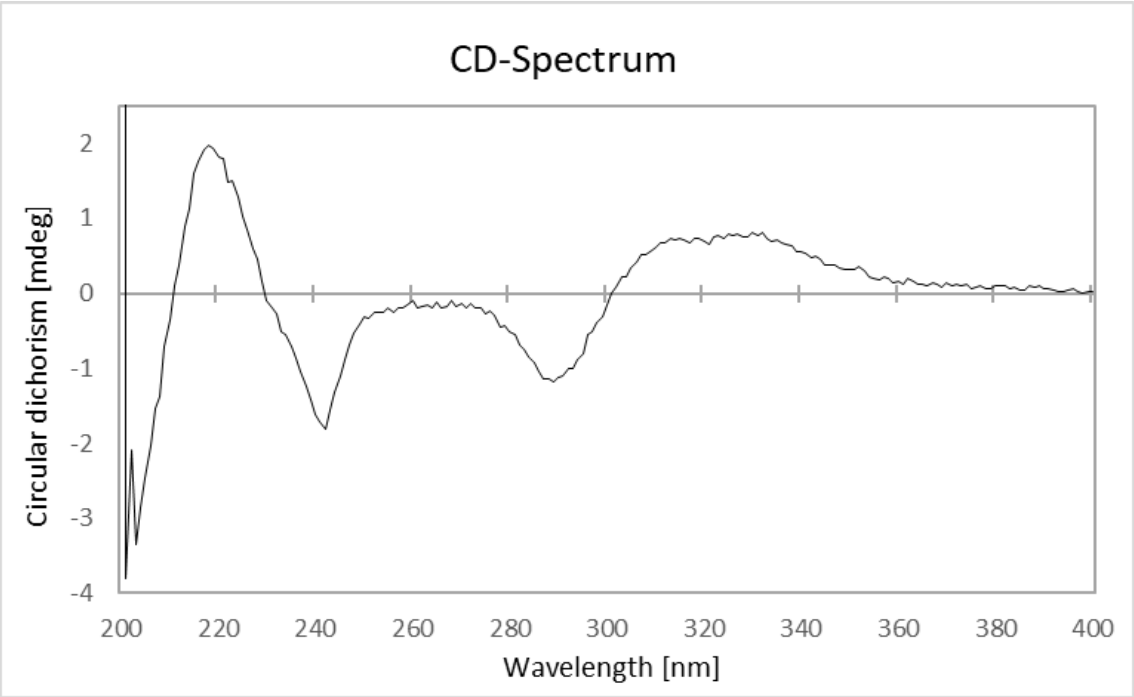

Figure 27. CD spectrum of AK-PG01 (c= 2.88*10-5 mol/L, MeOH). A mean curve was calculated from a total of five measurements in the ranges 200–400 nm.

The results of the ATR-FTIR measurements are shown in Figure 28. The spectrum is displayed as % transmittance versus wavenumber in the range between 4000 to 400 cm^{-1}. Background and sample were scanned 256 times. Possible sources of characteristic bands include the O–H stretching at 3354.61 cm^{-1} and the CH_2 stretching and scissoring at 2918.62 cm^{-1} and 1454.85 cm^{-1} [50]. The typical alkyl phenyl C=O stretching would be around 1690–1680 cm^{-1}. However, electron-withdrawing and electron-donating substituents on the aromatic ring can cause shifts of this band. Additionally, OH groups in *ortho* position to the carbonyl group lower the C=O frequency, as they are intramolecularly bonded to the C=O group [51]. Therefore, a C=O band at 1617.14 cm^{-1} could be plausible. The band at 1518.88 cm^{-1} could be from the *p*-substituted B-rings semi-circle stretch and in-plane C–H bend [52]. The band at 1345.43 cm^{-1} could stem from the involving C–O–H bend. The two bands at 1080.77 and 1034.52 cm^{-1} could correspond to the out of phase C–C–O stretch of secondary and primary alcohols respectively [53]. However, bands in the range between 1150–1060 $cm^{-1}$and 1115–1080 cm^{-1} could also stem from the antisymmetric C–O–C stretch of an aliphatic ether, or the symmetric COCOC stretch of an

acetal. Additional ether bands include the aryl–O stretch of an aromatic ether in the range of 1310–1210 cm^{-1} [54].

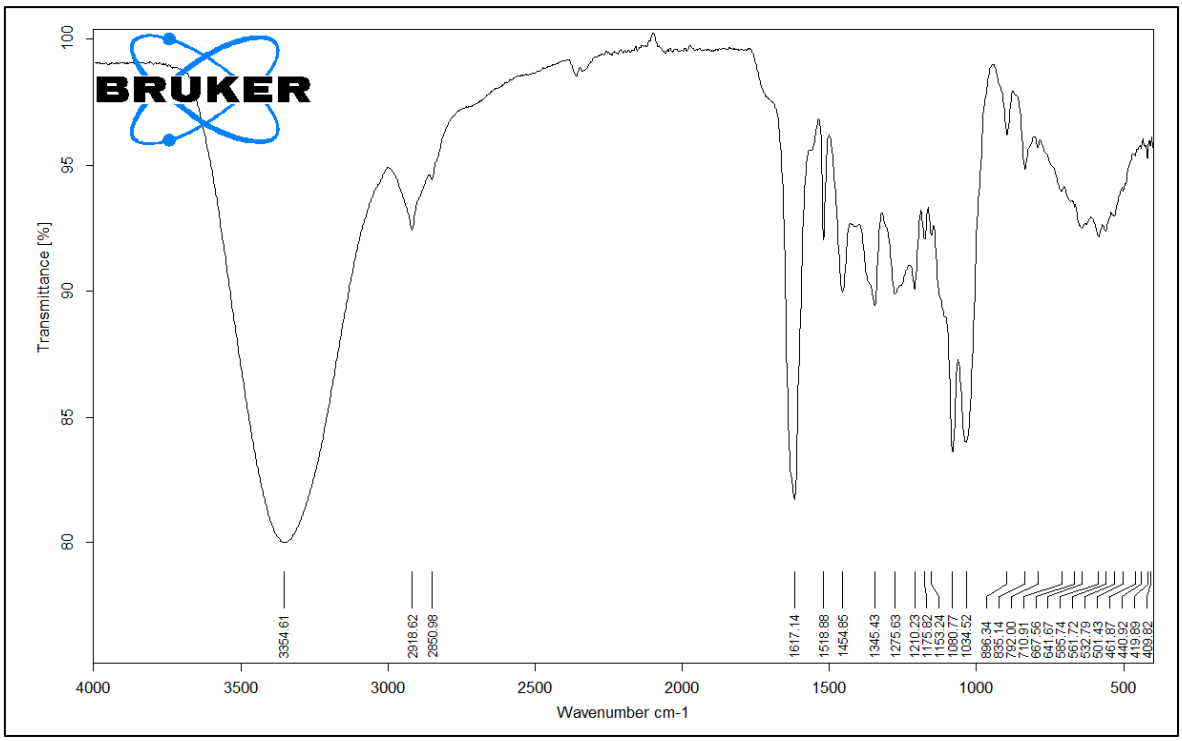

Figure 28. ATR-FTIR spectrum of AK-PG01. Transmittance % is shown in the ranges 4000 to 400 cm^{-1}.

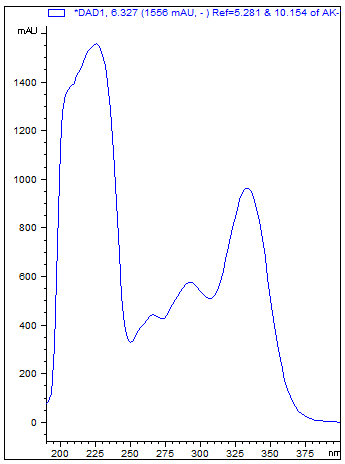

The obtained $[\alpha]_D^{20}$ value of AK-PG01 was +2.70 (MeOH, 1.67 mg/mL). For the evaluation of the log ε values, absorptions were measured at the maxima in the UV spectrum in the ranges 180–400 nm (Figure 29). The log ε results are 4.24 (226 nm), 3.73 (268 nm), 4.06 (290 nm) and 3.63 (334 nm).

Figure 29. UV-absorption spectrum of AK-PG01 in the range of 180-400 nm.

A possible biosynthetic pathway is shown in Figure 30. The twofold *C*-glycosylation could have occurred as described by Ito et al. [17]. After ring closure and dehydration, the flavone derivate is formed. Because AK-PG01 possesses two sp^3 hybridized carbons on positions 2 and 3, a subsequent hydrogenation of the double bond is suggested. This results in the formation of two products with either the *S* or *R* configuration on carbon 2, respectively. Both configurations have been isolated from natural sources [49].

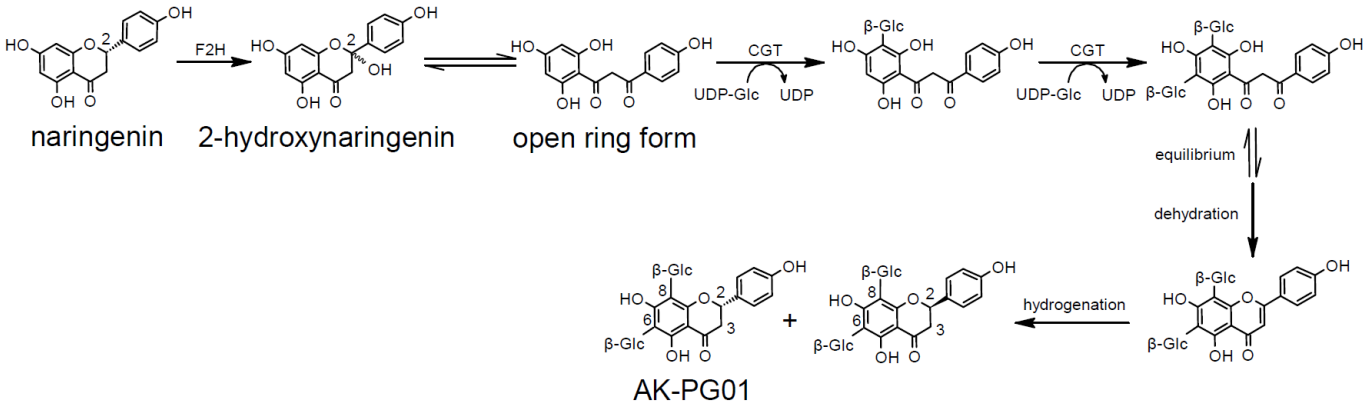

Figure 30. Possible biosynthetic pathway of AK-PG01. Uridine diphosphate (UDP), flavanone 2-hydroxylase (F2H), *C*-glycosyltransferase (CGT) [13,17].

3.2.2. 6'-*O*-β-D-Apiofuranosylsweroside (AK-PG02)

The NMR results of AK-PG02 are summarized in Table 9. Reference values stem from measurements of 6'-*O*-β-apiofuranosylsweroside in deuterated methanol, isolated from *Lonicera quinquelocularis* Hardw. [55]. The suggested structure with important COSY, NOESY and HMBC couplings is shown in Figure 31 a). AK-PG02 belongs to the secoiridoid class. Characteristic peaks of the secologanin moiety include the β proton of the α,β-unsaturated ester group at 7.59 ppm, the signal of the anomeric proton of the glucose moiety at 4.67 ppm and the three protons of the vinyl group at 5.28–5.55 ppm. The configuration of the stereoisomeric centers can be concluded from the biosynthetic pathway of secologanin and NMR shifts of the reference. The HMBC crosspeak between the H7 and the quaternary carbon C11, highly suggests a ring closure between the methyl ester and the aldehyde function of the secologanin moiety. The configurations of the sugar moieties are suggested through the $^3J_{H\text{-}H}$ coupling constants and NOESY crosspeaks.

However, as shown in Figure 31 b), D-apiose could form two different furanoid rings, the 3-*C*-(hydroxymethyl)-L-threofuranose and the 3-*C*-(hydroxymethyl)-D-erythrofuranose. However, the free form of apiose has never been found in nature [56]. NOESY crosspeaks of H5'' with H2'' and H4'' suggest the erythro-configuration. This is also in line with the

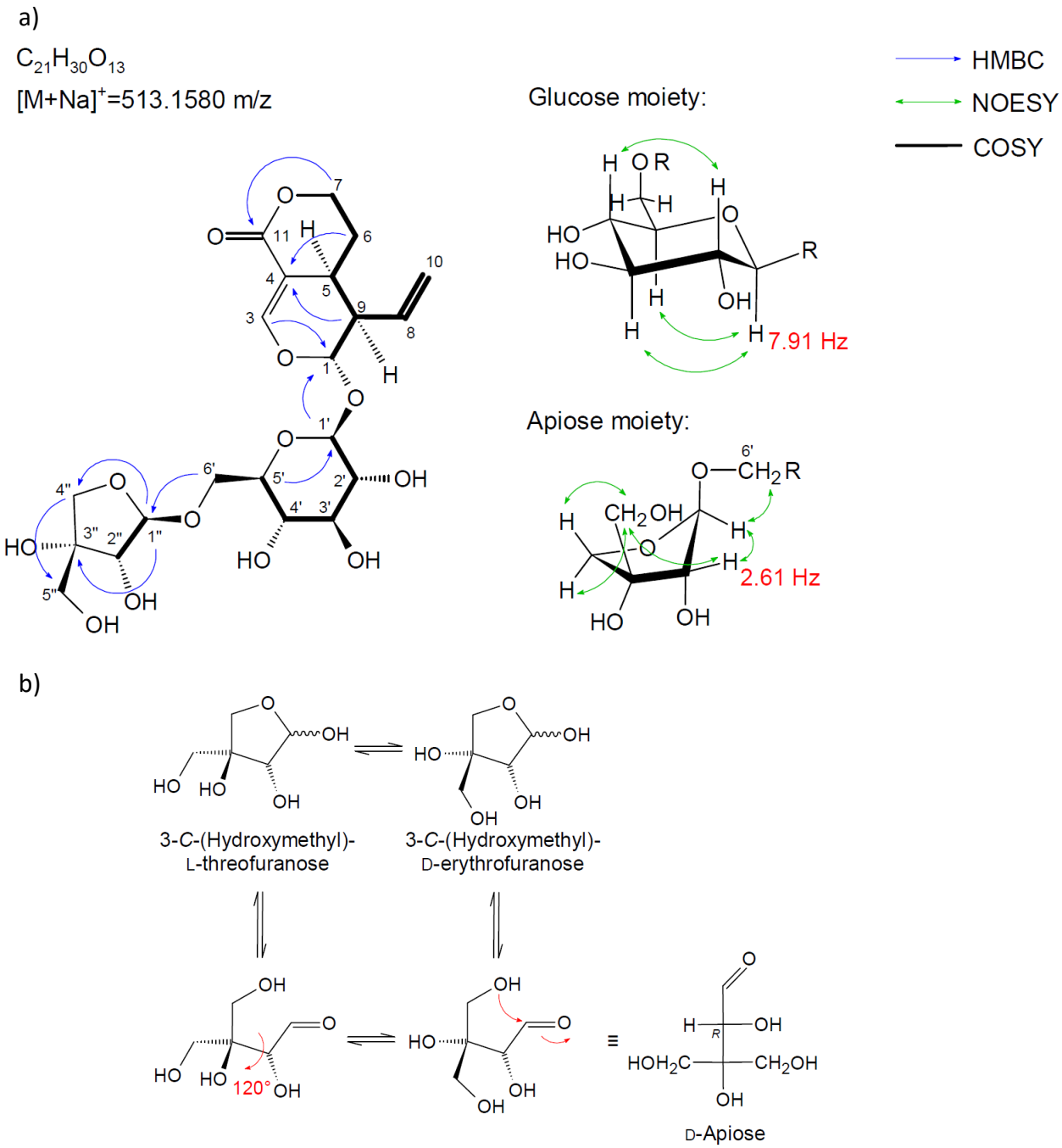

Figure 31. a) Structure of 6'-*O*-β-apio-D-furanosylsweroside (AK-PG02). HMBC crosspeaks are displayed as blue arrows, NOESY crosspeaks are displayed as green arrows and COSY crosspeaks are displayed as thick bonds. The coupling constants of the anomeric protons are shown in red. Apiose is shown in envelope ^{1}E configuration. b) Possible conversions of the free form of apiose. Unlike usual pentoses, the open-chain form of apiose only has a single chiral center [56].

NMR shifts of the reference [55]. Additionally, in nature the 3-*C*-(hydroxymethyl)-D-erythrofuranose, also known as D-*apio*-D-furanose is more common. The most common disaccharide consisting of apiose and glucose is β-D-apiofuranosyl-(1→6)-β-D-glucopyranose, also known as acuminose [56].

Table 9. NMR shift table of 6'-*O*-β-apio-D-furanosylsweroside (AK-PG02).

No.	Group	δ ^{13}C	Reference [55]	δ ^{1}H (multiplicity)	Reference [55]	HMBC coupling
			CD_3OD	s: singlet, d: duplet, t: triplet, m: multiplet, br: broad	CD_3OD	
Aglycone						
1	CH	98.3	98.1	5.46 (d)	5.45	H-3 (7.59), H-1' (4.67), H-9 (2.72)
3	CH	153.9	153.8	7.59 (d)	7.60	H-1 (5.46)
4	C_q	106.1	106.0	-	-	H-3 (7.59), H-9 (2.72), H-6 (1.77)
5	CH	28.6	28.4	3.15 (m)	3.13	H-3 (7.59), H-1 (5.46), H-7 (4.46, 4.37), H-9 (2.72), H-6 (1.77, 1.72)
6	CH_2	26.1	25.9	1.77 (m); 1.72 (ddd)	1.74	-
7	CH_2	69.8	69.7	4.46 (m); 4.37 (m)	4.40, 4.40	H-6 (1.72)
8	CH	133.4	133.2	5.55 (dt)	5.53	H-1 (5.46), H-10 (5.34), H-9 (2.72)
9	CH	43.9	43.8	2.72 (ddd)	2.72	H-8 (5.55), H-10 (5.34, 5.28)
10	CH_2	121.0	121.0	5.34 (dd), 5.28 (dd)	5.31, 5.31	H-9 (2.72)
11	C_q	168.5	168.4	-	-	H-3 (7.59), H-7 (4.46)
Acuminose moiety						
1'	CH	99.9	99.7	4.67 (d)	4,66	H-1 (5.46), H-2' (3.18), H-5' (3.46)
2'	CH	74.8	74.6	3.18 (t)	3,19	H-3' (3.37)
3'	CH	77.8	77.7	3.37 (t)	3,37	H-4' (3.29), H-2' (3.18)
4'	CH	71.6	71.4	3.29	3,30	H-6' (4.00), H-3' (3.37)
5'	CH	77.2	77.0	3.46 (dd)	3,46	H-6' (3.63)
6'	CH_2	68.7	68.5	4.00 (dd), 3.63 (t)	4,01 ;3,63	H-1'' (4.99), H-4' (3.29)
1''	CH	111.1	110.9	4.99 (d)	4.98	H-6' (4.00), H-4'' (3.98, 3.77), H-2'' (3.90), H-6' (3.63)
2''	CH	77.8	77.8	3.90 (d)	3.90	H-4'' (3.77)
3''	C_q	80.5	80.4	-	-	H-1'' (4.99), H-4'' (3.98, 3.77), H-5'' (3.57)
4''	CH_2	75.1	74.9	3.98 (d), 3.77 (d)	3.97, 3.76	H-1'' (4.99)
5''	CH_2	65.6	65.5	3.57	3.56	H-4'' (3.98), H-2'' (3.90)

The results of the ATR-FTIR measurements are shown in Figure 32. The spectrum is displayed as % transmittance versus wavenumber in the range between 4000 to 400 cm^{-1}. Background and sample were scanned 256 times. In addition to the bands corresponding to alkyl, alcohol, ether, or carbonyl groups which were discussed thoroughly for AK-PG01, AK-PG02 possesses an α,β-unsaturated ester and a vinyl function. The first of which shows characteristic C=O and C=C bands at 1689.00 cm^{-1} and 1613.60 cm^{-1} [51]. The vinyl group would show C=CH_2 stretching at 3090–3075 cm^{-1} and C=C stretching at around 1650 cm^{-1} [57]. However, both bands overlap with frequencies of other functional groups present in the molecule.

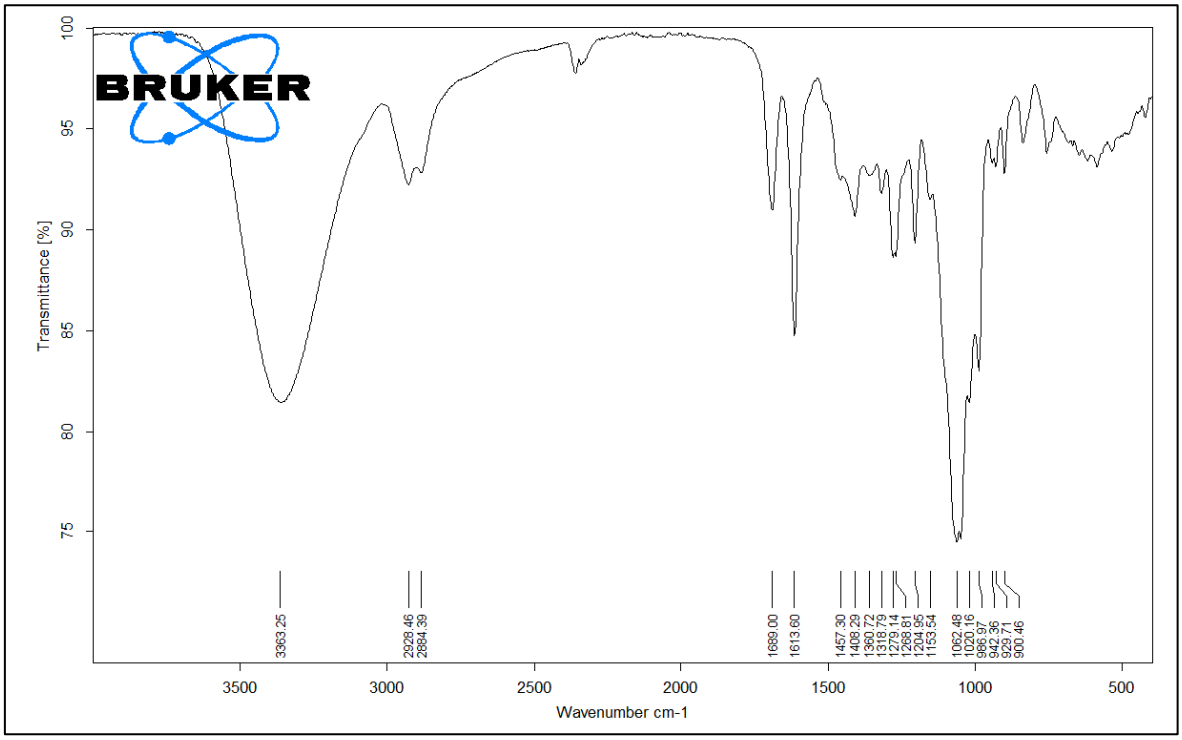

Figure 32. ATR-FTIR spectrum of AK-PG02. Transmittance % is shown in the ranges 4000 to 400 cm^{-1}.

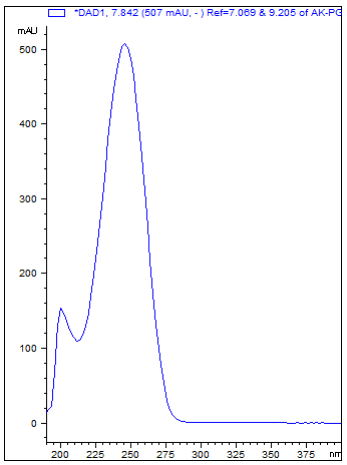

AK-PG02 has a specific rotation $[\alpha]_D^{20}$ of –11.79 (MeOH, 1.87 mg/mL). The log ε value at the UV-absorption maximum shown in Figure 33 is 3.81 (246 nm).

Figure 33. UV-absorption spectrum of AK-PG02 in the range of 180-400 nm.

Possible biosynthetic pathways are shown in Figure 34. Path a) describes an initial hydrolysis step to segologanic acid, which can form a six-membered ring with the carbon of the aldehyde function. After a subsequent formal reductive dehydroxylation step, sweroside is formed. A third step includes the apiosylation of the glucose moiety to form acuminose. The donor, UDP-apiose, is synthesised from UDP-D-glucuronic acid [56]. Path b) describes an initial apiosylation followed by a hydrolysis and a reduction step. Both ways would lead to AK-PG02. Although, in nature the D-erythrofuranoid form of apiose is more common, according to https://www.reaxys.com the L-threofuranose-apiose form of AK-PG02 has been isolated from *Pterocephalus hookeri* [58]. However, NMR spectroscopic data of that compound is not available.

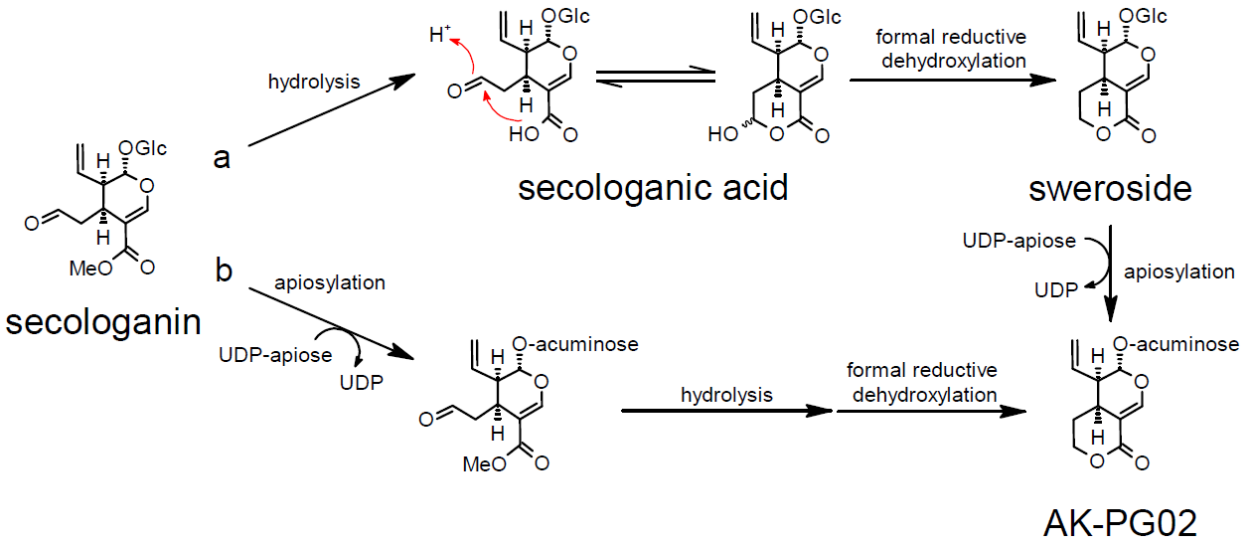

Figure 34. Possible biosynthetic pathways of AK-PG02. Uridine diphosphate (UDP) [56].

3.2.3. Glomerulatine A (AK-PG03)

The NMR results of AK-PG03 are summarized in Table 10. Reference values stem from measurements of (8-8a),(8'-8a')-tetradehydro-3a(*S*),3a'(*S*)-calycanthine (glomerulatine A) in deuterated benzene [9] and (8-8a),(8'-8a')-tetradehydro-3a(*R*),3a'(*R*)-isocalycanthine in deuterated chloroform [59]. The isocalycanthine-like structure was isolated from *Palicourea colorata* (Hoffmanns. ex Willd.) Delprete & J.H.Kirkbr. [59]. Interestingly, only eleven signals of each H and C atoms can be seen in the NMR spectra, suggesting a symmetric, dimeric structure of the molecule. Additionally, the ESI-MS spectrum is showing signals of $[M+H]^+$ at 343.1920 m/z and of $[M+2H]^{2+}$ at 172.0996 m/z, with a M+1 signal at a

distance of ~0.5 m/z (Figure 35). The suggested structure of the monomer with important COSY, NOESY and HMBC couplings is shown in Figure 36 (top).

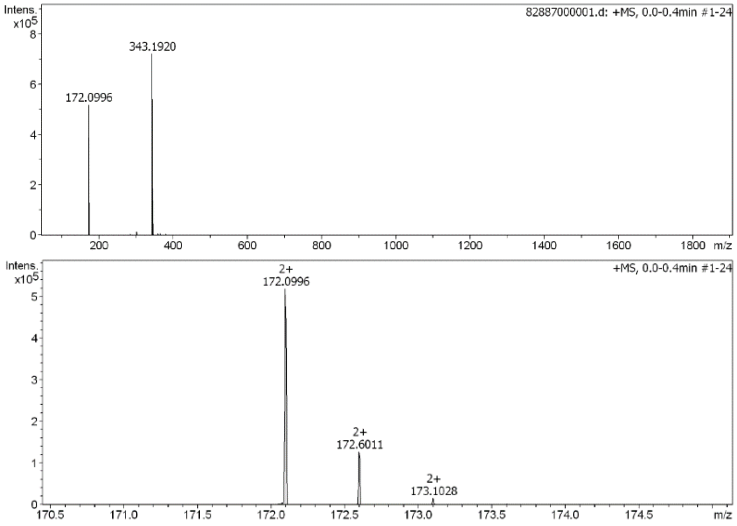

Figure 35. ESI-MS results of AK-PG03 measurements. The whole spectrum (top) with $[M+H]^+$ and $[M+2H]^{2+}$ signals and the magnification (bottom) of the $[M+2H]^{2+}$ signal with M+1 signals at a distance of ~0.5 m/z are shown.

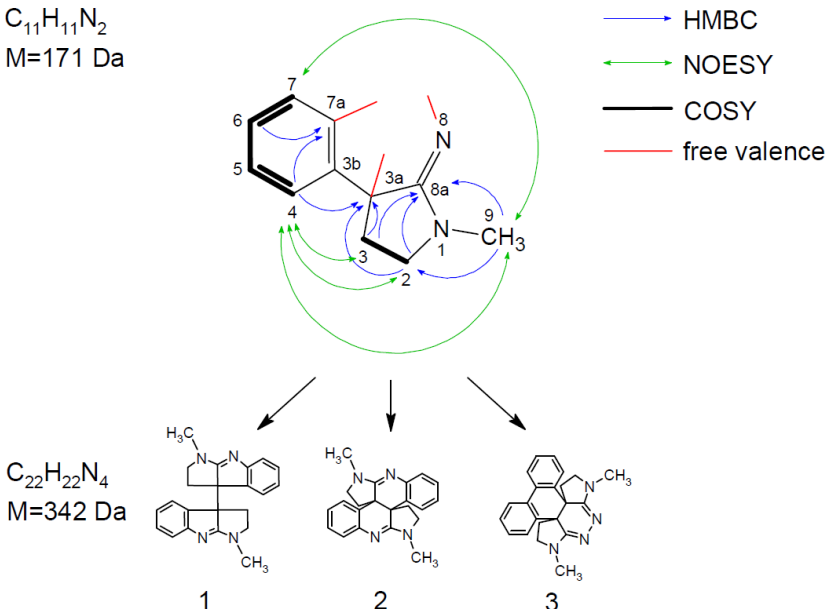

Figure 36. Supposed structure of the AK-PG03 monomer. HMBC crosspeaks are displayed as blue arrows, NOESY crosspeaks are displayed as green arrows, COSY crosspeaks are displayed as thick bonds and free valences are displayed in red. Possible dimers that do not contain a four-membered ring are shown below.

Table 10. NMR shift table of AK-PG03 and glomerulatine A / tetradehydroisocalycanthine.

No.	Group	δ ^{13}C	Reference [9,59] Glomerulatine A / Tetradehydroisocalycanthine C_6D_6 / $CDCl_3$		δ ^{1}H (multiplicity) s: singlet, d: duplet, t: triplet, m: multiplet, br: broad	Reference [9,59] Glomerulatine A / Tetradehydroisocalycanthine C_6D_6 / $CDCl_3$		HMBC coupling
2$^{(\prime)}$	CH_2	50.1	48.2	48.5	3.61 (m), 3.55 (t)	3.03, 2.61	3.57, 3.43	H-9 (3.26)
3$^{(\prime)}$	CH_2	30.8	30.3	29.9	2.59 (m), 1.60 (dd)	1.94, 1.37	2.43, 1.70	H-2 (3.61, 3.55)
3a$^{(\prime)}$	C_q	50.9	49.1	48.9	-	-	-	H-4 (6.66), H-2 (3.55), H-3 (2.59, 1.60)
3b$^{(\prime)}$	C_q	127.1	126.4	125.6	-	-	-	H-7 (6.97), H-5 (6.73), H-3 (2.59, 1.60)
4$^{(\prime)}$	CH	124.4	123.7	123.0	6.66 (dd)	6.77	6.66	H-6 (7.02)
5$^{(\prime)}$	CH	123.4	122.3	121.9	6.73 (dt)	6.65	6.70	H-7 (6.97)
6$^{(\prime)}$	CH	129.4	128.9	128.2	7.02 (dt)	6.96	7.03	H-4 (6.66)
7$^{(\prime)}$	CH	124.2	125.0	123.9	6.97 (dd)	7.47	7.03	H-5 (6.73)
7a$^{(\prime)}$	C_q	146.5	147.3	145.8	-	-	-	H-6 (7.02), H-4 (6.66)
8a$^{(\prime)}$	C_q	167.2	165.1	165.0	-	-	-	H-2 (3.55), H-9 (3.26), H-3 (1.60)
9$^{(\prime)}$	CH_3	31.6	30.9	31.1	3.26 (s)	2.92	3.28	-

Coupling of the protons H2 and H3 with C8a in the HMBC suggest the presence of a five membered ring. The monomer has three free valences, and multiple possible ways to form a dimer (Figure 36 (bottom)). Dimers that contain four-membered rings were not included as their occurrence in nature is rather improbable. Of the three possibilities, the first two seemed more likely, due to their resemblance of tryptamine. The main difference between the chimonanthine-like (1) and the isocalycanthine-like (2) structure is the number of bonds between the monomers. Consequently, tandem MS was performed on AK-PG03, as these two structures would differ in their fragmentation pattern. The results of the tandem MS measurement suggest the isocalycanthine-like structure. Additionally, the two structures can be differentiated by the shift of the C3a, which is ~64 ppm in the chimonanthine and ~50 ppm in the isocalycanthine-like structure [59,60].

However, due to the symmetric nature of this molecule, the HMBC signals of the two CH_2 groups, H2 and H3, onto the same quaternary carbon could just as well be explained with a six-membered ring. Because the carbons 8a and 8a' are equivalent (Figure 37). Additionally, the NMR signals of the calycanthine and isocalycanthine-type are very similar (Table 10). There are, however, differences of ^{1}H shifts due to the solvent [9,59].

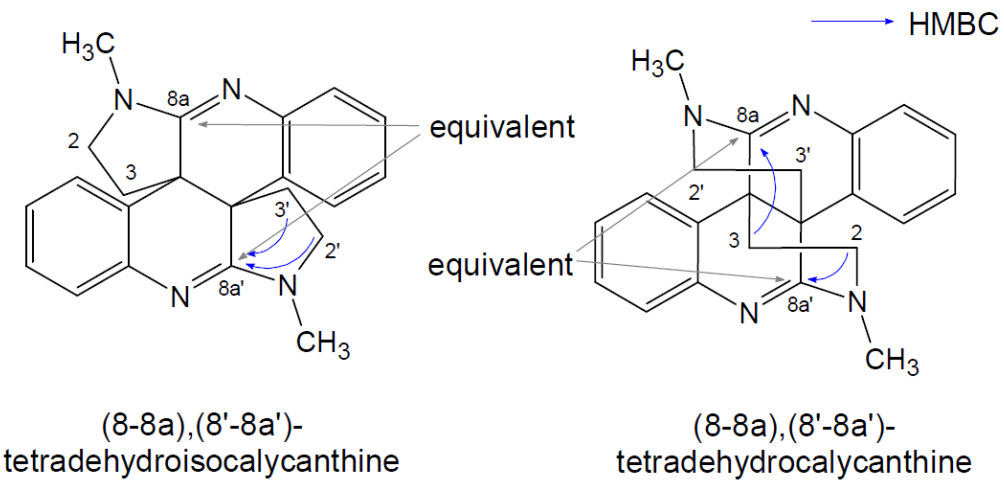

Figure 37. Structures of the isocalycanthine-like (left) and the calycanthine-like (right) molecule. The $^{3}J_{C\text{-}H}$ couplings between H2 and H3 with C8a$^{(\prime)}$ are highlighted. Both structures explain the HMBC crosspeak, because C8a and C8a' are equivalent.

Moreover, in order to differentiate between those two structures, Solis et al. [9] conducted a molecular mechanics study. The ^{1}H spectra for the H2 and H3 protons of the calycanthine and isocalycanthine-like structures were simulated to compare them with the spectrum of glomerulatine A. The experimentally obtained ^{1}H spectra of AK-PG03 and glomerulatine A and the simulated spectrum for the calycanthine-type are shown in Figure 38. Unlike the NMR measurement mentioned above (Table 10), Solis et al. [9] used $CDCl_3$ instead of C_6D_6 for the experimental ^{1}H NMR spectrum of glomerulatine A. Therefore, the proton signals of H2 are at δ 3.45 and 3.58, and the proton signals of H3 are at δ 1.70 and 2.45. These shifts are similar to the NMR results from Verotta et al. [59] of the isocalycanthine-like compound (Table 10).

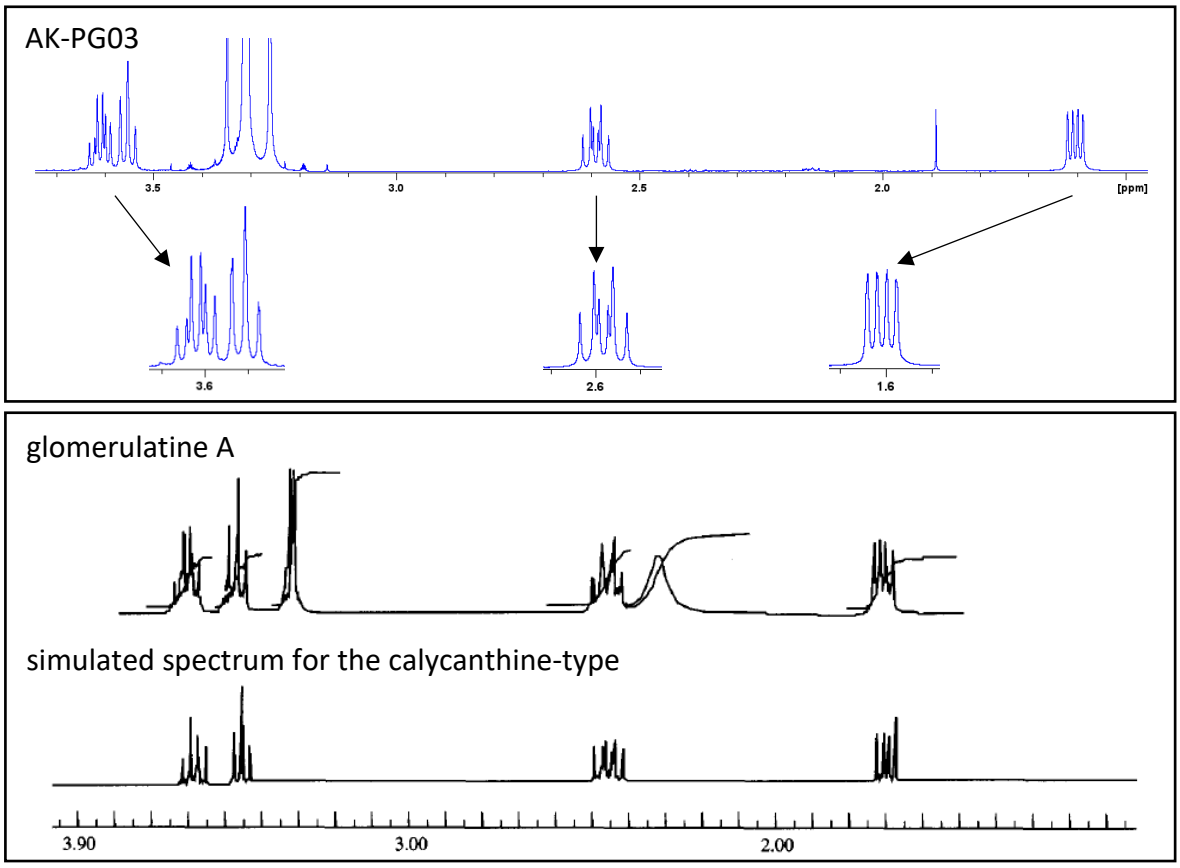

Figure 38. Comparison of ^{1}H spectra of AK-PG03 and glomerulatine A with a simulated ^{1}H spectrum of the calycanthine-type [9]. The glomerulatine A spectrum was measured at 400 MHz [9]. Because of the different solvents, there are differences in shifts. However, the peak shape of AK-PG03 and glomerulatine A are very similar.

Because of the similarities of the signal shapes in the ^{1}H spectra, it can be concluded that AK-PG03 has similar coupling constants and structural conformation as glomerulatine A. The suggested structure with important COSY, NOESY and HMBC couplings is shown in Figure 39 a). CD spectroscopic results of glomerulatine A conducted by Solis et al. [9] indicated the *S*-configuration and polarimetric measurements showed that this compound is laevorotatory with a value of –466 in $CHCl_3$ [9], which is in line with the results of AK-PG03 as will be shown below. These results suggest the 3a(*S*),3a'(*S*) configuration, as the *R,S* and *S,R*-configurations are superimposable and thus achiral (Figure 39 b). Although chimonanthine is known to convert into calycanthine under acidic conditions [33,34], and glomerulatine A was isolated under acidic conditions [9], AK-PG03 was isolated without the use of acid-base extraction methods. Suggesting that these compounds do not solely occur *in vitro* as artefacts.

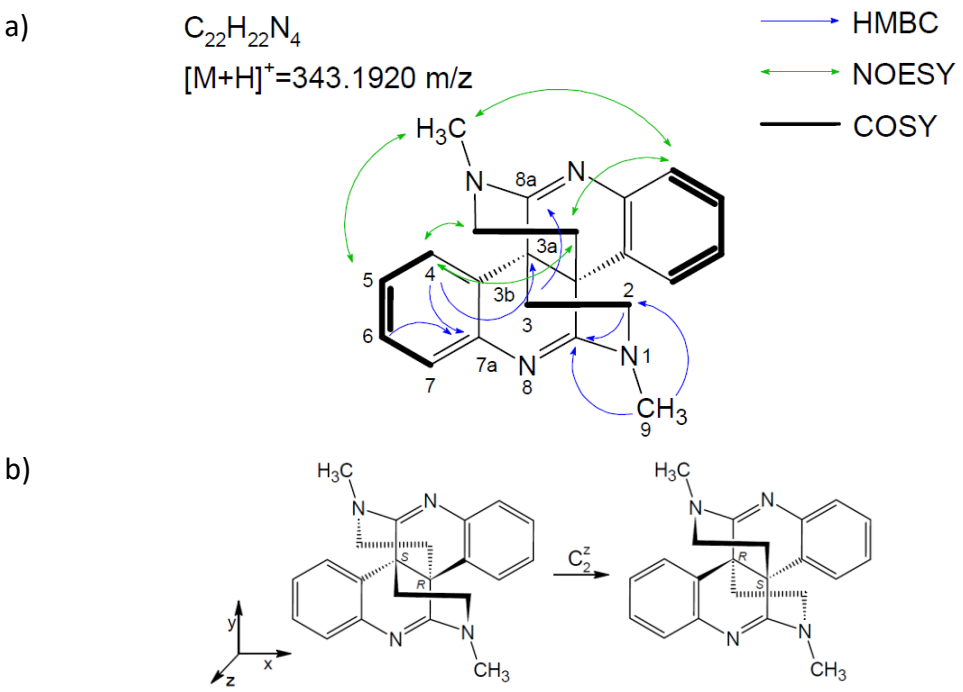

Figure 39. a) Structure of (8-8a),(8'-8a')-tetradehydro-3a(*S*),3a'(*S*)-calycanthine (AK-PG03). HMBC crosspeaks are displayed as blue arrows, NOESY crosspeaks are displayed as green arrows and COSY crosspeaks are displayed as thick bonds. b) The superimposition of the 3a(S), 3a'(R) configuration with the 3a(*R*), 3a'(*S*) configuration after a rotation of 180 ° around the z axis.

The results of the ATR-FTIR measurements are shown in Figure 40. The spectrum is displayed as % transmittance versus wavenumber in the range between 4000 to 400 cm^{-1}. Background and sample were scanned 256 times. Characteristic absorptions include the broad band at 3332.57 cm^{-1} that could be either from remnants of methanol which did not evaporate, residues of water, or R_3N^+–H stretching of the protonated tertiary amine [61]. Additionally, this compound possesses a *N*,*N*-disubstituted amidine group N–C=N. The C=N stretching would absorbs at 1633–1619 cm^{-1} [62]. The band at 1588.66 cm^{-1} and the much weaker one at 1570.78 cm^{-1} could from the *ortho*-disubstituted benzene [52].

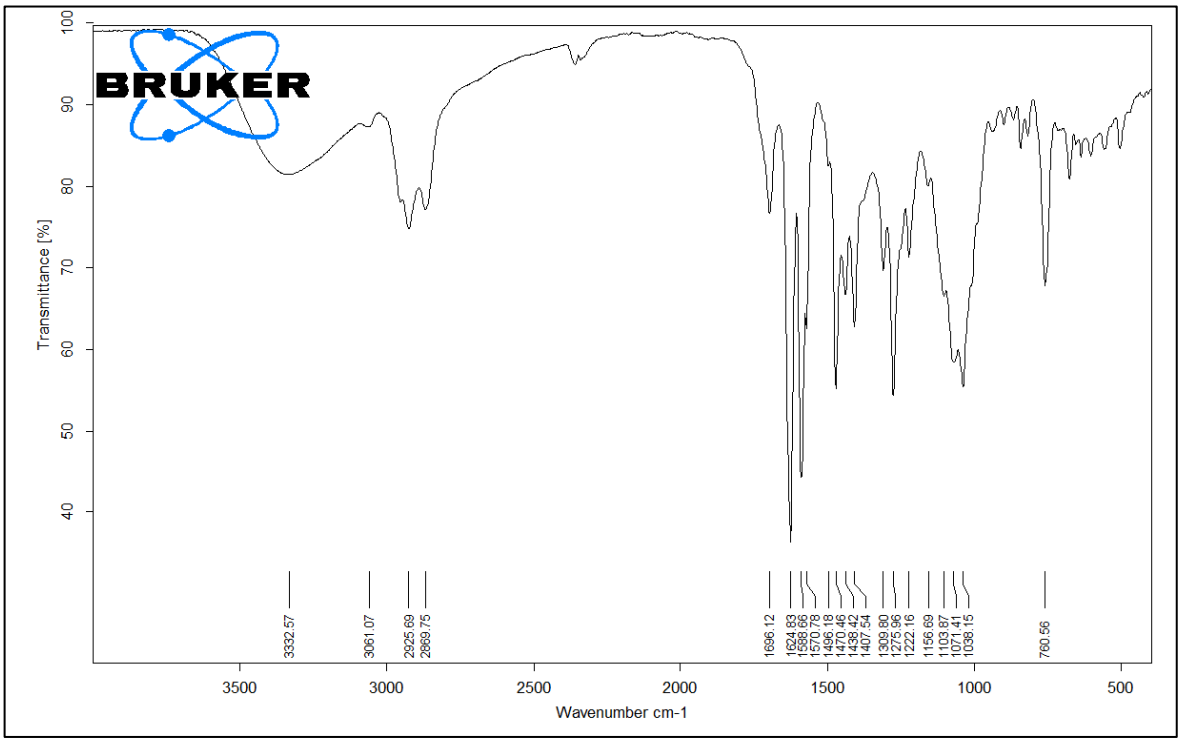

Figure 40. ATR-FTIR spectrum of AK-PG03. Transmittance % is shown in the ranges 4000 to 400 cm^{-1}.

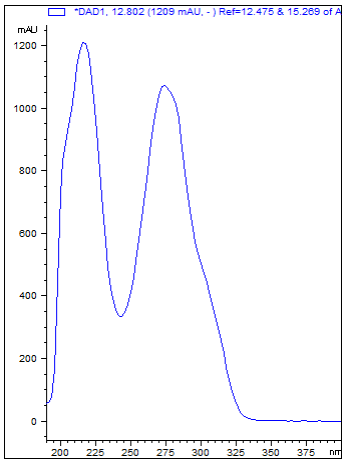

The obtained $[\alpha]_D^{20}$ value of AK-PG03 is –30.81 (MeOH, 6.53 mg/mL). It is therefore laevorotatory, similarly to glomerulatine A [9]. For the evaluation of the log ε values, absorptions were measured at the maxima at 218 and 274 nm and the shoulder at 300 nm in the UV spectrum in the ranges 180–400 nm (Figure 41). The log ε results are 3.68 (218 nm), 3.57 (274 nm) and 3.50 (300 nm).

Figure 41. UV-absorption spectrum of AK-PG03 in the range of 180-400 nm.

A possible biosynthetic pathway is shown in Figure 42. As already mentioned, under acidic conditions, chimonanthine forms into the thermodynamically more stable calycanthine form [33]. However, specific enzymes may catalyse this reaction. Subsequent dehydrogenation steps of the carbons 8a and 8a' and the nitrogens 8 and 8' result in the formation of AK-PG03. Interestingly, tetradehydrocalycanthine 3a(*S*), 3a'(*S*) is laevorotatory, although calycanthine 3a(*S*), 3a'(*S*) is dextrorotatory.

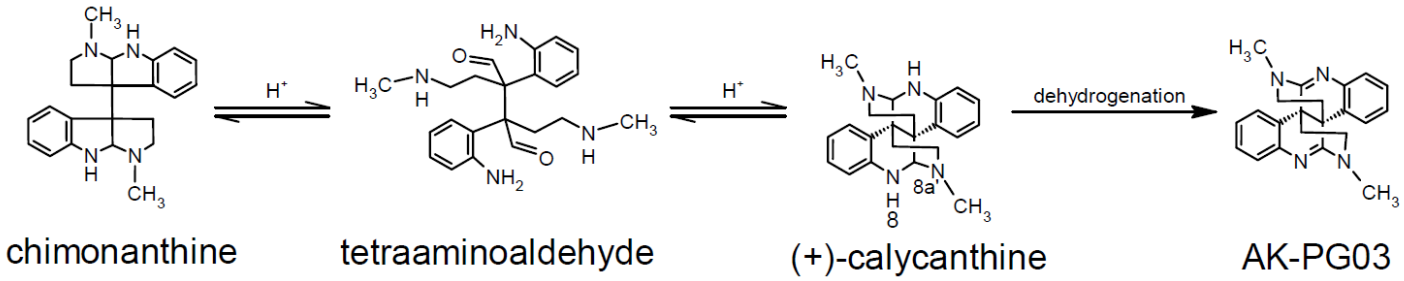

Figure 42. Possible biosynthetic pathways of AK-PG03 [33].

3.2.4. AK-PG04

The NMR results of AK-PG04 are summarized in Table 11 and Table 12. Reference values stem from measurements of 1-desmethyl-*meso*-chimonanthine in deuterated chloroform [60] and isoalstrostine A in deuterated methanol. The suggested structure with important COSY, NOESY and HMBC couplings is shown in Figure 43 a). Noticeable are the characteristic peaks from the α,β-unsaturated ester groups of the secologanin moieties and the aromatic signals of the cyclotryptamine moieties A and B. Similar to AK-PG01, some signals appear twofold or broad. A possible reason for this could be the property of the *meso*-chimonanthine moiety to form a major and a minor conformer as shown in Figure 43 b). Likewise, there are two signals in the HPLC chromatograms, after several seperation attempts. Nethertheless, the yield of 3.2 mg is too little to risk losses on further isolation processes. One major difference between those two conformers is the shift of the signals of the protons H4 and H4'. Depending on the protons position relative to the aromatic plane, their signals are shifted upfield towards δ 5.62 and 5.67 instead of δ 7.28 and 7.32 [60]. This shift difference of the two protons H4 and H4' was not observed in compounds with the 3a(*S*),3a'(*S*)-chimonanthine structure [63]. Therefore, a *meso*-chimonanthine like structure is implied. The 3a(*S*) stereochemistry is suggested by the similarities of the shifts of isoalstrostine A. Because of its relatively large molecular mass of $[M+H]^+$ 1073.4581 m/z, a ROESY experiment was performed to be able to differentiate between NOE signals and chemical exchange. Even though the NMR shifts are similar to the desmethyl-*meso*-chimonanthine structure, expected NOEs such as between the protons H8a and H8a', H4' and H3 or H4 and H3' are not observable [60]. After thorough research this is the first mentioning of the existence of chimonanthine-alstrostines.

Table 11. NMR shift table of AK-PG04 (1-desmethyl-*meso*-chimonanthine moiety).

No.	Group	δ ^{13}C	Reference [60] Isoalstrostine A / Desmethyl-*meso*-chimonanthine CD_3OD / $CDCl_3$ major / minor		δ ^{1}H (multiplicity) s: singlet, d: duplet, t: triplet, m: multiplet, br: broad		Reference [60] Isoalstrostine A / Desmethyl-*meso*-chimonanthine CD_3OD / $CDCl_3$ major / minor	HMBC coupling
1-Desmethyl-*meso*-chimonanthine moiety								
2	CH_2	53.0	53.3	44.9 / 44.6	3.23 (m), 2.20 (m, br)	3.39; 2.42	3.18–2.73 / 3.18	-
3	CH_2	32.7	36.8	35.7 / 37.6	2.80 (m), 2.37 (m)	2.48; 2.42	2.60–2.40 / 2.60	-
3a	C_q	63.0	-	62.9 / 63.6	-	-	-	H-2 (3.23, 2.20)
3b	C_q	132.9	133.2	132.2 / 131.3	-	-	-	H-7 (6.56)
4	CH	n.d.	125.3	123.9 / 124.3	6.32 (br)	7.30	7.28 / 5.62	-
5	CH	118.8	119.7	118.5 / 117.7	6.43 (br)	6.79	6.80 / 6.28	H-7 (6.56)
6	CH	129.5	131.0	128.2 / 128.7	7.05 (m)	7.23	7.10 / 6.91	-
7	CH	109.8	110.4	109.1 / 108.2	6.56 (d)	6.61	6.46 / 6.49	-
7a	C_q	152.0	153.3	151.8 / 151.0	-	-	-	H-6 (7.05), H-4 (6.23)
8a	CH	77.3	79.4	79.3 / 82.4	4.87 (s)	4.71	4.32 / 5.42	H-7'' (5.75), H-2 (3.23, 2.20)
1'N-CH_3		37.6	-	35.1 / 35.1	2.34 (s)	-	2.32 / 2.47	-
2'	CH_2	54.1	-	51.9 / 51.7	2.55–2.43 (br)	-	2.82 / 2.82–2.42	1'N-CH_3 (2.34)
3'	CH_2	36.8	-	38.1 / 36.4	2.43 (m), 2.12 (m)	-	2.10 / 2.10	-
3a'	C_q	63.1	-	64.0 / 63.3	-	-	-	H-2' (2.55–2.43)
3b'	C_q	134.4	-	130.0 / 131.3	-	-	-	H-7' (6.52)
4'	CH	n.d.	-	124.4 / 124.1	7.18 (m, br)	-	5.67 / 7.32	-
5'	CH	118.9	-	118.0 / 118.8	6.72 (m, br)	-	6.30 / 6.82	H-7' (6.52)
6'	CH	129.4	-	128.4 / 128.0	7.04 (m)	-	6.91 / 7.10	-
7'	CH	110.4	-	108.2 / 109.1	6.52 (d)	-	6.48 / 6.48	H-5' (6.72)
7a'	C_q	152.5	-	150.3 / 151.5	-	-	-	H-6' (7.04), H-4' (7.18)
8a'	CH	85.2	-	82.4 / 82.4	4.56 (s)	-	5.42 / 4.32	1'N-CH_3 (2.34)

Table 12. NMR shift table of AK-PG04 (secologanin moieties).

No.	Group	δ ^{13}C	Reference Isoalstrostine A CD_3OD	δ ^{1}H (multiplicity)	Reference Isoalstrostine A CD_3OD	HMBC coupling
Secologanin-aglycon moieties						
1''	CH	97.9	97.2	5.52 (d)	5.31	H-3'' (7.34), H-1* (4.72), H-9'' (2.63)
1'''	CH	98.3	98.1	5.53 (m)	5.51	H-3''' (7.50), H-1** (4.71), H-9''' (2.54)
3''	CH	152.9	153.2	7.34 (d,)	7.44	H-1'' (5.52)
3'''	CH	152.7	152.6	7.50(s)	7.49	H-1''' (5.53)
4''	C_q	112.1	111.0	-	-	H-3'' (7.34)
4'''	C_q	113.1	112.5	-	-	H-3''' (7.50)
5''	CH	36.7	36.8	3.29 (m)	3.27	H-3'' (7.34), H-7'' (5.75)
5'''	CH	30.5	28.0	3.03 (br)	3.15	H-3''' (7.50)
6''	C_q	n.d.	116.8	-	-	-
6'''	CH_2	36.8	33.1	1.75 (br), 1.73 (br)	2.19; 2.11	-
7''	CH	134.2	133.4	5.75 (s)	5.70	-
7'''	CH	55.4	53.1	4.25 (br)	4.01	H-7'' (5.75)
8''	CH	137.5	137.0	5.54 (m)	5.54	H-10'' (5.09)
8'''	CH	135.4	135.9	5.79 (m, br)	5.86	-
9''	CH	47.6	47.4	2.63 (m)	2.57	H-10'' (5.09)
9'''	CH	47.5	45.2	2.54 (m)	2.81	H-10''' (5.38, 5.30)
10''	CH_2	118.8	119.2	5.09 (m)	5.18	-
10'''	CH_2	119.8	120.4	5.38 (d), 5.30 (d)	5.47, 5.41	-
11''	C_q	169.6	168.9	-	-	H-3'' (7.34), 11''-OCH_3 (3.45)
11'''	C_q	169.8	169.3	-	-	H-3''' (7.50), 11'''-OCH_3 (3.71)
11''-OCH_3		51.8	51.7	3.45 (s)	3.66	-
11'''-OCH_3		52.3	51.8	3.71 (s)	3.66	-
Glucose moieties						
1*	CH	100.2	100.2	4.72 (d)	4.68	H-1'' (5.52), H-2* (3.20)
1**	CH	100.2	99.9	4.71 (d)	4.63	H-1''' (5.53), H-2** (3.09)
2*	CH	74.6	74.7	3.20 (dd)	3.17	H-3*(3.35)
2**	CH	74.7	74.6	3.09 (dd)	3.11	H-3** (3.36)
3*	CH	78.2	78.1	3.35 (m)	3.35	H-2* (3.20)
3**	CH	78.3	78.3	3.36 (m)	3.07	H-2** (3.09)
4*	CH	71.4	71.4	3.31 (m)	3.29	H-3*(3.35), H-5* (3.31)
4**	CH	71.4	71.4	3.36 (m)	3.23	H-3** (3.36), H-5** (3.32)
5*	CH	78.4	78.4	3.31 (m)	3.31	H-3*(3.35)
5**	CH	78.4	78.0	3.32 (m)	3.35	H-3** (3.36)
6*	CH_2	62.7	62.6	3.92 (dd), 3.74 (m)	3.90, 3.69	-
6**	CH_2	62.6	62.6	3.88 (dd), 3.70 (m)	3.50, 3.22	-

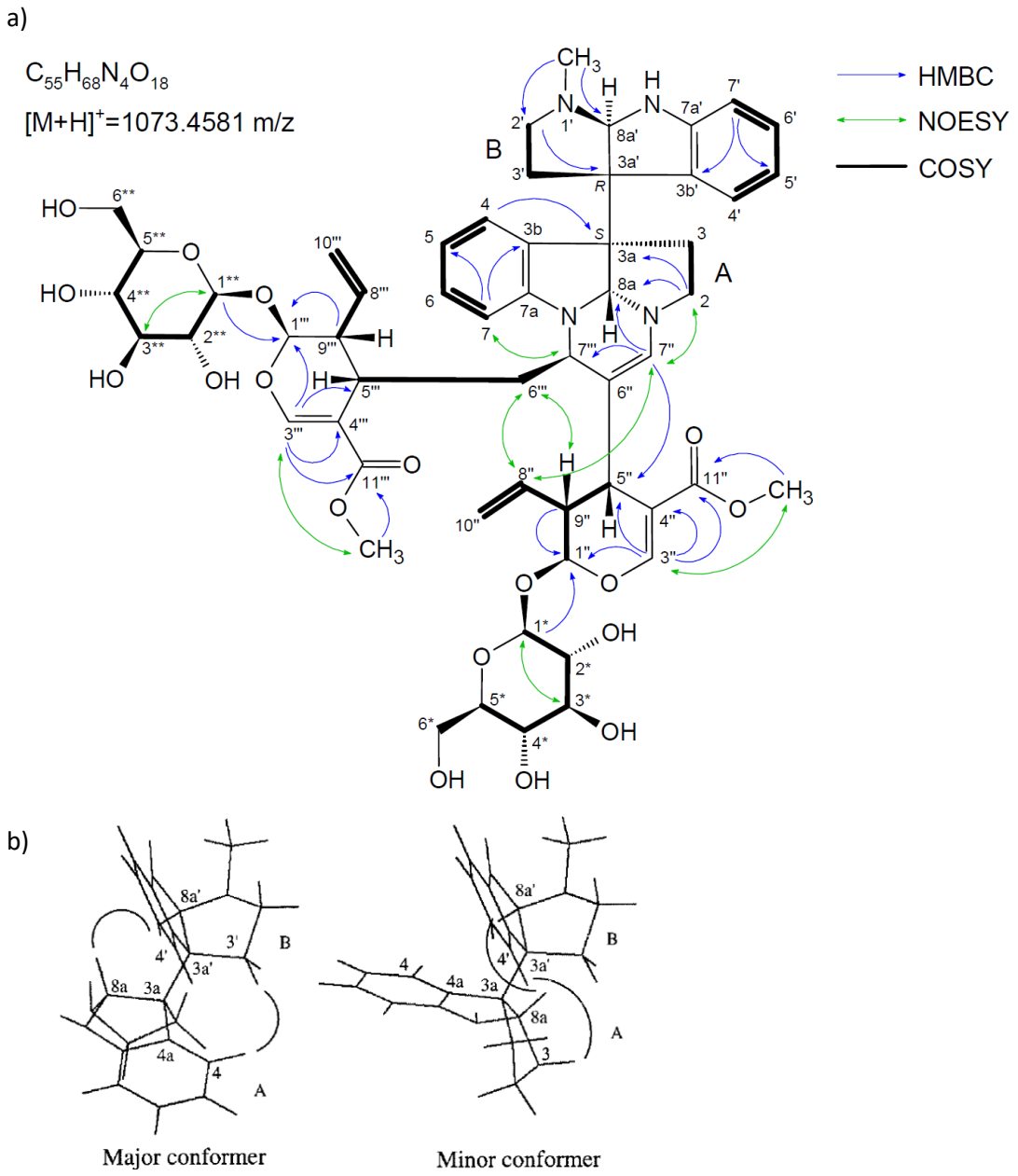

Figure 43. a) Structure of AK-PG04. HMBC crosspeaks are displayed as blue arrows, NOESY crosspeaks are displayed as green arrows and COSY crosspeaks are displayed as thick bonds. b) Shows the energy-minimized structure and indicated NOEs of 1-desmethyl-*meso*-chimonanthine [60].

The results of the ATR-FTIR measurements are shown in Figure 44. The spectrum is displayed as % transmittance versus wavenumber in the range between 4000 to 400 cm^{-1}. Background and sample were scanned 256 times. The spectrum looks very similar to that of AK-PG02, because many functional groups occur in both compounds such as the aromatic ring, the vinyl group, the –OH groups of the glucose moieties and the α,β-unsaturated ester group.

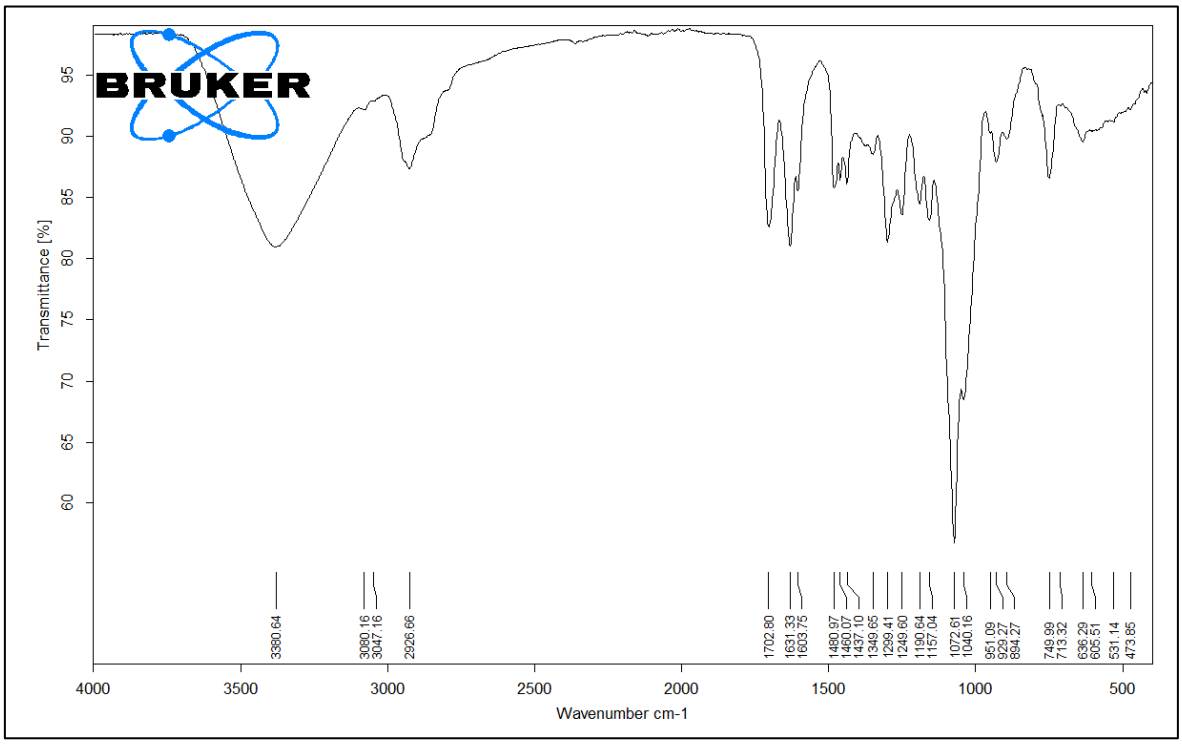

Figure 44. ATR-FTIR spectrum of AK-PG04. Transmittance % is shown in the ranges 4000 to 400 cm^{-1}.

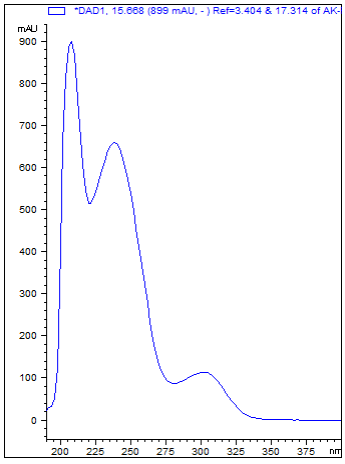

The obtained $[\alpha]_D^{20}$ value of AK-PG04 was +0.26 (MeOH, 2.33 mg/mL). For the evaluation of the log ε values, absorptions were measured at the maxima in the UV spectrum in the ranges 180–400 nm (Figure 45). The log ε results are 4.56 (208 nm), 4.39 (238 nm) and 3.75 (302 nm).

Figure 45. UV-absorption spectrum of AK-PG04 in the range of 180-400 nm.

A possible biosynthetic pathway is shown in Figure 46. It resembles the proposed isoalstrostine A route apart from the *meso*-chimonanthine starting point [30]. The demethylation of *meso*-chimonanthine can result in the formation of two enantiomers, 3a(*S*), 3a'(*R*) and 3a(*R*) and 3a'(*S*). However, whether this reaction is enantioselective, and enzyme catalysed, is not yet known. Moreover, both, desmethyl-*meso*-chimonanthine and isoalstrostine A are known to occur in the *Psychotria* species *P. lyciiflora* and *P. luxurians*,

respectively [30,60]. It is therefore not unlikely, that a compound structurally related to both classes is present in another member of the *Psychotria* alliance.

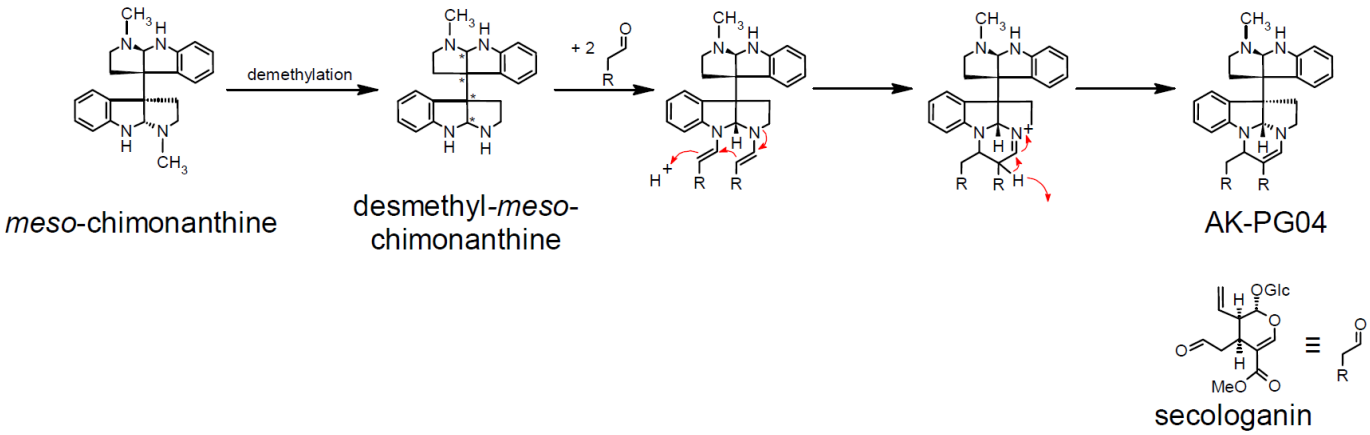

Figure 46. Possible biosynthetic pathways of AK-PG04 [30].

3.2.5. 1-(6-Amino-6-deoxy-α-D-glucosyl)-2,3-dipalmitylglycerol (AK-PG08)

The NMR results of AK-PG08 are summarized in Table 13. Reference values stem from measurements of rauvolfianine in deuterated DMSO-d_6 [64]. The suggested structure with important COSY, NOESY and HMBC couplings is shown in Figure 47. This compound belongs to the class of glycoglycerolipids. The coupling constant of the anomeric carbon suggests a α glycosidic conformation. Due to the amino group, the H6 proton shifts are at δ 3.34 and 2.92, whereas usual carbohydrates show H6 shifts of ~δ 3.90 and 3.70. Furthermore. the similarities of the CH_2 protons of the acyl chain cause a lot of overlapping. However, a CH_3:CH_2 ratio can be determined to estimate the average chain length of the fatty acids (Equation 3).

$$\frac{CH_3}{CH_2} = \frac{(\int \delta\ 0.98 + \int \delta\ 0.90) * \frac{1}{3}}{(\int \delta\ 2.80 + \int \delta\ 2.34 + \int \delta\ 2.06 + \int \delta\ 1.61 + \int \delta\ 1.33) * \frac{1}{2}}$$

$$= \frac{\frac{0.35 + 5.87}{3}}{\frac{0.53 + 4.16 + 2.18 + 4.28 + 44.70}{2}} = \frac{2.07}{27.93} \sim \frac{2\ CH_3}{28\ CH_2}$$

Equation 3. Calculation of the CH_3:CH_2 ratio for the estimation of the fatty acid chain length.

For this calculation, the integrals of CH_3 and CH_2 signals of the fatty acid moiety mentioned in Table 13 as well as CH_3 and CH_2 signals of unsaturated fatty acids were used. Nevertheless, it should be mentioned that these calculations are not fully accurate, because ideally only protons with the same relaxation time should be compared. Characteristic proton shifts of unsaturated fatty acids include olefinic protons at δ 5.35, CH_2 groups next to a double bond at δ 2.06, CH_2 groups between two double bonds at δ 2.80 and the CH_3 two bonds away of a double bond at 0.98 (Figure 48). These shifts are similar to the values obtained in deuterated chloroform by Tyl et al. [65].

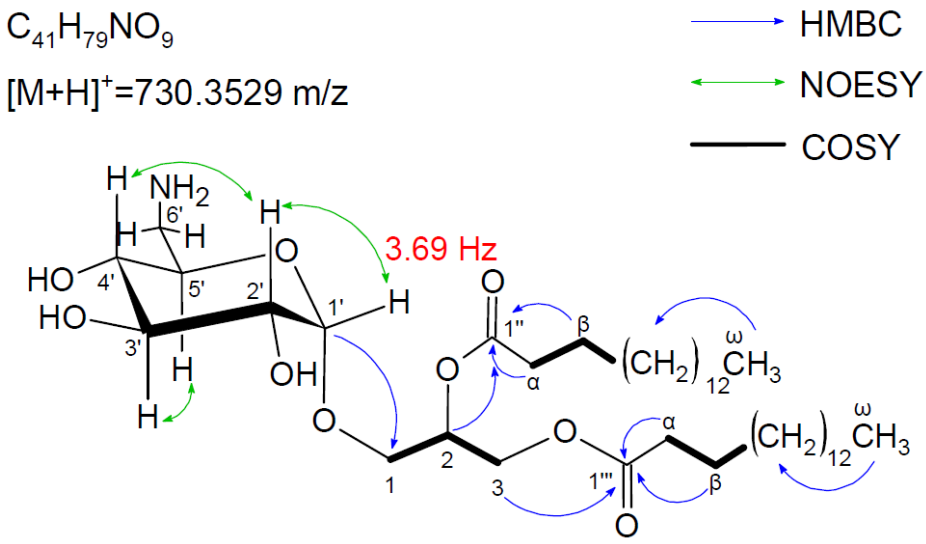

Figure 47. Structure of 1-(6-amino-6-deoxy-α-D-glucosyl)-2,3-dipalmitylglycerol (AK-PG08). HMBC crosspeaks are displayed as blue arrows, NOESY crosspeaks are displayed as green arrows and COSY crosspeaks are displayed as thick bonds. The small coupling constant of a α-glycosidic anomeric proton is shown in red.

Table 13. NMR shift table of 1-(6-amino-6-deoxy-α-D-glucosyl)-2,3-dipalmitylglycerol (AK-PG08).

No.	Group	δ ^{13}C	Reference [64] DMSO-d_6	δ ^{1}H (multiplicity) s: singlet, d: duplet, t: triplet, m: multiplet, br: broad	Reference [64] DMSO-d_6	HMBC coupling
Glycerol moiety						
1	CH_2	67.2	64.3	4.11(dd), 3.58(dd)	3.89, 3.39	H-2 (5.32), H-1' (4.77), H-3 (4.51, 4.19)
2	CH	71.8	69.4	5.32 (m)	5.13	H-3 (4.19), H-1 (4.11, 3.58)
3	CH_2	64.4	62.3	4,51(dd), 4.19(dd)	4.34, 4.14	H-1 (4.11, 3.58)
6-Amino-6-deoxy-D-glucose moiety						
1'	CH	100.0	98.0	4.77 (d)	4.40	H-1 (4.11, 3.58), H-5'(4.07), H-3'(3.63)
2'	CH	73.5	71.3	3.41 (dd)	3.17	H-3'(3.63)
3'	CH	75.0	72.6	3.63 (t)	3.36	H-1' (4.77), H-5'(4.07), H-2' (3.41), H-4'(3.09)
4'	CH	75.0	74.0	3.09 (t)	2.86	H-5'(4.07), H-3'(3.63), H-2' (3.41), H-6'(3.34, 2.92)
5'	CH	69.9	68.2	4.07 (t)	3.76	H-1' (4.77), H-6'(3.34, 2.92), H-4'(3.09)
6'	CH_2	54.3	54.4	3.34 (dd), 2.92(dd)	2.89, 2.52	H-5'(4.07), H-4'(3.09)
Fatty acid moiety						
1''$^{(\prime)}$	C_q	175.0	172.2	-	-	H-2 (5.32), H-3 (4.51, 4.19), Hα-2''$^{(\prime)}$ (2.34); Hβ-3''$^{(\prime)}$ (1.61)
2''$^{(\prime)}$	α-CH_2	35.0	33.1	2.34 (m)	2.25	Hβ-3''$^{(\prime)}$ (1.61)
3''$^{(\prime)}$	β-CH_2	26.0	24.1	1.61 (m)	1.48	Hα-2''$^{(\prime)}$ (2.34), H-N/A (1.25-1.40)
N/A	CH_2	23.3–33.1	21.8–31.0	1.25–1.40	1.24	Hω (0.90), Hβ-3''$^{(\prime)}$ (1.61)
ω	ω-CH_3	14.5	13.6	0.90	0.84	H-N/A (1.25–1.40)

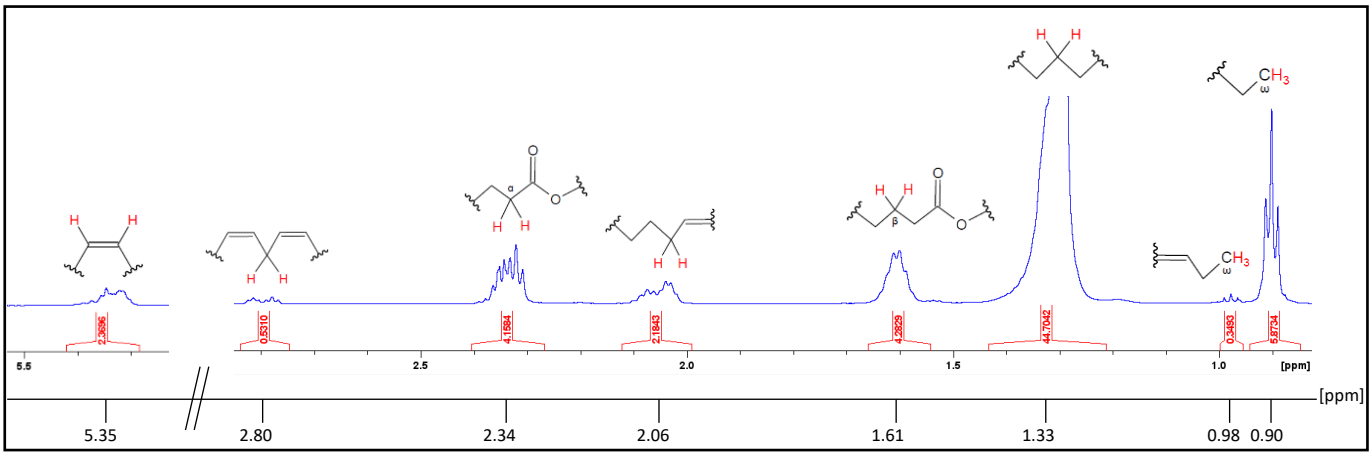

Figure 48. ^{1}H spectrum of protons of the fatty acid moiety. Corresponding functional groups are shown above, and integrals are shown below each signal.

The CH_3:CH_2 ratio of 2:28 suggests a fatty acid chain length of 16 carbons, one CH_3 group, 14 CH_2 groups and one carboxylic carbon. Consequently, the molecular mass of AK-PG08 is ~729 Da, which is corresponding to the results of the ESI-MS measurement, that shows a $[M+H]^+$ peak at 730.3529 m/z. Interestingly, there are multiple signals at distances

of around 28 m/z apart from each other, suggesting C_2H_4 differences of the acyl chains. However, varieties in chain lengths of glycolipids are nothing unusual.

The results of the ATR-FTIR measurements are shown in Figure 49. The spectrum is displayed as % transmittance versus wavenumber in the range between 4000 to 400cm^{-1}. Background and sample were scanned 256 times. Noticeable are the strong absorptions at frequencies of 2919.71 and 2851.07 cm^{-1}, which could correspond to the antisymmetric and symmetric stretching of the abundant CH_2 groups respectively. Additionally, skeletal vibrations at 721.13 and 1168.00 cm^{-1} could come from the $(CH_2)_n$ in phase rocking and C–C skeletal stretching respectively [50]. Additionally, already discussed frequencies of the carbohydrate moiety and carboxyl function are present.

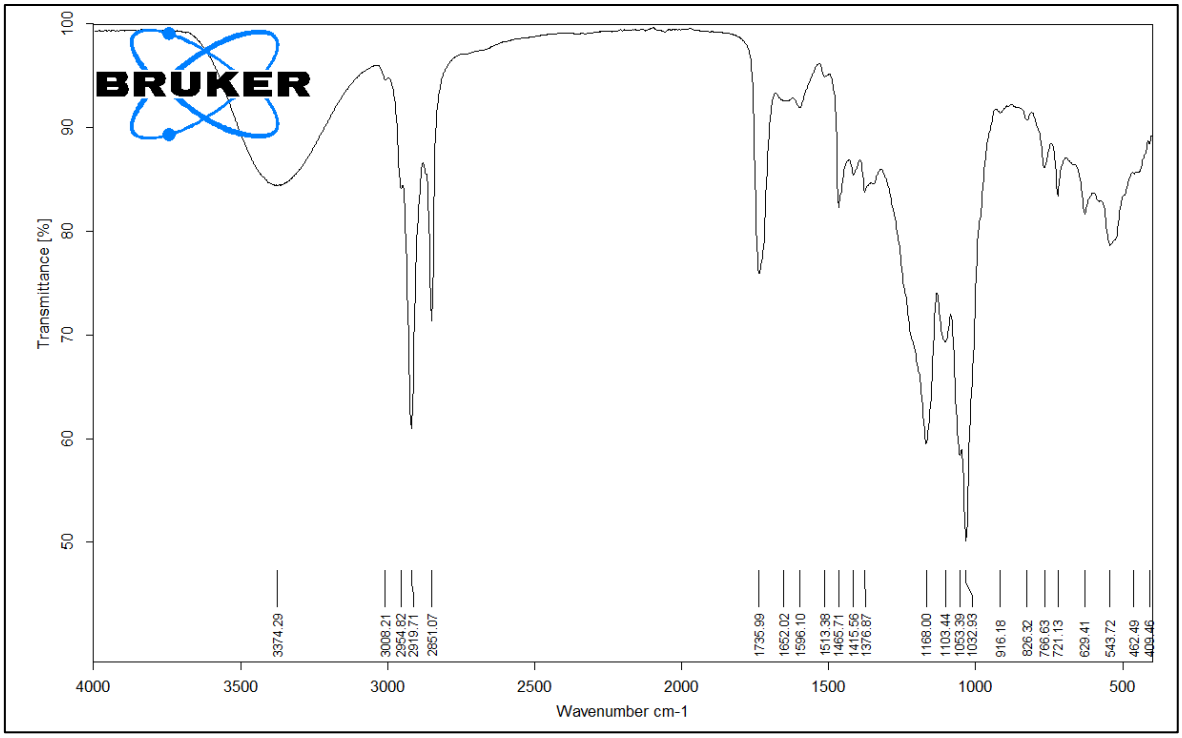

Figure 49. ATR-FTIR spectrum of AK-PG08. Transmittance % is shown in the ranges 4000 to 400 cm^{-1}.

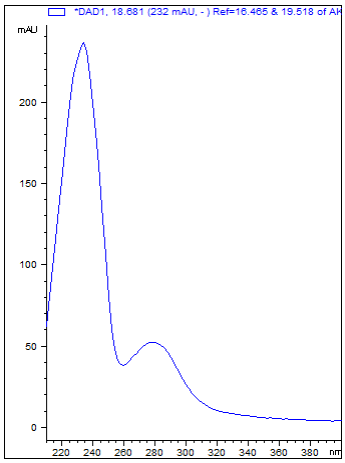

The obtained $[\alpha]_D^{20}$ value of AK-PG08 was +2.47 (MeOH, 4.53 mg/mL). For the evaluation of the log ε values, absorptions were measured at the maxima in the UV spectrum in the ranges 210–400 nm (Figure 50). The log ε results are 3.60 (234 nm) and 3.09 (278 nm).

Figure 50. UV-absorption spectrum of AK-PG08 in the range of 210-400 nm.

3.3. Biological and chemical assay results

3.3.1. Antioxidant activity assay

Radical scavenging activity of root, stem bark and leaf extracts of *P. glomerulata* and the controls L-ascorbic acid and α-tocopherol was assessed with the DPPH method. Samples and control were measured as triplicates. Absorbance of DPPH at 517 nm and 700 nm as reference was measured after 30 min of incubation in the dark. Then, EC_{50} values were calculated via https://www.ic50.tk. The results of the antioxidant activity assay are shown in Table 14. Although each of the three extracts showed antioxidant activity, their EC_{50} are much higher compared to the controls. Of those three, the root extract seems to have the highest EC_{50} value and therefore the lowest antioxidative activity. However, significant differences were not calculated.

Table 14. Results of the antioxidant activity assay.

Sample	Concentration range [mg/mL–µg/mL]	EC_{50}±SD after 30 min [mg/mL]
L-Ascorbic acid	0.25 – 0.12	3.28 ±0.55 $*10^{-3}$
α-Tocopherol	0.5 – 0.24	8.46 ±0.73$*10^{-3}$
Leaf	3.1 – 1.51	0.2780 ±0.0015
Stem bark	10.05 – 9.81	0.2658 ±0.0247
Root	8.35 – 8.15	0.3356 ±0.0289

3.3.2. Non-choice feeding experiment

The inhibitory effect of root, stem bark and leaf extracts on growth of neonatal *Spodoptera littoralis* against (–)-nicotine as control. Concentrations were tested as triplicates and the concentrations used were 500 and 1500 ppm nicotine for the PC and 500, 1000 and 2000 ppm for each extract solution. Then, ten neonatal larvae were added to each sample. After an incubation period of 4 d the weight of the ten larvae was determined. The average weight gain as well as the weight gain relative to the NC in % are shown in Table 15. None of the three plant extracts showed a significant inhibitory effect on weight gain. However, this might be because of the small sample size.

Table 15. Results of the non-choice feeding experiment.

Sample	Concentration [ppm]	Average weight ±SD [mg]	Average weight relative to NC [% m/m(NC)]
Leaf	500	11.85 ±2.15	96
	1000	12.77 ±2.18	103
	2000	12.61 ±2.42	102
Stem bark	500	12.92 ±3.05	104
	1000	11.42 ±3.00	92
	2000	10.83 ±3.52	87
Root	500	15.25 ±1.20	123
	1000	10.92 ±2.15	88
	2000	13.08 ±3.64	106
(–)-Nicotine	500	7.82 ±2.67	63
	1500	4.08 ±1.71	33

3.3.3. Leaf disc choice test

Gustatory effects of leaf, stem bark and root extracts as well as the controls, caffeine and D-(–)-salicin on 10-day-old larvae of *S. littoralis* was evaluated using the leaf disc choice test. 13 mm Leaf discs of *Lactuca sativa* L. were treated with either plant extract or control and tested against each other. Samples were prepared in triplicates and the combinations chosen were root, stem bark and leaf extract against the solvent, each plant extract against the solvent and lastly each plant extract against each PC. The test lasted for 105 min. If there were no bite marks on any leaf, the test was not stopped until the other day. ImageJ software was used to evaluate the eaten area. The eaten amounts of each leaf disc are shown in Table 16. The samples are leaf= L, stem bark= SB, root= R extracts and the controls are solvent, caffeine and D-(–)-salicin. Because of the small number of samples and the relatively large standard deviations, no significant effect can be observed. In other words, the larvae did not differentiate between plant extracts and control and ate whatever disc they first reached.

Table 16. Results of the leaf disc choice test.

Sample	Sample area eaten ±SD [%]			Control area eaten ±SD [%]
L+SB+R+solvent	28.9 ±50.0	36.2 ±48.3	50.2 ±46.3	11.5 ±20.0
L+solvent		73.4 ±46.0		100 ±0
SB+solvent		66.7 ±57.7		86.4 ±23.5
R+solvent		69.3 ±28.3		8.4 ±14.5
L+salcin		33.3 ±57.7		66.7 ±57.7
SB+salcin		0 ±0		90.3 ±10.3
R+salcin		28.5 ±49.3		48.0 ±41.9
L+caffeine		33.3 ±57.7		43.2 ±21.6
SB+caffeine		34.7 ±56.6		25.9 ±24.1
R+caffeine		38.1 ±54.1		8.9 ±15.4

Leaf= L, stem bark= SB, root= R extracts

Overall, the extracts of *P. glomerulata* showed little effects in the antioxidant activity assay and no significant effects in the biologic tests. However, because mixtures of compounds were tested, it cannot be concluded that the isolated substances also would not show an effect. Unfortunately, tests with the isolated components were not possible, as the yield was not sufficient. In addition to that, to obtain statistically significant results with the leaf disc choice test, larger sample numbers are needed. Because it seemed like the larvae were eaten the leaf they first reached. Therefore, in most samples there was a probability of 50 % it would show an effect.

4. Conclusion and outlook

Because of the investigation of multiple solvent phases, it was possible to isolate five compounds that differ vastly from their molecular structure and their lipophilicity from the leaf extract of *Palicourea glomerulata* (Figure 51). Additionally, previous findings of glomerulatine A were able to be replicated without the use of acid-base extraction methods. Suggesting that its presence is not only *in vitro* as an artefact. Furthermore, compounds that are scarcely found in nature such as *C*-glycosylflavanonoids and 6-amino-6-deoxy-glycoglycerolipids were found in the leaf extract as well. Moreover, this present study is the first mentioning of a novel type of alkaloid, that is structurally related to cyclotryptamines and alstrostines. However, the biologic synthesis of non-strictosidine MIAs is not fully understood.

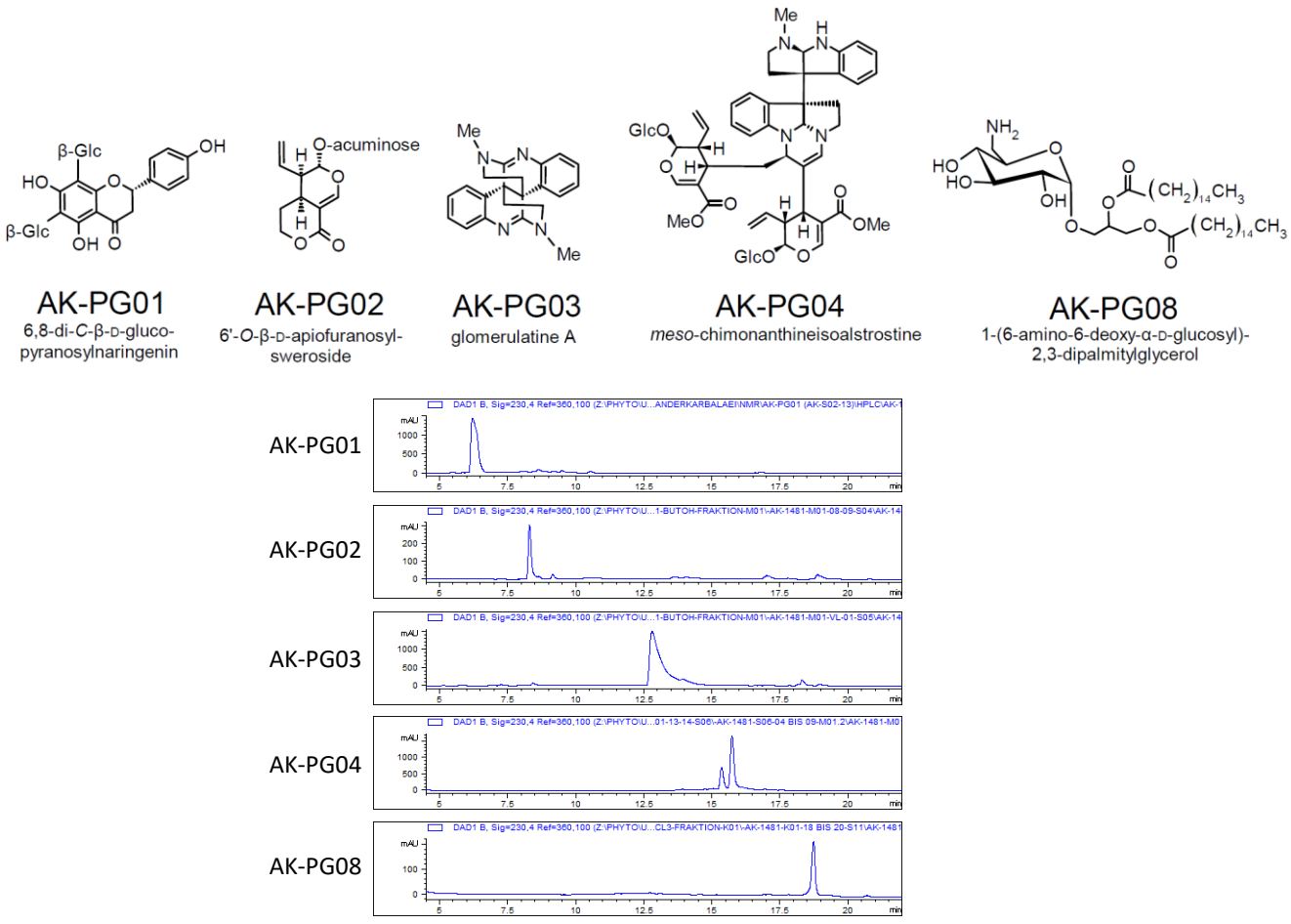

Figure 51. Summary of all isolated compounds (top). The HPLC chromatograms of each substance, showing the differences in their lipophilicity (bottom).

Another aspect this study succeeded to show is the complexity of structure elucidation, as the spectra of each compound brought their own unique challenges. For example, the presence of rotamers in *C*-glycosylflavanonoids and *meso*-chimonanthine derivates, or the similarities in the NMR spectra of calycanthine-, and isocalycanthine-type structures.

The results of the biological assay did not indicate any significant effects. However, this might be because of the low concentrations and in the case of the leaf disc choice test, low number of samples used. Additionally, non-purified extracts were tested. Therefore, conclusions on possible effects of the isolated compounds cannot be drawn.

Overall, plants are able to produce a large diversity of specialized metabolites, and the application of modern isolation techniques can help to find novel structures in already studied species. This study contributed to the further understanding of the chemical profile of *Palicourea glomerulata*. However, as no significant effects regarding plant protection in the form of radical scavenging and herbivore repelling activity were measured, it is unclear why the plant produces these compounds. Therefore, future studies enlightening the reasoning of their synthesis as well as the assessment of other potential effects for the plant and human health are needed.

5. References

[1] M. Heinrich, J. Mah, V. Amirkia. Alkaloids used as medicines: Structural phytochemistry meets biodiversity-An update and forward look. Molecules, 2021, volume 26(7), 1836. DOI: 10.3390/molecules26071836.

[2] D. Martins, C.V. Nunez. Secondary metabolites from Rubiaceae species. Molecules, 2015, volume 20(7), 13422–13495. DOI:10.3390/molecules200713422.

[3] R. Tiwari, C.S. Rana. Plant secondary metabolites: a review. International Journal of Engineering Research and General Science, 2015, volume 3(5), 661–670.

[4] Royal Botanic Gardens Kew, Plants of the World Online: *Palicourea glomerulata* (Donn.Sm.) Borhidi, URL: https://powo.science.kew.org/taxon/urn:lsid:ipni.org:names:77115607-1. (retrieved on 23.01.2022)

[5] N. Calixto, M. Pinto, S. Ramalho, M. Burger, A. Bobey, M.C. Marx Young, V. Bolzani, A. Pinto. The genus *Psychotria*: Phytochemistry, chemotaxonomy, ethnopharmacology and biological properties. Journal of the Brazilian Chemical Society, 2016, volume 27(8), 1355–1378. DOI: 10.5935/0103-5053.20160149.

[6] M.G. Simpson. Plant systematics (second edition). 8 - Diversity and classification of flowering plants: Eudicots. Elsevier/Academic Press: Amsterdam, Boston, 2010, volume 2, 275–448. DOI: 10.1016/B978-0-12-374380-0.50008-7. URL: <https://www.sciencedirect.com/topics/pharmacology-toxicology-and-pharmaceutical-science/rubiaceae>. (retrieved on 20.03.2022)

[7] A. Berger, K. Valant-Vetschera, J. Schinnerl, L. Brecker. A revised classification of the sister tribes Palicoureeae and Psychotrieae (Rubiaceae) indicates genus-specific alkaloid accumulation. Phytochemistry Reviews, 2021, *in press*. DOI: 10.1007/s11101-021-09769-x.

[8] S.G. Razafimandimbison, C.M. Tylor, N. Wikström, T. Pailler, A. Khodabandeh, B. Bremer. Phylogeny and generic limits in the sister tribes Psychotrieae and Palicoureeae (Rubiaceae): Evolution of schizocarps in *Psychotria* and origins of

bacterial leaf nodules of the Malagasy species. American Journal of Botany, 2014, volume 101(7), 1102–1126. DOI: 10.3732/ajb.1400076.

[9] P.N. Solís, A.G. Ravelo, J.A. Palenzuela, M.P. Gupta, A. González, J.D. Phillipson. Quinoline alkaloids from *Psychotria glomerulata*. Phytochemistry, 1997, volume 44(5), 963–969. DOI: 10.1016/S0031-9422(96)00583-3.

[10] Y. Ji, M. Yu, B. Wang, Y. Zhang. The extraction, separation, and purification of alkaloids in the natural medicine. Journal of Chemical and Pharmaceutical Research, 2014, volume 6(1), 338–345.

[11] J. Xiao, A. Capanoglu, A.R. Jassibi, A. Miron. Advance on the flavonoid *C*-glycosides and health benefits. Critical Reviews in Food Science and Nutrition, 2016, volume 56(1), 29–45. DOI: 10.1080/10408398.2015.1067595.

[12] P.G. Pietta. Flavonoids as antioxidants. Journal of Natural Products, 2000, volume 63(7), 1035–1042. DOI: 10.1021/np9904509.

[13] P. Y. Lam, A. Lui, L. Wang, H. Liu, T. Umezawa, Y. Tobimatsu, C. Lo. Tricin biosynthesis and bioengineering. Frontiers in Plant Science, 2021, volume 12, 733198. DOI: 10.3389/fpls.2021.733198.

[14] I.J. Flores-Sanchez, R. Verpoorte. Plant polyketide synthases: A fascinating group of enzymes. Plant Physiology and Biochemistry, 2009, volume 47(3), 167–174. DOI: 10.1016/j.plaphy.2008.11.005.

[15] J.M. Jez, J.P. Noel. Reaction mechanism of chalcone isomerase. pH dependence, diffusion control, and product binding differences. The Journal of Biological Chemistry, 2002, volume 277(2), 1361–1369. DOI: 10.1074/jbc.M109224200.

[16] N. Putkaradze, D. Teze, F. Fredslund, D.H. Welner. Natural product *C*-glycosyltransferases- a scarcely characterised enzymatic activity with biotechnological potential. Natural Product Reports, 2021, volume 38(3), 432–443. DOI: 10.1039/D0NP00040J.

[17] T. Ito, S. Fujimoto, F. Suito, M. Shimosaka, G. Taguchi. *C*-Glycosyltransferases catalyzing the formation of di-*C*-glucosyl flavonoids in citrus plants. The Plant Journal, 2017, volume 91(2), 187–198. DOI: 10.1111/tpj.13555.

[18] Y. Du, H. Chu, K. Ivan, C. Lo. CYP93G2 is a flavanone 2-hydroxylase required for *C*-glycosylflavone biosynthesis in rice. Plant Physiology, 2010, volume 154(1), 324–333. DOI: 10.1104/pp.110.161042.

[19] L.J. El-Naggar, J.L. Beal. Iridoids. A review. Journal of Natural Products, 1980, volume 43(6), 649–707. DOI: 10.1021/np50012a001.

[20] L.-F. Tietze. Secologanin, a biogenetic key compound? Synthesis and biogenesis of the iridoid and secoiridoid glycosides. Angewandte Chemie International Edition, 1983, volume 22(11), 828–841. DOI: 10.1002/anie.198308281.

[21] H. Yamane, K. Konno, M. Sabelis, J. Takabayashi, T. Sassa, H. Oikawa. Chemical Defence and Toxins of Plants. Comprehensive Natural Products II: Chemistry and Biology. Mander L., Lui H.-W., Eds.; Elsevier: Oxford, 2010, volume 4, 339–385. DOI: 10.1016/B978-008045382-8.00099-X

[22] B. Dinda, S. Debnath, Y. Harigaya. Naturally occurring iridoids. A review, part 1. Chemical and Pharmaceutical Bulletin, 2007, volume 55(2), 159–222. DOI: 10.1248/cpb.55.159.

[23] K. Miettinen, L. Dong, N. Navrot, T. Schneider, V. Burlat, J. Pollier, L. Woittiez, S. Van der Krol, R. Lugan, T. Ilc, R. Verpoorte, K.-M.Oksman-Caldentey, E. Martinoia, H. Bouwmeester, A. Goossens, J. Memelink, D. Werck-Reichhart. The seco-iridoid pathway from *Catharanthus roseus*. Nature Communications, 2014, volume 5(1), 3606. DOI: 10.1038/ncomms4606.

[24] J. Zhou, C. Wang, L. Yang, E.-S. Choi, S.-W. Kim. Geranyl diphosphate synthase: an important regulation point in balancing a recombinant monoterpene pathway in *Escherichia coli*. Enzyme and Microbial Technology, 2015, volume 68, 50–55. DOI: 10.1016/j.enzmictec.2014.10.005.

[25] A. Contin, R. Van der Heijden, A.W.M. Lefeber, R. Verpoorte. The iridoid glucoside secologanin is derived from the novel triose phosphate/pyruvate pathway in a

Catharanthus roseus cell culture. FEBS Letters, 1998, volume 434(3), 413–416. DOI: 10.1016/S0014-5793(98)01022-9.

[26] W. Eisenreich, A. Bacher, D. Arigoni, F. Rohdich. Biosynthesis of isoprenoids via the non-mevalonate pathway. Cellular and Molecular Life Sciences, 2004, volume 61(12), 1401–1426. DOI: 10.1007/s00018-004-3381-z.

[27] C.C. Burke, M.R. Wildung, R. Croteau. Geranyl diphosphate synthase: cloning, expression, and characterization of this prenyltransferase as a heterodimer. Proceedings of the National Academy of Sciences of the United States of America, 1999, volume 96(23), 13062–13067. DOI: 10.1073/pnas.96.23.13062.

[28] F. Geu-Flores, N.H. Sherden, V. Courdavault, V. Burlat, W.S. Glenn, C. Wu, E. Nims, Y. Cui, S.E. O'Connor. An alternative route to cyclic terpenes by reductive cyclization in iridoid biosynthesis. Nature, 2012, volume 492(7427), 138–142. DOI: 10.1038/nature11692.

[29] H. Yamamoto, N. Katano, A. Ooi, K. Inoue. Secologanin synthase which catalyzes the oxidative cleavage of loganin into secologanin is a cytochrome P450. Phytochemistry, 2000, volume 53(1), 7–12. DOI: 10.1016/S0031-9422(99)00471-9

[30] C. Kornpointner, A. Berger, F. Traxler, A. Hadžiabdić, M. Massar, J. Matek, L. Brecker, J. Schinnerl. Alkaloid and iridoid glucosides from *Palicourea luxurians* (Rubiaceae: Palicoureeae) indicate tryptamine- and tryptophan-iridoid alkaloid formation apart the strictosidine pathway. Phytochemistry, 2020, volume 173, 112296. DOI: 10.1016/j.phytochem.2020.112296.

[31] S.E. O'Connor, J.J. Maresh. Chemistry and biology of monoterpene indole alkaloid biosynthesis. Natural Product Reports, 2006, volume 23(4), 532–547. DOI: 10.1039/B512615K.

[32] J. Stöckigt, L. Barleben, S. Panjikar, E.A. Loris. 3D-Structure and function of strictosidine synthase-the key enzyme of monoterpenoid indole alkaloid biosynthesis. Plant Physiology and Biochemistry, 2008, volume 46(3), 340–355. DOI: 10.1016/j.plaphy.2007.12.011.

[33] A. Steven, L.E. Overman. Totalsynthese komplexer Cyclotryptaminalkaloide: stereokontrollierter Aufbau quartärer Kohlenstoffstereozentren. Angewandte Chemie, 2007, volume 119(29), 5584–5605. DOI: 10.1002/ange.200700612.

[34] G.W. Kirby, S.W. Shah, E.J. Herbert. Biosynthesis of chimonanthine from [2-^{3}H]-tryptophan and [2-^{3}H]-tryptamine. Journal of the Chemical Society C: Organic, 1969, volume 14(14), 1916–1919. DOI: 10.1039/J39690001916.

[35] A. Berger, K. Valant-Vetschera, J. Schinnerl, L. Brecker. Alkaloid diversification in the genus *Palicourea* (Rubiaceae: Palicoureeae) viewed from a (retro-)biogenetic perspective. Phytochemistry Reviews, 2021, *in press*. DOI: 10.1007/s11101-021-09768-y.

[36] D. Colombo, C. Gagliardi, M. Vetro, F. Ronchetti, M. Takasaki, T. Konoshima, N. Suzuki, H. Tokuda. New 6-amino-6-deoxy-glycoglycerolipids derived from 2-*O*-β-D-glucopyranosylglycerol: insights into the structure-activity relationship of glycoglycerolipids as anti-tumor promoters. Carbohydrate Research, 2013, volume 373, 64–74. DOI: 10.1016/j.carres.2013.03.007.

[37] R.J. Andersen, O. Taglialatela-Scafati. Avrainvilloside, a 6-deoxy-6-aminoglucoglycerolipid from the green alga *Avrainvillea nigricans*. Journal of Natural Products, 2005, volume 68(9), 1428–1430. DOI: 10.1021/np050161m.

[38] B.-N. Zhou, S. Tang, R.K. Johnson, M.P. Mattern, J.S. Lazo, E.R. Sharlow, K. Harich, D.G.I. Kingston. New glycolipid inhibitors of Myt1 kinase. Tetrahedron, 2005, volume 61(4), 883–887. DOI: 10.1016/j.tet.2004.11.013.

[39] X. Zeng, L. Xiang, C.-Y. Li, Y. Wang, G. Qiu, Z.-X. Zhang, X. He. Cytotoxic ceramides and glycerides from the roots of *Livistona chinensis*. Fitoterapia, 2012, volume 83(3), 609–616. DOI: 10.1016/j.fitote.2012.01.008.

[40] H.-J. Wu, C.-X. Li, G.-P. Song, Y.-X. Li. Synthesis of natural α-6-dehydroxy-6-aminoglucoglycerolipids. Chinese Journal of Chemistry, 2008, volume 26(9), 1641–1646. DOI: 10.1002/cjoc.200890296.

[41] Sigma Aldrich: Sephadex® LH-20, URL: <https://www.sigmaaldrich.com/AT/de/product/sigma/lh20100>. (retrieved on 23.01.2022)

[42] M. Burow, R. Müller, J. Gershenzon, U. Wittstock. Altered glucosinolate hydrolysis in genetically engineered *Arabidopsis thaliana* and its influence on the larval development of *Spodoptera littoralis*. Journal of Chemical Ecology, 2006, volume 32(11), 2333–2349. DOI: 10.1007/s10886-006-9149-1.

[43] M.S. Blois. Antioxidant determinations by the use of a stable free radical. Nature, 1958, volume 181(4617), 1199–1200. DOI: 10.1038/1811199a0.

[44] J.I. Glendinning, M. Tarre, K. Asaoka. Contribution of different bitter-sensitive taste cells to feeding inhibition in a caterpillar (*Manduca sexta*). Behavioral Neuroscience, 1999, volume 113(4), 840–854. DOI: 10.1037/0735-7044.113.4.840.

[45] S. Sato, T. Akiya, H. Nishizawa, T. Suzuki. Total synthesis of three naturally occurring 6,8-di-*C*-glycosylflavonoids: phloretin, naringenin, and apigenin bis-*C*-β-D-glucosides. Carbohydrate Research, 2006, volume 341(8), 964–970. DOI: 10.1016/j.carres.2006.02.019.

[46] Chemgapedia: Auswertung von ^{13}C-NMR-Spektren, URL: <http://www.chemgapedia.de/vsengine/vlu/vsc/de/ch/3/anc/nmr_spek/c_nmr_spektren.vlu/Page/vsc/de/ch/3/anc/nmr_spek/m_42/nmr_7_3/inkremente_m42te1102.vscml.html>. (retrieved on 23.02.2022)

[47] L. Brecker. Seinerzeit und heutzutage: Scoparin aus Besenginster. Nachrichten aus der Chemie, 2017, volume 65(5), 596–598. DOI: 10.1002/nadc.20174059954.

[48] G. Zhou, R. Yan, X. Wang, S. Li, J. Lin, J. Liu, Z. Zhao. The overlooked rotational isomerism of *C*-glycosyl flavonoids. Phytochemistry Reviews, 2019, volume 18(2), 443–461. DOI: 10.1007/s11101-019-09601-7.

[49] N. Okamura, A. Yagi, I. Nishioka. Studies on the constituents of zizyphi fructus. V. Structures of glycosides of benzyl alcohol, vomifoliol and naringenin. Chemical and Pharmaceutical Bulletin, 1981, volume 29(12), 3507–3514. DOI: 10.1248/cpb.29.3507.

[50] D. Lin-Vien, N.B. Colthup, W.G. Fateley, J.G. Grasselli. Chapter 2-Alkanes. The handbook of infrared and raman characteristic frequencies of organic molecules. Academic Press: Boston, San Diego, New York, London, Sydney, Tokyo, Toronto, 1991, volume 1, 9–28.

[51] D. Lin-Vien, N.B. Colthup, W.G. Fateley, J.G. Grasselli. Chapter 9- Compounds containing the carbonyl group. The handbook of infrared and raman characteristic frequencies of organic molecules. Academic Press: Boston, San Diego, New York, London, Sydney, Tokyo, Toronto, 1991, volume 1, 117–154.

[52] D. Lin-Vien, N.B. Colthup, W.G. Fateley, J.G. Grasselli. Chapter 17- Aromatic and heteroaromatic rings. The handbook of infrared and raman characteristic frequencies of organic molecules. Academic Press: Boston, San Diego, New York, London, Sydney, Tokyo, Toronto, 1991, volume 1, 277–306.

[53] D. Lin-Vien, N.B. Colthup, W.G. Fateley, J.G. Grasselli. Chapter 4- Alcohols and phenols. The handbook of infrared and raman characteristic frequencies of organic molecules. Academic Press: Boston, San Diego, New York, London, Sydney, Tokyo, Toronto, 1991, volume 1, 45–60.

[54] D. Lin-Vien, N.B. Colthup, W.G. Fateley, J.G. Grasselli. Chapter 5- Ethers and peroxides. The handbook of infrared and raman characteristic frequencies of organic molecules. Academic Press: Boston, San Diego, New York, London, Sydney, Tokyo, Toronto, 1991, volume 1, 61–72.

[55] S. Kumar, O.P. Sati, V.D. Semwal, M. Nautiyal, S. Sati, Y. Takeda. Iridoid glycosides from *Lonicera quinquelocularis*. Phytochemistry, 2000, volume 53(4), 499–501. DOI: 10.1016/S0031-9422(99)00426-4.

[56] M. Pičmanová, B.L. Møller. Apiose: one of nature's witty games. Glycobiology, 2016, volume 26(5), 430–442. DOI: 10.1093/glycob/cww012.

[57] D. Lin-Vien, N.B. Colthup, W.G. Fateley, J.G. Grasselli. Chapter 6- Alkenes. The handbook of infrared and raman characteristic frequencies of organic molecules. Academic Press: Boston, San Diego, New York, London, Sydney, Tokyo, Toronto, 1991, volume 1, 73–94.

[58] W.-X. Wang, S.-Y. Luo, Y. Wang, L. Xiang, X.-H. Liu, C. Tang, Y. Zhang. Pterocephanoside A, a new iridoid from a traditional Tibetan medicine, *Pterocephalus hookeri*. Journal of Asian Natural Products Research, 2021, volume 23(12), 1189–1196. DOI: 10.1080/10286020.2020.1860951.

[59] L. Verotta, T. Pilati, M. Tatò, E. Elisabetsky, T.A. Amador, D.S. Nunes. Pyrrolidinoindoline Alkaloids from *Psychotria colorata*1. Journal of Natural Products, 1998, volume 61(3), 392–396. DOI: 10.1021/np9701642.

[60] V. Jannic, F. Guéritte, O. Laprévote, L. Serani, M.T. Martin, T. Sévenet, P. Potier. Pyrrolidinoindoline alkaloids from *Psychotria oleoides* and *Psychotria lyciiflora*. Journal of Natural Products, 1999, volume 62(6), 838–843. DOI: 10.1021/np9805387.

[61] D. Lin-Vien, N.B. Colthup, W.G. Fateley, J.G. Grasselli. Chapter 10- Compounds containing $–NH_2$, –NHR, and $–NR_2$ groups. The handbook of infrared and raman characteristic frequencies of organic molecules. Academic Press: Boston, San Diego, New York, London, Sydney, Tokyo, Toronto, 1991, volume 1, 155–178.

[62] D. Lin-Vien, N.B. Colthup, W.G. Fateley, J.G. Grasselli. Chapter 12- Double bond containing nitrogen atoms. The handbook of infrared and raman characteristic frequencies of organic molecules. Academic Press: Boston, San Diego, New York, London, Sydney, Tokyo, Toronto, 1991, volume 1, 191–211.

[63] H. Takayama, Y. Matsuda, K. Masubuchi, A. Ishida, M. Kitajima, N. Aimi. Isolation, structure elucidation, and total synthesis of two new chimonanthus alkaloids, chimonamidine and chimonanthidine. Tetrahedron, 2004, volume 60(4), 893–900. DOI: 10.1016/j.tet.2003.11.034.

[64] R. Ebeh Messanga, N.B. Dominique Serge, A. Abouem A Zintchem, M.N.[II] Norbert, M.N. Del Esther Florence, B.D. Patrick Hervé, N. Maximilienne Ascension, A. Alex De Théodore, P. Dieudonné Emmanuel, G.B. Christian, U. Koert. Rauvolfianine, a new antimycobacterial glyceroglycolipid and other constituents from *Rauvolfia caffra*. Sond. (Apocynaceae). Natural Product Research, 2018, volume 32(16), 1971–1976. DOI: 10.1080/14786419.2017.1356832.

[65] C.E. Tyl, L. Brecker, K.-H. Wagner. ^{1}H NMR spectroscopy as tool to follow changes in the fatty acids of fish oils. European Journal of Lipid Science and Technology, 2008, volume 110(2), 141–148. DOI: 10.1002/ejlt.200700150.

List of figures

List of tables

List of equations